

SANDIA REPORT

REFERENCE COPY C.2

SAND91-8233 • UC-113
Unlimited Release
Printed August 1991

Coal Combustion Science Quarterly Progress Report April - June 1991



SAND91-8233
0002
UNCLASSIFIED

08/91
142F SN STAC

Principal Investigators:

- Task 1. Coal Devolatilization ----- Thomas H. Fletcher
- Task 2. Coal Char Combustion---- Robert H. Hurt
- Task 3. Fate of Mineral Matter---- Larry L. Baxter

Edited by Donald R. Hardesty

Prepared by
Sandia National Laboratories
Albuquerque, New Mexico 87185 and Livermore, California 94551-0969
for the United States Department of Energy
under Contract DE-AC04-76DP00769

Issued by Sandia National Laboratories, operated for the United States Department of Energy by Sandia Corporation.

NOTICE: This report was prepared as an account of work sponsored by an agency of the United States Government. Neither the United States Government nor any agency thereof, nor any of their employees, nor any of the contractors, subcontractors, or their employees, makes any warranty, express or implied, or assumes any legal liability or responsibility for the accuracy, completeness, or usefulness of any information, apparatus, product, or process disclosed, or represents that its use would not infringe privately owned rights. Reference herein to any specific commercial product, process, or service by trade name, trademark, manufacturer, or otherwise, does not necessarily constitute or imply its endorsement, recommendation, or favoring by the United States Government, any agency thereof or any of their contractors or subcontractors. The views and opinions expressed herein do not necessarily state or reflect those of the United States Government, any agency thereof or any of their contractors or subcontractors.

This report has been reproduced from the best available copy.

Available to DOE and DOE contractors from:

Office of Scientific and Technical Information
P.O. Box 62
Oak Ridge TN 37831

Prices available from (615) 576-8401, FTS 626-8401.

Available to the public from:

National Technical Information Service
U.S. Department of Commerce
5285 Port Royal Rd.
Springfield, VA 22161

NTIS price codes

Printed copy: A07

Microfiche copy: A01

SAND 91-8233

Unlimited Release
Printed August 1991

COAL COMBUSTION SCIENCE

QUARTERLY PROGRESS REPORT*

APRIL-JUNE 1991

Submitted By: Donald R. Hardesty
Sandia National Laboratories, Livermore
Combustion Research Facility

Submitted To: James D. Hickerson
Pittsburgh Energy Technology Center

* Research supported by the United States Department of Energy, Office of Fossil Energy, Pittsburgh Energy Technology Center

COAL COMBUSTION SCIENCE

QUARTERLY PROGRESS REPORT -- APRIL-JUNE 1991

Donald R. Hardesty
Combustion Research Facility
Sandia National Laboratories
Livermore, California

This document provides a quarterly status report of the Coal Combustion Science Program that is being conducted at the Combustion Research Facility, Sandia National Laboratories, Livermore, California. The information reported is for the period April-June 1991.

The objective of this activity is to support the Office of Fossil Energy in executing research on coal combustion science. This activity consists of basic research on coal combustion that supports both the Pittsburgh Energy Technology Center (PETC) Direct Utilization Advanced Research and Technology Development Program, and the International Energy Agency (IEA) Coal Combustion Science Project. Specific tasks for this activity include:

Task 1: Coal Devolatilization

The objective of this task is to characterize the physical and chemical processes that constitute the early devolatilization phase of coal combustion as a function of coal type, heating rate, particle size and temperature, and gas phase temperature and oxidizer concentration. During FY91 the emphasis is on data compilation and documentation of the chemical percolation devolatilization model. The principal investigator on this task is Thomas H. Fletcher.

Task 2: Coal Char Combustion

The objective of this task is to characterize the physical and chemical processes involved during coal char combustion as a function of coal type, particle size and temperature, and gas phase temperature and oxygen concentration. During FY91 the emphasis is on data compilation for the suite of PSOC coals, determination of the effect of devolatilization conditions on char reactivity, and determination of char reactivity at high carbon conversions. The principal investigator on this task is Robert H. Hurt.

Task 3: Fate of Mineral Matter During Coal Combustion

The objective of this task is to establish a quantitative understanding of the mechanisms and rates of transformation, fragmentation, and deposition of mineral matter in coal combustion environments as a function of coal type, particle size and temperature, the initial forms and distribution of mineral species in the unreacted coal, and the local gas temperature and composition. A particular goal is determining the importance of fragmentation in the evolution of the particle size distribution during coal combustion. The principal investigator on this task is Larry L. Baxter.

TABLE OF CONTENTS

	Page
Executive Summary	9
TASK 1: COAL DEVOLATILIZATION	
<i>T. H. Fletcher and D. R. Hardesty</i>	
OBJECTIVE FOR TASK 1	1-1
SUMMARY OF TECHNICAL PROGRESS	
DURING THIS QUARTER	1-2
Subtask 1.1. Compilation of Data from the Sandia Coal Devolatilization Experiments	1-2
Subtask 1.2. Documentation of the Chemical Percolation Devolatilization Model	1-11
PLANS FOR NEXT QUARTER	1-11
ACKNOWLEDGMENTS	1-11
NOMENCLATURE FOR TASK 1	1-11
REFERENCES FOR TASK 1 SECTION	1-12
PUBLICATIONS, PAPERS, AND PRESENTATIONS	1-12
MILESTONE SCHEDULE AND STATUS REPORT	1-13
 TASK 2: THE RATES AND MECHANISMS OF COAL CHAR COMBUSTION	
<i>R. H. Hurt and D. R. Hardesty</i>	
OBJECTIVE FOR TASK 2	2-1
SUMMARY OF TECHNICAL PROGRESS	
DURING THIS QUARTER.....	2-3
Subtask 2.1. Kinetic Analysis and Data Compilation for the PSOC Coal Suite	2-4
Subtask 2.3 Char Reactivity at High Carbon Conversion	2-56
PLANS FOR NEXT QUARTER	2-57
NOMENCLATURE FOR TASK 2	2-57
REFERENCES FOR TASK 2 SECTION	2-58
PUBLICATIONS, PAPERS, AND PRESENTATIONS	2-58
MILESTONE SCHEDULE AND STATUS REPORT	2-59

TABLE OF CONTENTS - continued

	Page
TASK 3: THE FATE OF MINERAL MATTER	
<i>L. L. Baxter and D. R. Hardesty</i>	
OBJECTIVES FOR TASK 3	3-1
SUMMARY OF TECHNICAL PROGRESS	
DURING THIS QUARTER	3-2
Subtask 3.1. Release of Inorganic Material During Coal Devolatilization and Char Oxidation	3-3
Subtask 3.2 The Evolution of Particle and Fly Ash Size Distributions	3-8
Subtask 3.3 Theoretical and Experimental Studies of Ash Deposition	3-30
TECHNOLOGY EXCHANGE FOR TASK 3	3-30
PLANS FOR NEXT QUARTER	3-31
ACKNOWLEDGMENTS	3-31
NOMENCLATURE FOR TASK 3	3-32
REFERENCES FOR TASK 3 SECTION	3-33
PUBLICATIONS, PAPERS, AND PRESENTATIONS	3-33
APPENDIX for TASK 3	3-34
MILESTONE SCHEDULE AND STATUS REPORT	3-55

COAL COMBUSTION SCIENCE

QUARTERLY PROGRESS REPORT APRIL - JUNE 1991

EXECUTIVE SUMMARY

Task 1: Coal Devolatilization

The primary emphasis during this quarter was on the compilation of data from the Sandia coal devolatilization experiments into one comprehensive document. These data are being assembled into the document in tables in an appendix as a function of coal type, and are discussed in the text of the document by topic. The main body of the document is a discussion of apparatus, analysis techniques, and results. In addition to this work, the journal paper describing the CPD model was completed during this quarter; the paper was submitted for publication in *Energy and Fuels*. A draft copy of the paper was sent to PETC, and a Sandia report will be issued after comments from all reviewers are addressed.

In the course of this work, several new observations were made that contribute new insights into the mechanisms of coal devolatilization. These insights include an analysis of the relationship between the composition of the devolatilized char and the coalification band, an interpretation of the oxygen content of the fully devolatilized chars as a function of coal rank, and further elucidation of the chemical structure and molecular weight of chars.

Task 2: The Rates and Mechanisms of Coal Char Combustion

Activities during this quarter focused on the kinetic analysis and data compilation for the suite of PSOC coals. The technique developed in the previous quarter for determining n^{th} -order global kinetic parameters was applied this quarter to seven coals from the PSOC suite of ten. This technique yielded n^{th} -order global kinetic parameters that successfully describe that data from both the optical and tracer experiments.

For each of the seven coals, the complete set of combustion parameters were determined, comprising the global kinetic parameters n , E , and A (reaction order, activation energy, and preexponential factor), the burning mode parameter, α , (describing the particle diameter evolution), the char structural parameters ω and ρ_o (swelling factor and initial char density) and the product ratio parameters, A_c , E_c (which determine the CO/CO_2 product ratio). These sets of parameters were used to calculate combustion rates, q , and burnout times, τ_{50} , for the coal chars under a chosen set of standard conditions representative of the various environments encountered in pulverized coal fired boilers. The presentation of combustion rates or burnout times under chosen standard conditions allows a direct comparison of the reactivity of various coals, something that is not possible from values of A , E , and n alone.

Further, the characteristic burnout times reflect the influence of not only A , E , and n , but of *all* of the measured combustion parameters.

Task 3: The Fate of Mineral Matter

During this quarter, analyses of elemental release rates from a spherical oil agglomerate product (SOAP) were conducted in the CCL. Overall mass loss is determined as a function of residence time within approximately 10 relative percent. From these data, the release of inorganic and organic constituents of the SOAP are determined.

Of the eight major inorganic components of SOAP, only two were found to be released to the gas phase in appreciable amounts during combustion. These are sodium and potassium, both alkali metals. At the latest stage of combustion monitored during these tests (95 ms), approximately 35 and 50 percent of these elements, respectively, is released.

Elemental release rates of the organic constitutions were also determined. Hydrogen and oxygen are found to leave the SOAP in significantly larger fractions than the overall mass loss. Sulfur is released faster; nitrogen is released slightly faster; carbon is released slightly slower. These results are consistent with similar experimental results for pulverized coal under similar conditions.

Also during the quarter, analyses of char fragmentation for coals with a broad variation in rank, geographic origin, ash loading, and ash type were completed. Results indicate that the extent of fragmentation increases with increasing initial char diameter, decreases with increasing ash loading, increases with increasing rank, and is sensitive to mineral grain size distribution. These results are consistent with results reportedly earlier for a smaller suite of coals.

Future Work

On the coal devolatilization task, the primary emphasis during the next quarter is the completion of the first draft of the comprehensive document containing the data from the Sandia devolatilization experiments.

Also during the next quarter, on the char combustion task kinetic parameters will be determined for the remaining three coals in the PSOC suite and the data compilation will be completed. In addition, reactivity measurements will be performed on chars previously collected from the CCL under various devolatilization conditions. Results of the literature search and scoping experiments will be used to formulate a research plan on the topic of carbon reactivity at high conversions. The plan will identify research priorities on both the fundamental and applied aspects of this problem that will serve to define future work in this area. Finally, reactivity measurements will be performed on another proprietary coal-derived product and the results will be reported to PETC under separate cover.

In the mineral matter area, during the next quarter, the first version of ADLVIC will be completed. Preparations will be initiated for release of the code to PETC and other interested parties. A complete discussion of ADLVIC will be included in the next quarterly report. This discussion and documentation will include validation of the model predictions at many different combustion scales. Also, progress in developing ADLVIC II, a more detailed ash deposition model, will be reported.

PROJECT TITLE: COAL COMBUSTION SCIENCE

**TASK 1: DOCUMENTATION OF COAL
DEVOLATILIZATION RESEARCH
PERFORMED AT SANDIA FROM 1985
TO 1991**

ORGANIZATION: Sandia National Laboratories, Livermore

CONTRACT: FWP 0709

REPORTING PERIOD: April 1 - June 30, 1991

REPORTED BY: T. H. Fletcher and D. R. Hardesty

Phone: FTS 234-2584 and 234-2321

OBJECTIVE FOR TASK 1

The overall objectives of the coal devolatilization research at Sandia are to characterize coal devolatilization behavior as a function of time, temperature, heating rate, and coal type, and to relate the observed behavior to the chemical structure of the parent coal. Research emphasis in FY91 is placed on documentation and closure of both experimental and modeling activities pertaining to coal devolatilization research. This task is therefore divided into two subtasks:

SUBTASK 1.1 COMPILATION OF DATA FROM THE SANDIA COAL DEVOLATILIZATION EXPERIMENTS

Objective: To compile all of the experimental data obtained in the Coal Devolatilization Laboratory (CDL) at Sandia, along with the corresponding interpretation of data, into one comprehensive document. Data obtained in collaboration with other laboratories will be included in this report.

Deliverables: A comprehensive document containing all coal devolatilization data obtained with PETC funding at Sandia, along with data interpretation.

SUBTASK 1.2 DOCUMENTATION OF THE CHEMICAL PERCOLATION DEVOLATILIZATION MODEL

Objective: To complete the documentation of the chemical percolation devolatilization (CPD) model, including improvements to treat crosslinking and the effects of pressure. Relationships between model parameters and experimentally measured chemical structures in coal and coal chars will be examined. Emphasis will be placed on closure and documentation, including journal publications and technical presentations, as well

as a summary report. Sandia code licensing guidelines will be examined prior to distribution and the delivery of the code to PETC will be expedited.

Deliverables: An engineering model of coal devolatilization based on the chemical structure of the parent coal, including a summary report describing model formulation and validation.

SUMMARY OF TECHNICAL PROGRESS DURING THIS QUARTER

The primary emphasis during this quarter was on the compilation of data from the Sandia coal devolatilization experiments into one comprehensive document (Subtask 1.1). These data are being assembled into the document in tables in an appendix as a function of coal type, and are discussed in the text of the document by topic. The main body of the document is a discussion of apparatus, analysis techniques, and results.

Under Subtask 1.2, the internal review of the journal paper describing the CPD model was completed during this quarter; the paper was submitted for publication in *Energy and Fuels*. A draft copy of the paper was sent to PETC, and a Sandia report will be issued after comments from the journal review panel are addressed.

SUBTASK 1.1 COMPILATION OF DATA FROM THE SANDIA COAL DEVOLATILIZATION EXPERIMENTS

The focus of work during this quarter was preparation of the comprehensive document, and is proceeding according to schedule. The data from the char and tar samples from five different coals, collected in the Coal Devolatilization Laboratory (CDL) in two separate gas temperature conditions and in the Char Combustion Laboratory (CCL), have now been assembled into tables suitable for inclusion in the appendix. These data include elemental organic and inorganic analyses of char samples, NMR analyses of char and tar samples, apparent densities, mercury porosimetry and N₂ BET internal surface area data, and the extent of mass release, residence time, and temperature history determined for each sample. The sizing-pyrometry data for each experimental condition have also been assembled in tables for inclusion in an appendix. Copies of the Penn State analyses of the unpulverized coal will be included in that appendix for reference.

The main body of the document is currently organized into the following chapters:

1. Introduction
2. Apparatus
3. Sample Analysis Techniques
4. Summary of Experiments Performed
5. Results and Discussion of CDL experiments in 100% N₂
6. Results and Discussion of Additional Experiments
7. Conclusions

During this quarter, an outline of the document was sent to PETC for review and approval. Work on the main body of the document is proceeding according to schedule. Drafts of Chapters 1 through 4 have been completed, and a draft of Chapter 5, which contains the bulk of the discussion of results, is nearing completion. In the course of the document preparation, several new observations were made that contribute new insights into mechanisms of coal devolatilization. These insights are summarized below in this quarterly report.

Elemental Compositions of Chars During Devolatilization

Char Composition Relative to the Coalification Band

The elemental compositions of chars collected at different residence times during devolatilization have been examined, and elemental release rates of C, H, O, N, and S have been discussed in previous quarterly reports as a function of coal type. Pyrolysis reaction rates have recently been extrapolated to geologic time scales and correlated with increases in coal rank [Solomon, et al., 1991]. This implies that changes in elemental composition of coal chars may follow the coalification process [Van Krevelen, 1981]. During this quarter, the elemental compositions of coal chars during devolatilization are examined relative to the coalification band. The coalification band used in this analysis is expressed on a plot of the hydrogen to carbon ratio versus the oxygen to carbon ratio, as shown in Fig. 1.1. The elemental compositions of most raw coals lie in the band shown, with the low rank coals to the right of the bend at high oxygen to carbon ratios. Graphite lies at the lower left origin. The five coals used in the Sandia coal devolatilization experiments lie in the coalification band, with the highest rank coal (PSOC-1508D Pocahontas #3 lv bituminous) located in the narrow region below the bend at low oxygen to carbon ratios.

The data shown in Fig. 1.1 are from char samples collected as a function of residence time in the 1250 K gas condition in the CDL. The arrows represent the change in elemental composition of the chars as a function of residence time. It is clear that the progress of chars during devolatilization in these experiments does not follow the coalification band, with the exception of the low volatile bituminous coal (PSOC-1508D). The location of the final chars in these experiments all lie in a much closer region on this chart than the original coals, which is expected.

Oxygen Content of Fully-Devolatilized Chars

The fully-devolatilized chars from the low rank coals contain surprisingly large amounts of oxygen. The lignite char collected at the longest residence time in the 1250 K gas condition in the CDL contains 10% oxygen on a dry ash-free (daf) basis, while the subbituminous coal contains 7.4% (daf) oxygen. This is due to the large amount of oxygen in the parent coals (25% and 17% daf, respectively). In contrast, chars from the two high volatile bituminous coals (PSOC-1493D and PSOC-1451D) at the same location contain 5 to 6% daf oxygen, while the char from the low volatile coal (PSOC-1508D) contains

3.5% daf oxygen. The oxygen in these chars may be released during pyrolysis at higher temperatures, but most likely the oxygen is released during the initial stages of char combustion in practical coal flames. The oxygen in coal chars often serves as a crosslinking bridge between adjacent aromatic clusters (Ar-O-Ar), and is stable enough to survive at typical devolatilization temperatures. Oxygen contained in carboxyl groups (-COOH) leaves during the devolatilization process as CO₂, and is not found in significant quantities in fully-devolatilized coal chars.

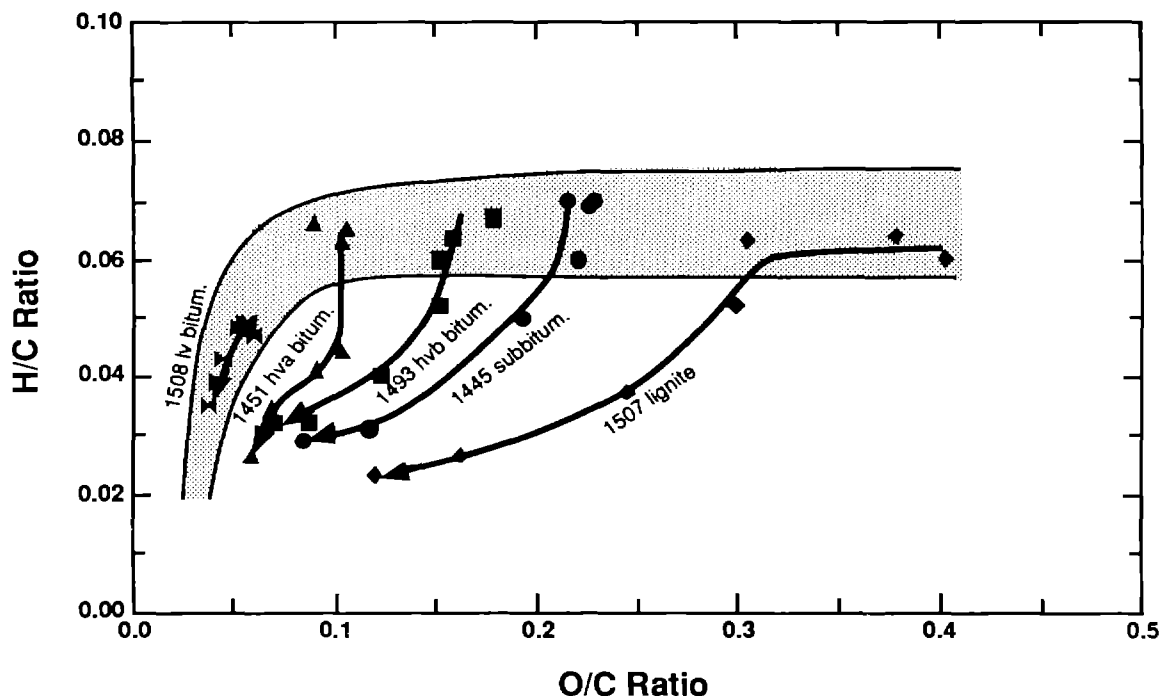


Figure 1.1 Coalification chart showing locations of initial coals and progress of chars during devolatilization, based on elemental composition.

Chemical Structure of Coal Chars During Devolatilization

New NMR Data for a Subbituminous Coal

Chars from four of the five coals were previously examined for chemical structure using ¹³C NMR spectroscopy. The NMR analyses are performed at the University of Utah in collaboration with Professor Ronald Pugmire and Dr. Mark Solum. Some of these results were previously published for two coals [Fletcher, et al., 1990; Pugmire, et al., 1991]. During this quarter, the results of the NMR analysis of char structure was completed for the final coal from the Sandia coal devolatilization laboratory: PSOC-1445D New Mexico Blue #1 subbituminous coal. These data are shown in Tables 1.1 and 1.2 for chars collected in the CDL in the 1250 K and 1050 K gas conditions, respectively.

Table 1.1
¹³C NMR Analyses of Chars from PSOC-1445D
New Mexico Blue #1 Subbituminous Coal
106-125 μm Size Fraction,
1250 K Gas Condition in the CDL (100% N₂)

Sampling Distance (mm)	0	70	250
Residence Time (ms)	0	77	238
Mass Release (% daf)	0.0	26.8	53.6
Aromatic carbon, $f_a = f_a' + f_a^C$	0.59	0.67	0.84
Carbonyl, f_a^C	0.06	0.08	0.05
Aromatic carbon, carbonyl subtracted, f_a'	0.53	0.56	0.79
Protonated aromatic carbon, f_a^H	0.19	0.22	0.36
Non-protonated aromatic C, $f_a^N = f_a^P + f_a^S + f_a^B$	0.34	0.34	0.43
Aromatic carbon with O attachment, f_a^P	0.07	0.07	0.05
Aromatic carbon with alkyl attachment, f_a^S	0.12	0.13	0.17
Aromatic bridgehead and inner carbon, f_a^B	0.15	0.14	0.21
Aliphatic carbon, f_{al}	0.41	0.33	0.16
Aliphatic CH and CH ₂ , f_{al}^H	0.30	0.25	0.12
Aliphatic CH ₃ and non-protonated carbon, f_{al}^*	0.11	0.08	0.04
Aliphatics with oxygen attachment, f_{al}^O	0.07	0.10	0.08
Proton spin-relaxation time, $T_{1\rho}^{Har}$ (ms)	4.7	2.1	7.3
Total carbons per cluster	26	21	16
Aromatic carbons per cluster, C	14	12	13
Aliphatic carbons per cluster	12	9	3
Total attachments per cluster, $\sigma + I$	5.0	4.3	3.6
Bridges and loops per cluster, B_C	2.1	2.6	3.0
Side chains per cluster	2.9	1.7	0.6
Fraction of intact bridges per cluster, p	0.42	0.60	0.82
Average cluster molecular weight	410	335	225
Side chain molecular weight, m_δ	47	43	18

Table 1.2
¹³C NMR Analyses of Chars from PSOC-1445D
New Mexico Blue #1 Subbituminous Coal
106-125 μm Size Fraction,
1050 K Gas Condition in the CDL (100% N₂)

Sampling Distance (mm)	0	50	80	120	180	250
Residence Time (ms)	0	59	88	123	180	253
Mass Release (% daf)	0.0	0.0	6.1	30.8	39.0	46.9
Aromatic carbon, $f_a = f_a' + f_a^C$	0.59	0.58	0.59	0.64	0.65	0.74
Carbonyl, f_a^C	0.06	0.05	0.05	0.06	0.06	0.10
Aromatic carbon, carbonyl subtracted, f_a'	0.53	0.53	0.54	0.58	0.59	0.64
Protonated aromatic carbon, f_a^H	0.19	0.16	0.17	0.20	0.20	0.23
Non-protonated aromatic C, $f_a^N = f_a^P + f_a^S + f_a^B$	0.34	0.37	0.37	0.38	0.39	0.41
Aromatic carbon with O attachment, f_a^P	0.07	0.07	0.06	0.06	0.08	0.07
Aromatic carbon with alkyl attachment, f_a^S	0.12	0.13	0.14	0.13	0.14	0.15
Aromatic bridgehead and inner carbon, f_a^B	0.15	0.17	0.17	0.19	0.17	0.19
Aliphatic carbon, f_{al}	0.41	0.42	0.41	0.36	0.35	0.26
Aliphatic CH and CH ₂ , f_{al}^H	0.30	0.30	0.30	0.26	0.25	0.20
Aliphatic CH ₃ and non-protonated carbon, f_{al}^*	0.11	0.12	0.11	0.10	0.10	0.06
Aliphatics with oxygen attachment, f_{al}^O	0.07	0.07	0.08	0.10	0.08	0.12
Proton spin-relaxation time, $T_{1\rho}^{Har}$ (ms)	4.7	4.7	3.5	3.1	3.2	2.5
Total carbons per cluster	26	30	28	28	24	22
Aromatic carbons per cluster, C	14	16	15	16	14	14
Aliphatic carbons per cluster	12	14	13	12	10	8
Total attachments per cluster, $\sigma + l$	5.0	6.0	5.6	5.3	5.2	4.8
Bridges and loops per cluster, B_C	2.0	2.0	2.5	2.5	2.9	3.5
Side chains per cluster	3.0	4.0	3.1	2.8	2.3	1.3
Fraction of intact bridges per cluster, p	0.42	0.40	0.45	0.47	0.55	0.73
Average cluster molecular weight	410	496	419	417	359	316
Side chain molecular weight, m_{δ}	47	49	42	41	36	30

The NMR data for the Blue #1 coal have been incorporated into the appendices in the comprehensive document, and are currently being analyzed prior to incorporation into the main body of the comprehensive document. These data are consistent with results discussed in the previous quarterly report regarding average cluster molecular weights in other coals. The initial cluster molecular weight for the subbituminous coal is 410 amu, which lies between the values of 440 amu observed for the Zap lignite and 270 amu observed for the Illinois #6 hvb bituminous coal. The cluster molecular weight of the fully-devolatilized char from the subbituminous coal (238 ms) in the 1250 K gas condition in the CDL is 225 amu, which is close to that observed for fully-devolatilized chars from other coals under these conditions (see Fig. 1.2).

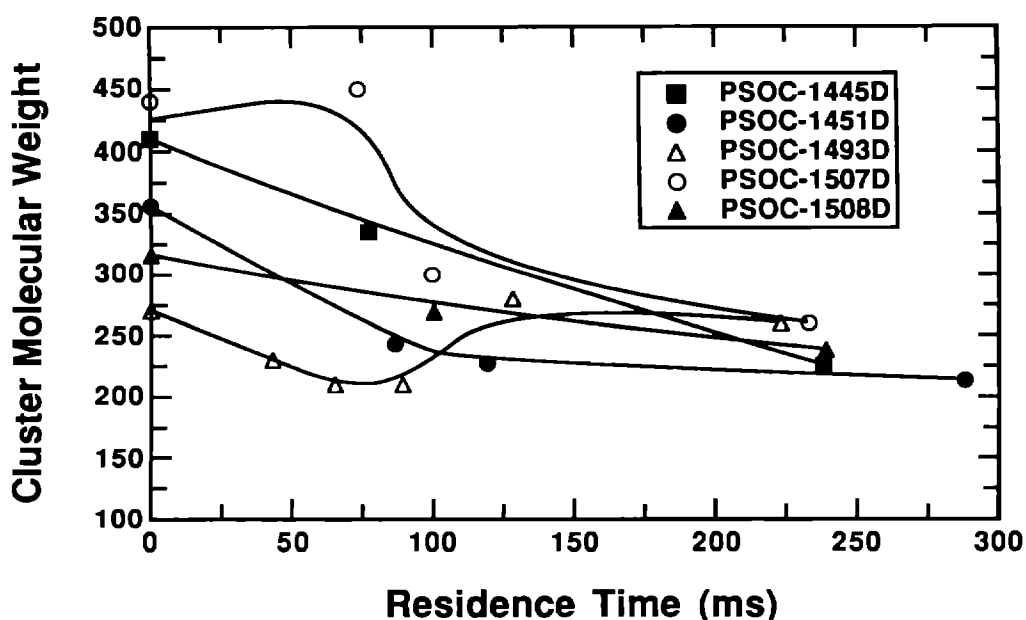


Figure 1.2 Average cluster molecular weights in coals and chars collected in the 1250 K gas condition in the CDL, determined from ^{13}C NMR analyses. Parent coals are represented at 0 ms residence time.

Molecular Weights of Attachments to Clusters

Another comparison of chemical structure as a function of coal rank is the average molecular weight of attachments to clusters in the parent coal. Attachments to clusters include labile bridges (ϵ), char bridges (c), and side chains (δ). As explained by Fletcher, et al. [1991], the molecular weight of attachments m_{att} can be calculated from the cluster molecular weight by subtracting the mass in the aromatic fused structure (the number of aromatic carbons per cluster C_{clust} multiplied by the molecular weight of carbon M_C) and dividing by the number of attachments per cluster ($\sigma+1$):

$$m_{att} = \frac{M_{clust} - C_{clust} M_C}{\sigma + 1} \quad (1.1)$$

The definition of the molecular weight per cluster (M_{clust}) used here includes the mass in the aromatic part of the cluster plus the surrounding aliphatic material. The cluster molecular weight therefore includes the mass of side chains and one-half the molecular weights of labile bridges and char bridges attached to the cluster, as follows:

$$m_{att} = \frac{\mathcal{L} \frac{m_b}{2} + c \frac{m_{char}}{2} + \delta m_\delta}{\mathcal{L} + c + \delta} \quad (1.2)$$

where \mathcal{L} , c , and δ represent the populations of labile bridges, char bridges, and side chains, respectively. The factor of 2 in the m_b and m_c terms reflects the fact the only one-half of an intact bridge is attributed to a cluster. Unreacted coals contain very few char bridges (i.e., $c = 0$), and hence Eq. 1.2 reduces to the relation $m_{att} = m_\delta$ assuming that $m_\delta = m_b/2$. For fully-devolatilized chars, $\mathcal{L} = 0$, and Eq. 1.2 becomes:

$$m_{att} = \frac{c \frac{m_{char}}{2} + \delta m_\delta}{c + \delta} \quad (1.3)$$

Side chain molecular weights have been thus determined for all five parent coals examined in the Sandia devolatilization experiments ($m_\delta = m_{att}$ for unreacted coals), as shown in Fig. 1.3. Side chain molecular weights for other parent coals are also shown, as reported by Solum, et al. [1989] for the Argonne premium coals [Vorres, 1989] and for three coals examined at Advanced Fuel Research (AFR) [Serio, et al., 1987]. The continuous lines in this figure represent linear correlations of the data. The oxygen content of the parent coal is an indicator of coal rank; the oxygen content of the parent coal decreases as coal rank increases. The side chain molecular weights of the parent coals exhibit a definite trend as a function of coal rank; values of m_δ range from 52 amu in the lignite and subbituminous coal (25% daf oxygen) to 13 amu for the highest rank coal (Pocahontas #3 lv bituminous, Argonne sample).

The average molecular weights of attachments to clusters in fully-devolatilized coal chars are also shown in Fig. 1.3. The fully-devolatilized chars are from the longest residence time (~ 250 ms) in the 1250 K gas condition experiments conducted in the Sandia CDL in 100% N_2 . The molecular weights of side chains for the fully-devolatilized chars vary from 18 to 11 amu, which is not a significant dependence on coal rank. This coincides with the data on average cluster molecular weights for these chars (Fig. 1.2), which do not exhibit a significant rank dependence, either. The fully-devolatilized chars do not contain any labile bridges, and hence the attachments to the cluster consist solely of char bridges and side chains. The side chains present in the "fully-devolatilized" chars are stable enough to remain with the char at typical devolatilization temperatures (800 to 1100 K). The average value of m_{att} in the fully-devolatilized chars is low enough (11 to 18 amu) to

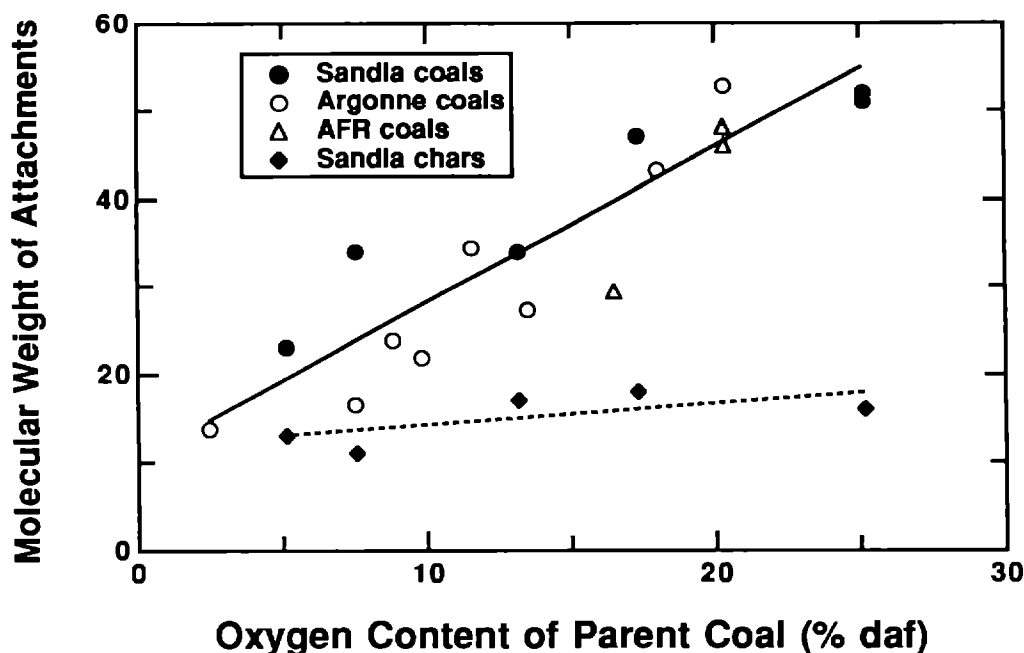


Figure 1.3 Average molecular weight of attachments to aromatic clusters in unreacted and fully-devolatilized coals as a function of coal type. Data for non-Sandia coals are taken from Solum, et al. [1989]. Fully-devolatilized chars are from the longest residence time (~ 250 ms) in the 1250 K gas condition in the CDL.

compare with side chains consisting of one atom (12 amu for carbon, 16 amu for oxygen). Low molecular weight side chains may consist mainly of methyl groups (15 amu) and OH groups (17 amu), which are more stable than longer side chains such as COOH or ethyl groups (C₂H₅).

Molecular weights of char bridges in fully-devolatilized chars are thought to be smaller than molecular weights of labile bridges and side chains in the parent coal. These char bridges fall into three categories: (a) biphenyl bridges, where a bridge is formed between neighboring carbons on different aromatic clusters (Ar-Ar); (b) ether-type bridges where a single oxygen atom forms a bridge between neighboring clusters (Ar-O-Ar); and (c) a carbon bridge, thought to mainly consist of single carbon atoms between clusters (Ar-C-Ar). These three types of char bridges are illustrated in Fig. 1.4. Two bridges may link the same two aromatic clusters, and are hence only the sum of bridges and loops is determined. The molecular weights of these three types of char bridges are low enough to be consistent with the NMR determinations of m_{att} shown in Fig. 1.3 for coal chars: 0 amu for biphenyl bridges; 16 amu for oxygen bridges, and 12 amu for carbon bridges.

The measured changes in the average molecular weight of attachments to clusters as a function of coal rank and during devolatilization, as well as the measured cluster molecular

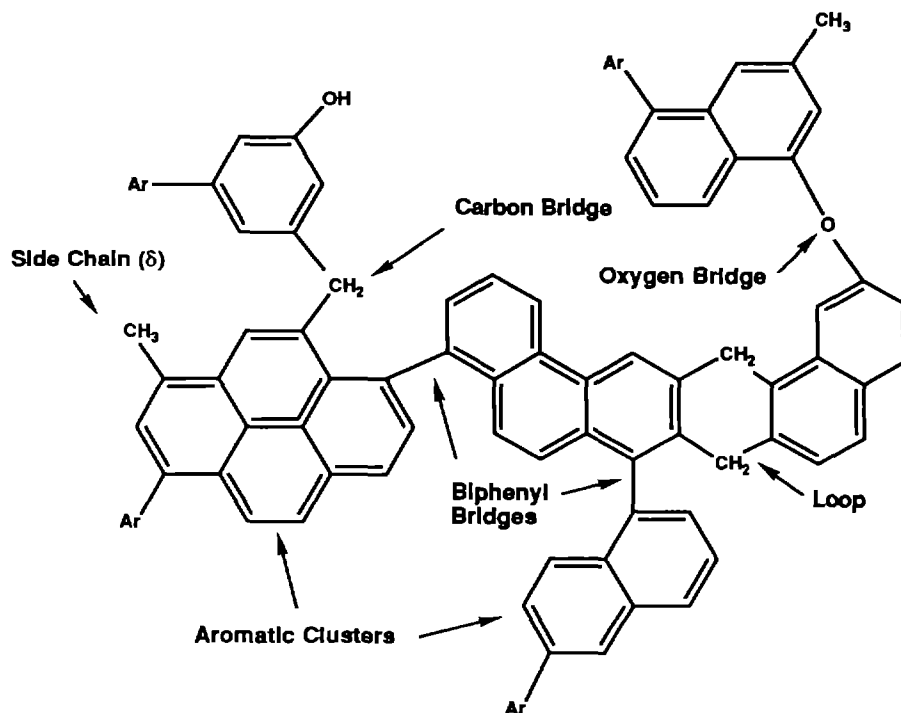


Figure 1.4 Characteristic chemical structures found in fully-devolatilized coal chars, illustrating the postulated forms of char bridges.

weights, present a critical test for devolatilization models based on chemical mechanisms. Network-based devolatilization models, like the CPD model [Grant, et al., 1989], calculate the populations of labile bridges, char bridges, and side chains (gas precursors), and hence permit calculation of m_{all} from Eq. 1.2 as a function of coal type and the extent of devolatilization. Since m_{δ} and m_c are not measured independently, the data do not indicate whether the decrease in m_{all} during to devolatilization is due to a change in m_{δ} or an increase in the population of char bridges (c). Changes in m_{δ} as a function of the extent of reaction could be modeled by assuming that a certain fraction of the side chain material consists of $-CH_3$ and $-OH$ groups that are so tightly bound to the aromatic rings that they can be considered to be inert. The average value of m_{δ} would then change as a function of time, since it would be a combination of reactive and inert side chains.

The comparison of predicted and measured values of m_{all} as a function of residence time and coal type is only one example of how the NMR analyses of char particles provides new insights into the coal devolatilization process. These NMR data are also valuable in (a) selecting input coefficients for such models that better coincide with chemical structures that exist in coal and char, and (b) providing quantitative data for evaluation of proposed mechanisms and rate coefficients in such models, and (c) determining the chemical structures of the residual chars for better understanding of fundamental char reaction rates and mechanisms.

SUBTASK 1.2 DOCUMENTATION OF THE CHEMICAL PERCOLATION DEVOLATILIZATION MODEL

A journal article describing the most recent improvements to the CPD model was finished during this quarter. This paper is titled, "A Chemical Percolation Model for Devolatilization: 3. Chemical Structure as a Function of Coal Type," authored by Thomas H. Fletcher, Alan R. Kerstein, Ronald J. Pugmire, and David M. Grant. This paper has now cleared internal Sandia review, and has been submitted for publication to *Energy and Fuels*. A draft copy of this paper was forwarded to PETC at the time of submission to the journal, and a Sandia report will be issued after comments from the journal reviewers are addressed.

PLANS FOR NEXT QUARTER

The primary emphasis for next quarter is the completion of the first draft of the comprehensive document containing the data from the Sandia Devolatilization experiments. This draft will be sent to PETC for review, and will be completed during the next quarter. A paper will be prepared during the next quarter for presentation at the Seventh Annual Coal Preparation, Utilization, and Environmental Control Contractors Conference to be held in Pittsburgh, Pennsylvania, July 15-18, 1991.

ACKNOWLEDGMENTS

Special thanks to Alan R. Kerstein at Sandia for many useful discussions regarding the NMR data. Special thanks also to Professor Ronald J. Pugmire and Dr. Mark S. Solum at the University of Utah for their continued collaboration. The work at the University of Utah is supported through the Advanced Combustion Engineering Research Center at Brigham Young University and the University of Utah, which is supported by the National Science Foundation (NSF), 23 industrial firms, and DOE/PETC. Additional support at the Univ. of Utah is provided through the Consortium for Fossil Fuel Liquefaction Science by DOE/PETC.

NOMENCLATURE FOR TASK 1

Ar	aromatic cluster
c	char bridge
C_{clust}	number of carbons per aromatic cluster
δ	side chain to aromatic cluster
m_{att}	molecular weight of an attachment to an aromatic cluster
m_b	molecular weight of a labile bridge
m_c	molecular weight of a char bridge
m_δ	average molecular weight of a side chain to an aromatic cluster
M_C	molecular weight of carbon
M_{clust}	average molecular weight of an aromatic cluster, including attachments
$\sigma+1$	coordination number (number of attachments per cluster)

REFERENCES FOR TASK 1 SECTION

- Fletcher, T. H., M. S. Solum, D. M. Grant, S. Critchfield, and R. J. Pugmire, *Twenty-Third Symp. (Int.) on Com.* (in press, 1990).
- Fletcher, T. H., A. R. Kerstein, R. J. Pugmire, and D. M. Grant, "A Chemical Percolation Model for Devolatilization: 3. Chemical Structure as a Function of Coal Type," submitted for publication to *Energy and Fuels* (1991). See also Fletcher, T. H. and D. R. Hardesty, "Coal Combustion Science: Task 1, Coal Devolatilization," DOE/PETC Quarterly Progress Report for October to December, 1990, edited by D. R. Hardesty, Sandia Report No. SAND91-8210, available NTIS (1991).
- Pugmire, R. J., M. S. Solum, D. M. Grant, S. Critchfield, and T. H. Fletcher, *Fuel*, **70**, 414 (1991).
- Serio, M. A., D. G. Hamblen, J. R. Markham, and P. R. Solomon, *Energy & Fuels*, **1**, 38 (1987).
- Solum, M. S., R. J. Pugmire, and D. M. Grant, *Energy & Fuels*, **3**, 187 (1989).
- Solomon, P. R., D. G. Hamblen, M. A. Serio, Z. Yu, and S. Charpenay, "Can Coal Science Be Predictive," *ACS Div. of Fuel Chem. prepr.*, **36**:1, 267 (1991).
- Van Krevelen, D. W., *Coal Science and Technology 3. Coal*, Elsevier, New York, p. 113 (1981).
- Vorres, K. S., "Users' Handbook for the Argonne Premium Coal Sample Bank," Argonne National Laboratory, supported by DOE contract W-31-109-ENG-38 (September, 1989). Also Vorres, K. S., *ACS Div. Fuel Chem. prepr.*, **32**:4, 221 (1987).

PUBLICATIONS, PAPERS, AND PRESENTATIONS

During April, an invited paper was presented in the Storch award ceremony at the National ACS Meeting in Atlanta. The paper discusses mass transfer issues during coal pyrolysis, with a focus on methods for estimating vapor pressures of tar and metaplast. This paper was entitled, "Predicting Vapor Pressures of Tar and Metaplast During Coal Pyrolysis," authored by T. H. Fletcher, D. M. Grant, and R. J. Pugmire.

A paper entitled, "Structural Evolution of Matched Tar-Char Pairs in Rapid Pyrolysis Experiments," authored by R. J. Pugmire, M. S. Solum, D. M. Grant, S. Critchfield, and T. H. Fletcher, appeared in *Fuel* (Vol. 70, p. 414, 1991).

A paper entitled, "A Chemical Percolation Model for Devolatilization: 3. Chemical Structure as a Function of Coal Type," authored by T. H. Fletcher, A. R. Kerstein, R. J. Pugmire, and D. M. Grant, was submitted for publication to *Energy and Fuels*.

PROJECT TITLE: COAL COMBUSTION SCIENCE

TASK 2: RATES AND MECHANISMS OF COAL CHAR COMBUSTION

ORGANIZATION: Sandia National Laboratories, Livermore

CONTRACT: FWP 0709

REPORTING PERIOD: April 1 - June 30, 1991

REPORTED BY: R. H. Hurt and D. R. Hardesty

Phone: FTS 234-3707 and 234-2321

OBJECTIVE FOR TASK 2

The objective of Task 2 is to characterize the combustion behavior of selected U.S. coals under conditions relevant to industrial pulverized coal-fired furnaces. An optical particle-sizing pyrometer is used to measure, *in situ*, the temperature, size, and velocity of individual burning coal char particles, from which kinetic parameters describing the combustion of a given coal are derived. Partially reacted char particles are also sampled and characterized to understand the physical and chemical transformations that accompany coal combustion. The ultimate goal of the task is the establishment of a data base of the high temperature reactivities of chars from strategic U.S. coals, from which important trends may be identified and predictive capabilities developed.

Research is divided into three subtasks, in accordance with the FY91 project plan:

SUBTASK 2.1 KINETIC ANALYSIS AND DATA COMPILATION FOR THE PSOC COAL SUITE

Over the course of the PETC/Sandia Coal Combustion Science Program, extensive data have been obtained in the Char Combustion Laboratory (CCL) on the combustion rates of chars from a suite of ten PSOC parent coals. An additional large body of data has been obtained documenting the time-resolved rates of release of organic and inorganic coal constituents during combustion. These data form a unique body of information on the combustion behavior of chars from across the spectrum of commercially strategic U.S. coals.

It is at this point highly desirable to compile this information into archival data packages, so that the data and analyses may be a readily available resource for use by coal scientists and by U.S. industry. The completed compilation will become the basis

for the identification of trends and the development of correlations and predictive capabilities relevant to industrial combustion systems.

The archival data packages will contain the measurements of the temperature, size, and velocity of individual burning coal particles as well as rates of release of organic and inorganic coal constituents for each of the ten coals in the PSOC suite. The compilation will also contain n^{th} -order global kinetic parameters describing the combustion rate of each of the coals. The global rate parameters will be used to make a meaningful comparison of coal char reactivities over a broad range of temperature and pressure and to establish correlations between coal char reactivity and properties of the parent coal.

SUBTASK 2.2 THE EFFECT OF DEVOLATILIZATION CONDITIONS ON CHAR REACTIVITY

In pulverized coal combustion the process of devolatilization determines, to a large extent, the properties and thus the reactivity of the resulting char. The heating rate, final temperature, and gas environment can affect devolatilization yields and the chemical composition and physical structure of the char. Swelling coals, in particular, produce a variety of char particle morphologies ranging from dense consolidated particles to thin or thick walled cenospheres, depending in part on devolatilization conditions.

It is important to understand the influence of devolatilization conditions on char reactivity in order to relate reactivities measured in the CCL to those in other combustion systems with different heating rates and gas environments. Immediate emphasis is placed on characterizing potential differences in the chars produced in 6 and 12 mole% O₂ environments, as these differences impact kinetic studies of char oxidation performed in the CCL.

SUBTASK 2.3 CHAR REACTIVITY AT HIGH CARBON CONVERSION

There are many factors that potentially contribute to the unburned carbon content of flyash from industrial boilers, including:

- the presence of low-reactivity components in the coal
- the presence of large particles in the size distribution from the pulverizer
- encapsulation of carbon by fused ash
- particle trajectories through regions in the furnace having low oxygen concentration or temperature.

Few studies have addressed this industrially important and technically challenging problem due in part to the difficulties associated with generating and isolating significant quantities of the residual carbon in highly reacted samples.

The goal of Subtask 2.3 is to measure the reactivity of the residual carbon in highly reacted samples and to understand its implications for the problem of unburned carbon in flyash. To accomplish this goal, it is planned first to determine the mode of occurrence of carbon in flyash, and secondly, to isolate the carbon from highly reacted samples generated in the CCL or the Sandia Multifuel Combustor (MFC) and to measure its combustion reactivity. The reactivity of the residual carbon will be compared to the large body of existing data from the CCL at low to intermediate conversions. This study will generate insight into the origin of residual carbon in flyash and will suggest strategies for prediction and for remediation of the problem.

SUMMARY OF TECHNICAL PROGRESS DURING THIS QUARTER

In accordance with the FY91 work statement, activities during this quarter focused entirely on Subtask 2.1. The technique developed in the previous quarter for determining n^{th} -order global kinetic parameters was applied this quarter to seven coals from the PSOC suite of ten. This technique yielded n^{th} -order global kinetic parameters that successfully describe that data from both the optical and tracer experiments.

For each of the seven coals, the complete set of combustion parameters were determined, comprising the global kinetic parameters n , E , and A (reaction order, activation energy, and preexponential factor), the burning mode parameter, α , (describing the particle diameter evolution), the char structural parameters ω and ρ_o (swelling factor and initial char density) and the product ratio parameters, A_c , E_c (which determine the CO/CO_2 product ratio). These sets of parameters were used to calculate combustion rates, q , and burnout times, τ_{50} , for the coal chars under a chosen set of standard conditions representative of the various environments encountered in pulverized coal fired boilers. The presentation of combustion rates or burnout times under chosen standard conditions allows a direct comparison of the reactivity of various coals, something that is not possible from values of A , E , and n alone. Further, the characteristic burnout times reflect the influence of not only A , E , and n , but of *all* of the measured combustion parameters.

SUBTASK 2.1 KINETIC ANALYSES AND DATA COMPILATION FOR THE PSOC COAL SUITE

Introduction

In the previous quarterly report, an analysis was performed that identified the origin of the distinct linear groupings of single-particle rate constants observed on Arrhenius plots of data from the CCL. Based on the results of this analysis, a new technique was developed for the extraction of meaningful n^{th} -order global kinetic parameters and was successfully demonstrated on the data for PSOC-1508D, Pocahontas #3 low-volatile bituminous coal. The goal was to develop and demonstrate a standardized analysis technique for application to each of the PSOC coals. The existence of a standardized procedure is vital to the internal consistency of the data and analysis compilation and will allow meaningful comparisons of the combustion properties of different coals.

During this quarter, that technique was applied uniformly to data on the following seven coals in the PSOC suite (in rank order):

PSOC-1516D	Lower Kittaning	Pennsylvania, lvb
PSOC-1508D	Pocahontas #3	West Virginia, lvb
PSOC-1451D	Pittsburgh #8	Pennsylvania hvb
PSOC-1493D	Illinois #6	Illinois, hvb
PSOC-1502D	Hiawatha	Utah, hvb
PSOC-1488D	Dietz	Montana subbituminous
PSOC-1443D	Lower Wilcox	Texas lignite

For each of the seven coals, the complete set of combustion parameters were determined, comprising the global kinetic parameters n , E , and A (reaction order, activation energy, and preexponential factor), the burning mode parameter, α , (describing the diameter evolution), the char structural parameters ω , ρ_0 (swelling factor and initial char density) and the product ratio parameters, A_c , E_c (determining the CO/CO_2 product ratio). These sets of parameters were used to calculate combustion rates, q , and burnout times, τ_{50} , for the coal chars under a chosen set of standard conditions representative of the various environments encountered in pulverized coal-fired boilers.

Explanation of Combustion Parameters

In the following sections, the analysis techniques and the significance of each of the individual combustion parameters is discussed, and results for PSOC-1451, Pittsburgh #8 coal are presented as examples.

Global Kinetic Parameters A , E , and n .

The rate of char oxidation, q , (g C/s-m²-external surface) is described here by a kinetic law of the form:

$$q = k_s P_s^n \quad (2.1)$$

where

$$k_s = A e^{(-E/RT_p)} \quad (2.2)$$

A given coal has a unique set of values for A , E , and n , and this set is sufficient to determine the instantaneous combustion rate of a particle with known physical properties in thermal equilibrium with a specified environment.[†] The technique used for extracting A , E , and n for a given coal is described in detail in the previous quarterly report (Hurt and Hardesty, 1991). As discussed in the previous report, this approach attempts to describe the combustion behaviour of "typical" particles within a population of particles having differing reactivities and physical properties. This simple approach has the advantage of yielding a single rate law (single set of values for A , E , and n) for convenient incorporation in comprehensive combustion models. This approach should be capable of adequately describing the overall combustion behavior of any given coal at low-to-intermediate carbon conversions (< 90%). It will be seen in a later section, that this approach does successfully describe char combustion behavior in the CCL experiments, based on results from the seven coals analyzed to date.

The reaction order, n , is obtained by minimization of the sum of square residuals in a least-squares regression of $\ln k_s$ vs. T_p . In cases where the data are clearly insufficient to determine a statistically significant value of n , a value of 0.5 is adopted.^{††} Global kinetic parameters for PSOC-1451, Pittsburgh #8 coal char are presented, as an example, in Arrhenius form in Fig. 2.1.

Mode of Burning Parameter, α

The empirical mode of burning parameter, α , describes the evolution of the particle diameter and density during combustion, according to:

$$(\rho/\rho_o)_{daf} = (m/m_o)_{daf}^\alpha \quad (2.3)$$

where ρ_{daf} is defined to be the mass of carbonaceous, or combustible material in the particle, m_c , divided by the particle volume. The accompanying expression for

[†] Assuming CO to be the sole combustion product.

^{††} Based on the theory of reaction and diffusion in porous solids, and on extensive data at lower temperatures, the reaction order is expected to lie between 0.5 and 1 for carbon oxidation in zone II.

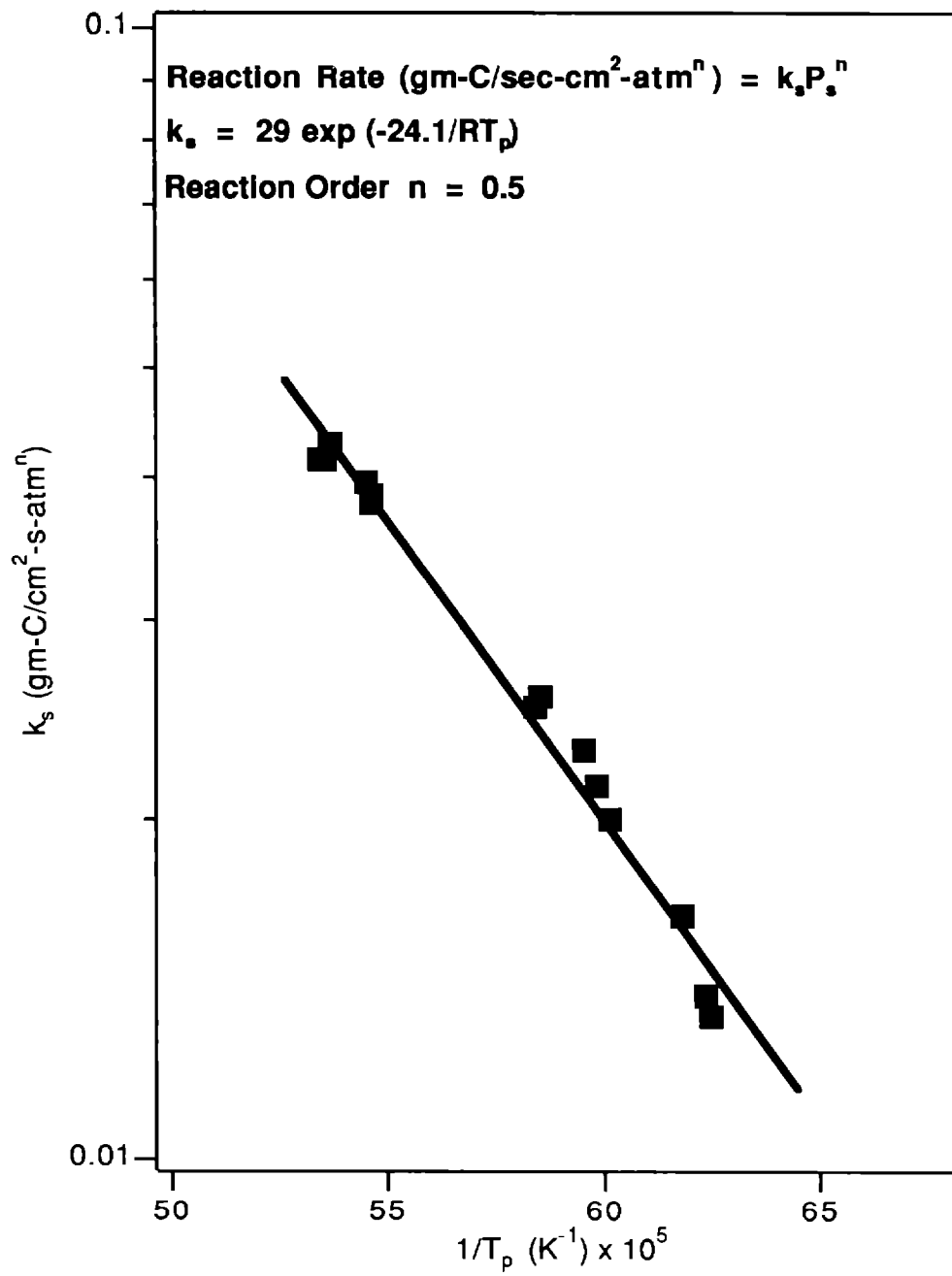


Figure 2.1 Arrhenius diagram and global kinetic parameters for PSOC-1451D, Pittsburgh #8 coal

diameter, related to Eq. 2.3 by a particle mass balance, is:

$$d/d_o = (m/m_o)_{daf}^{(1-\alpha)/3} \quad (2.4)$$

where $(1 - \alpha)/3$ is often referred to as the empirical parameter β (Mitchell, 1988). The densities and particle masses in Eqs. 2.3 and 2.4 refer to the values on an ash-free basis, which can be translated into particle densities and masses knowing the ash content of the initial char.

The subscript "o" refers here to the unreacted char, sampled at the point immediately following devolatilization and at the onset of oxidation. The parameter α thus describes the particle diameter evolution only during the char oxidation process. In the CCL experiments, the properties of the chars sampled from the 6.35 cm measurement height are used to approximate m_o , d_o , and ρ_o . This approach is based on the visual observation that this reactor position approximately marks the end of devolatilization and onset of char oxidation for most coals.

The value of α affects the overall burning rate primarily by determining the particle size and thus the available external surface area) at higher conversions. A value of 1 for α corresponds to constant diameter burning, while a value of 0 corresponds to constant density burning or shrinking core behavior. The value of α determined is a qualitative indication of the extent of internal reaction, related to the extent of O_2 penetration into the particle; as α approaches unity O_2 penetration depth and the extent of internal reaction increase. The value of α is not, however, a quantitative estimate of the amount of internal reaction, as other phenomena, such as fragmentation and carbon densification (Hurt et al., 1988) also influence the evolution of diameter and density.

The measured particle density evolution for PSOC-1451D, Pittsburgh #8 coal char is presented in Fig. 2.2 as an example, together with the predictions of the empirical relation Eq. 2.3 for the optimum value of α , 0.1.

Char Structural Parameters

Although particle size and density often have a relatively weak influence on the *instantaneous* oxidation rate, they are very important in determining the time required for complete char combustion. As α determines the evolution of size and density with combustion, we need only two additional combustion parameters that specify the *initial* char size and density, immediately following devolatilization. For coal particles of a given initial size, the average initial *char* particle diameter and density are determined by the extent of volatile release and the extent of swelling. Both of these parameters are highly rank dependent.

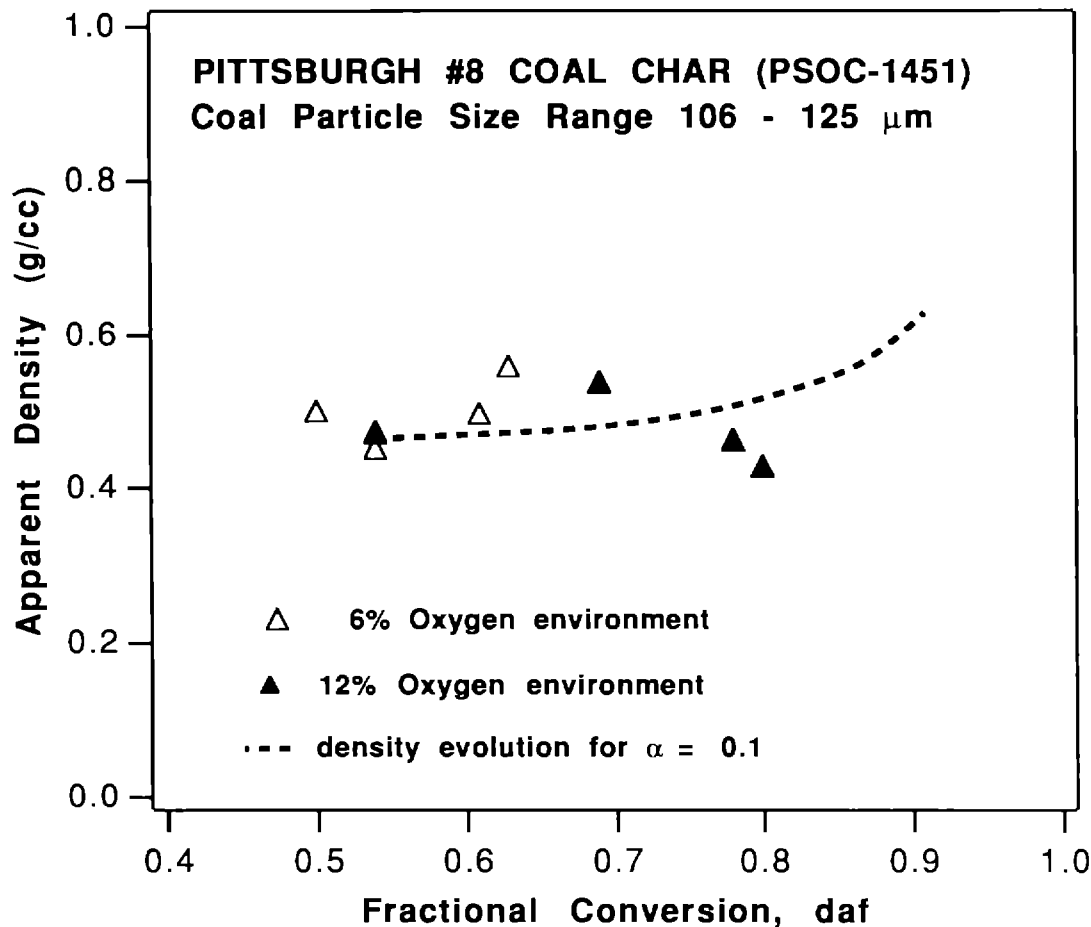


Figure 2.2 Measured (points) and predicted (curve) density evolution for PSOC-1451D, Pittsburgh #8 coal

To make predictions for coal particles of a given initial size, d_c , the two combustion parameters required are the initial char particle density, ρ_o , and the swelling factor, ω :

$$\omega \equiv d_o/d_c \quad (5)$$

where ρ_o and d_o are again taken to be the values at the 6.35 cm measurement height in the CCL reactor. Values of ω greater than unity correspond to swelling.

The initial char density, ρ_o , is directly measured by a technique involving the measurement of particle bed density, as described in earlier quarterly reports. The swelling factor can be calculated by one of two methods. In the first method, the ratio is taken of the mean particle size determined by the coded aperture technique applied at the 6.35 cm measurement height and the average of the initial particle size range determined by sieving. This technique is inaccurate, as it forms the ratio of sizes

determined by unrelated techniques operating on different principles. The second method utilizes the measured densities and conversions at the 6.35 cm measurement height according to:

$$\omega \equiv \frac{d_o}{d_c} = \left(\frac{m_o/m_c}{\rho_o/\rho_c} \right)^{1/3} \quad (2.6)$$

where all properties in Eq. 2.6 are on an ash-containing basis. This technique was applied uniformly to yield swelling factors under the rapid heating conditions present in the CCL. Note that the use of ω to obtain a char size distribution from an initial coal size distribution neglects any particle fragmentation occurring during devolatilization. The char structural parameters for PSOC-1451, Pittsburgh #8 coal char appear in Table 2.1 as examples.

Product Ratio Parameters

There is evidence that both CO and CO₂ are primary products of coal char combustion (Mitchell, 1988). Particularly at low combustion temperatures, some CO₂ may form at or near the particle surface, affecting both the mass and energy transport to and from the particle. Carbon dioxide formation tends to slow the reaction by requiring an additional half mole of oxygen to diffuse through the particle boundary layer to gasify a single mole of carbon. At the same time CO₂ production liberates more heat, raises the particle temperature, and thus increases the rate of the activated heterogeneous reactions. Depending on the properties of the particle and the gas phase, CO₂ formation may either increase or decrease the rate of combustion.

It has been observed (Mitchell, 1988) that some CO₂ formation must be assumed in order to reconcile the measured particle temperatures with the overall burning rates determined by the tracer techniques. For the set of PSOC coals, therefore, the following empirical expression is used to correlate the temperature dependence of the product ratio:

$$CO/CO_2 = A_c e^{(-E_c/RT_p)} \quad (2.7)$$

Both A_c and E_c were adjusted for each coal to provide an adequate fit to both the measured particle temperatures and the overall mass conversions determined by tracer techniques. The product ratio parameters for PSOC-1451, Pittsburgh #8 coal char in Table 2.1 as examples and the fit to the measured mass conversions appears in Fig. 2.3.

Table 2.1
Summary of Combustion Parameters for PSOC-1451, Pittsburgh #8 Coal

<p>Char oxidation rate parameters</p> $q = A \exp(-E/RT_p) P^n$	<p>A</p> <p>E</p> <p>n</p>	<p>29 gm-C / cm²-s-atmⁿ</p> <p>24 kcal / mole</p> <p>0.5 *</p>
<p>Product ratio parameters</p> $CO/CO_2 = A_c \exp(-E_c/RT_p)$	<p>A_c</p> <p>E_c</p>	<p>4.0 x 10⁴ *</p> <p>30 * kcal / mole</p>
<p>Burning mode parameter</p> $\rho/\rho_o = (m/m_o)^\alpha$ $d/d_o = (m/m_o)^{(1-\alpha)/3}$	<p>α</p>	<p>0.1</p>
<p>Char structural parameters</p> $\omega = d_o / d_c$ <p>(linear swelling factor)</p> <p>$\rho_o \equiv \rho$ at $z = 6.5$ cm</p> <p>(initial char particle density, daf)</p>	<p>ω</p> <p>ρ_{o,daf}</p>	<p>1.10</p> <p>0.385 gm / cm³</p>
<p>As an example, this parameter set yields a combustion rate, q, of 0.0032 gm/sq.cm-sec for a 100 μm particle in a gas with $T_g = 1600$ K containing 6 mole-% oxygen</p> <p>These product ratio parameters yield 6 mole-% carbon dioxide at 1900 K and 15 mole-% carbon dioxide at 1700 K</p> <p>* These particular parameters should be regarded as empirical parameters useful for the prediction of burning rates. They do not necessarily have fundamental significance or uniqueness for this data set.</p>		

Characteristic Times for 50% Carbon Conversion

Char reactivities are reported both as combustion rates, q , and burnout times, τ_{50} , under a chosen set of standard conditions representative of the various environments encountered in pulverized coal-fired boilers. A characteristic time for 50% carbon conversion, τ_{50} , can be defined as:

$$\tau_{50} \equiv \frac{\frac{1}{2} m_{p,daf}}{q_{25} A_{25}} \quad (2.8)$$

where $m_{p,daf}$ is the mass of carbonaceous (combustible) material in the unreacted char particle, q_{25} is the oxidation rate per unit external surface area, and A_{25} is the external surface area, both evaluated at 25% carbon conversion. Because the particle diameter changes between 0 and 50% carbon conversion, q and A are evaluated at the midpoint.

An expression for τ_{50} must be derived in terms of the set of combustion parameters presented for each of the PSOC coals. The quantity $m_{p,daf}$ is given by $[\rho_{o,daf} \pi d^3 / 6]$, and A_{25} is equal to πd_{25}^2 where d_{25} is the particle diameter at 25% carbon conversion, given by $d_o [(0.75)^{(1-\alpha)} / 3]$.

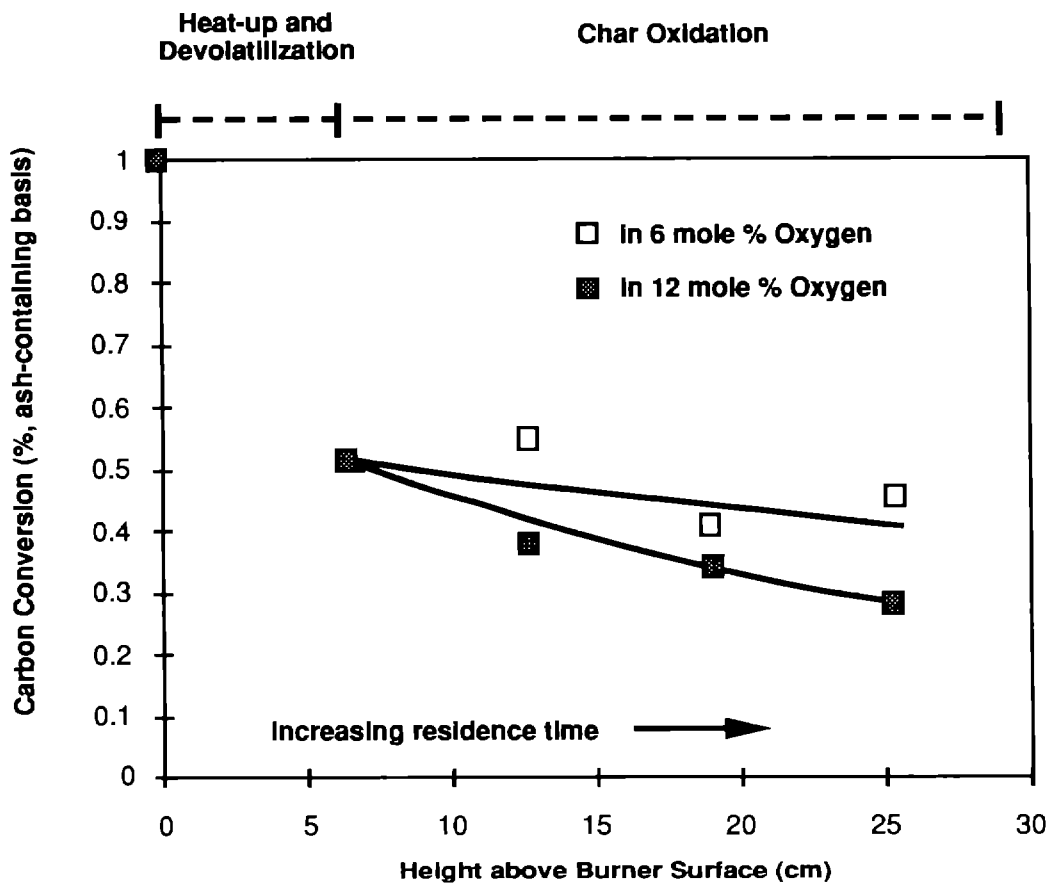


Figure 2.3 Conversion profiles from combustion experiments in the CCL for PSOC-1451, Pittsburgh #8 coal. Points are determined by inorganic tracer analysis on extracted samples. Curves are predictions using the rate constants derived from optical measurements.

Finally, relating d_o to the initial coal particle density by $d_o/d_c = \omega$, and substituting in Eq. 2.8, the following expression for τ_{50} is obtained :

$$\tau_{50} \equiv \frac{\omega d_c \rho_{o,daf}}{12 q_{25} 0.75^{2(1-\alpha)/3}} \quad (2.9)$$

The characteristic burnout time, τ_{50} , is thus seen to be a function of the instantaneous combustion rate, q , (a function of A , E , n , A_c , and E_c), the swelling factor, ω , the mode of burning parameter, α , and the initial char density, $\rho_{o,daf}$. Examples of burnout time predictions are presented in Figs. 2.4 - 2.6.

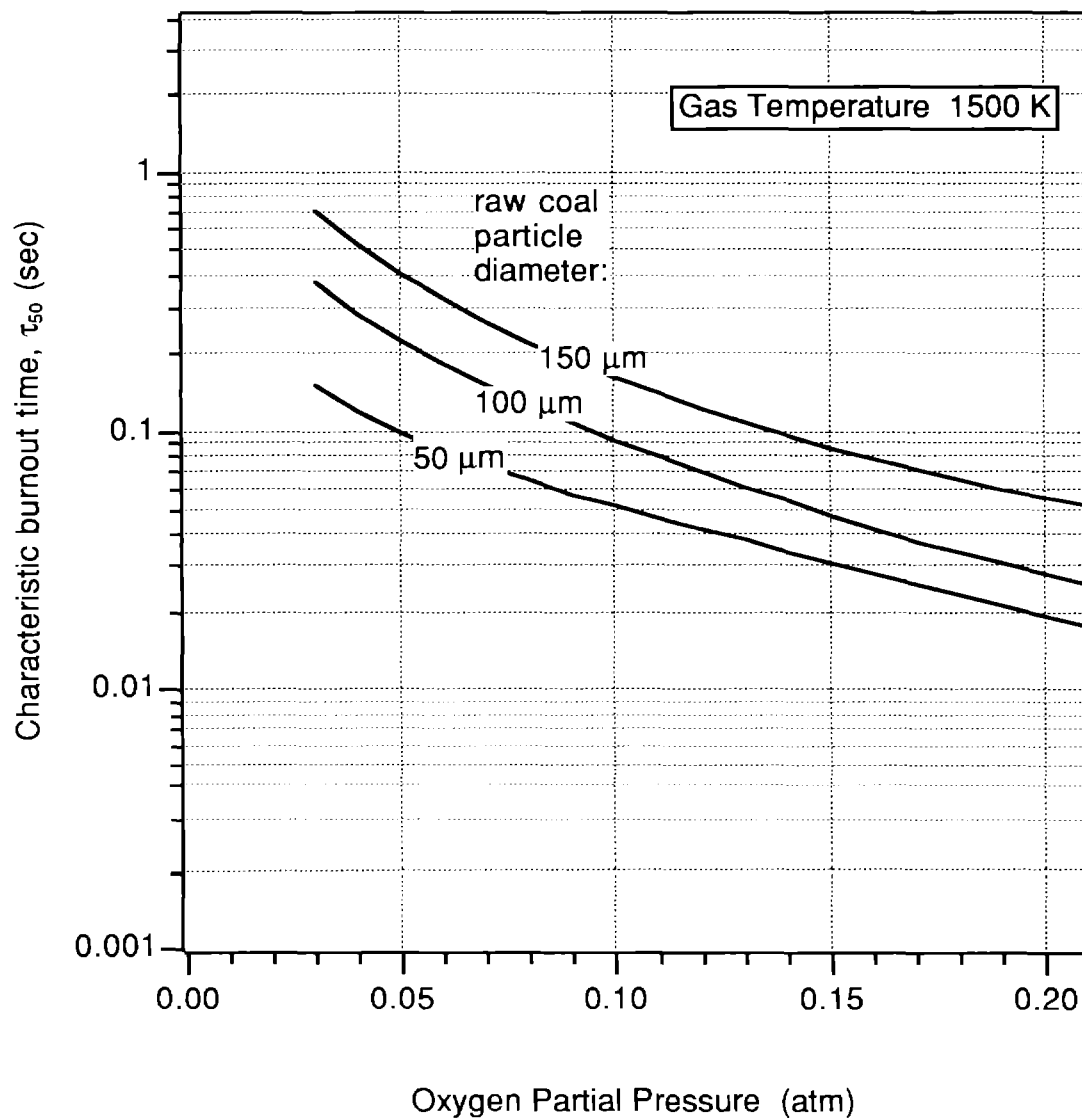


Figure 2.4 Predicted times for 50% completion of char combustion for PSOC-1451D, Pittsburgh #8 coal at 1500 K gas temperature.

Because swelling behavior and initial char density are interrelated, we can define a parameter, $\hat{\rho}_{o,daf} \equiv \omega^3 \rho_{o,daf}$, a hypothetical char density in the absence of swelling. For a given coal, $\hat{\rho}_{o,daf}$ is determined by the initial coal density and the coal volatile and ash content. Equation 2.9 can be rewritten as

$$\tau_{50} \equiv \frac{d_c \hat{\rho}_{o,daf}}{12 \omega^2 q_{25} 0.75^{2(1-\alpha)/3}} \quad (2.10)$$

to show that particle swelling ($\omega > 1$) *reduces* the burnout time. The relative importance of the kinetic and structural parameters to overall char reactivity will be

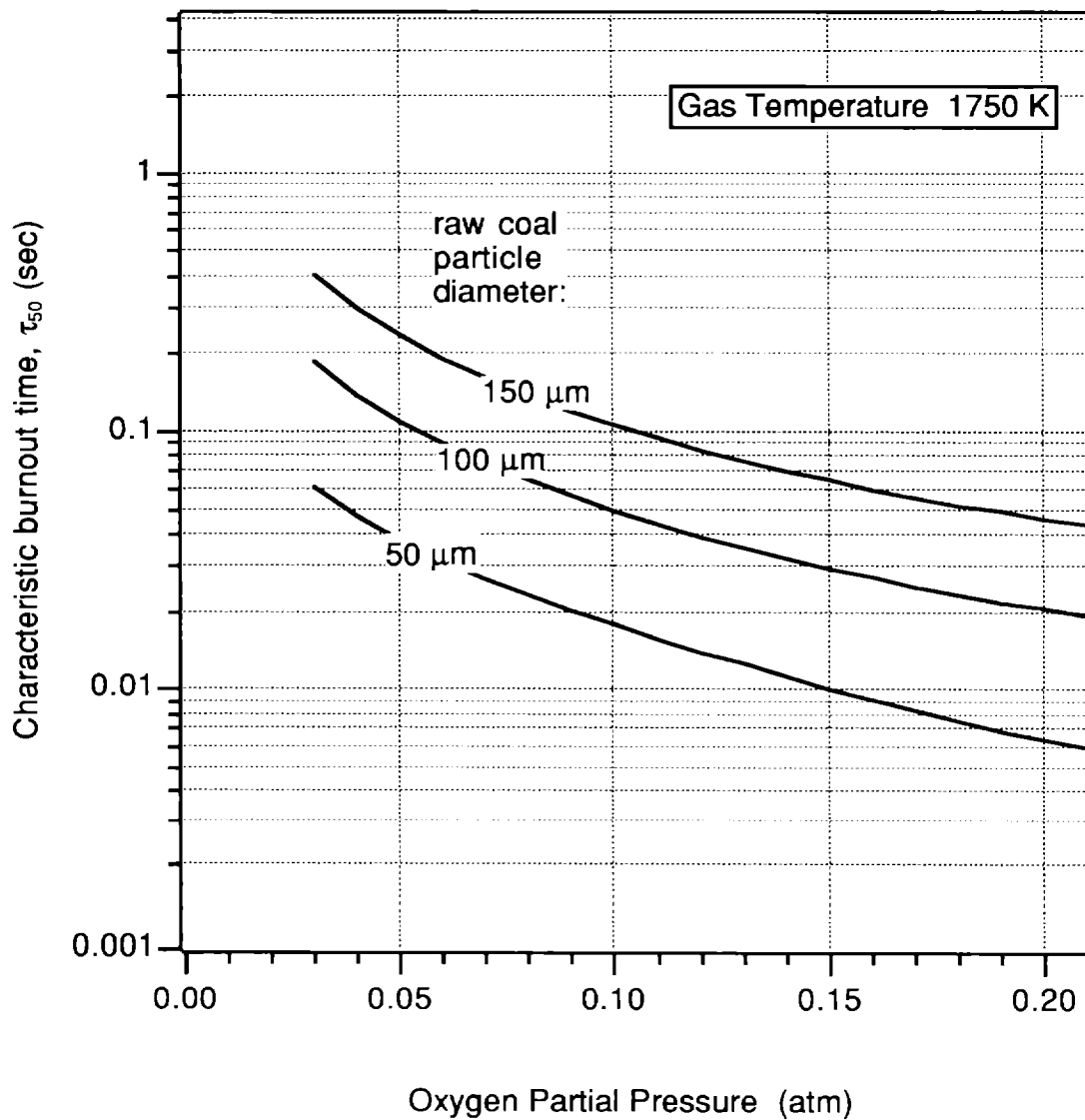


Figure 2.5 Predicted times for 50% completion of char combustion for PSOC-1451D, Pittsburgh #8 coal at 1750 K gas temperature.

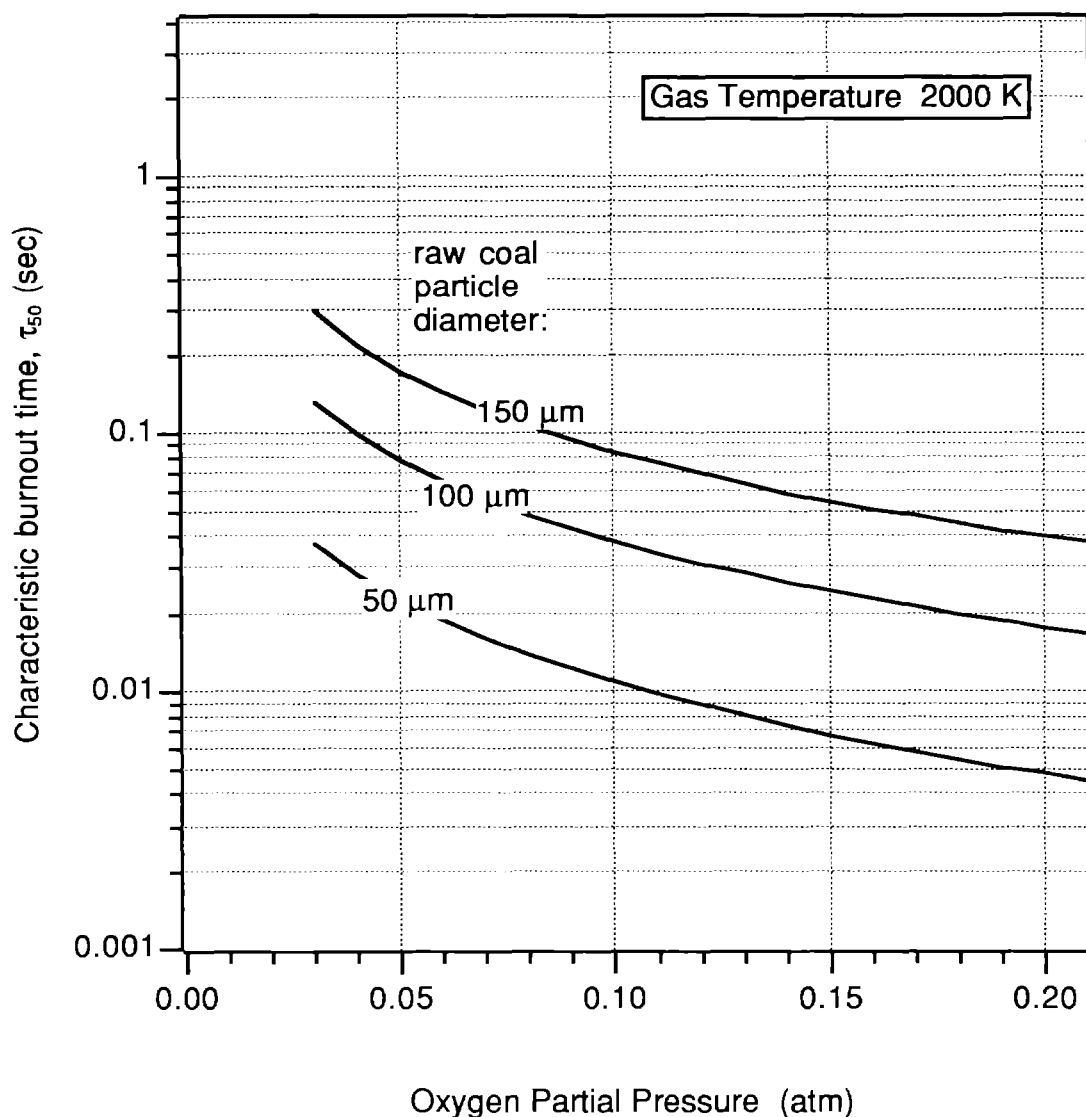


Figure 2.6 Predicted times for 50% completion of char combustion for PSOC-1451D, Pittsburgh #8 coal at 2000 K gas temperature.

discussed in more detail in the next quarterly report when the complete analysis set is available.

Summary of Results

In this section the primary results for the remaining six coals (of the seven completed to date) are presented, comprising Arrhenius plots, a summary table of combustion parameters, plots of density vs. conversion, profiles along the reactor height of tracer-calculated carbon conversions, and the burnout time predictions.

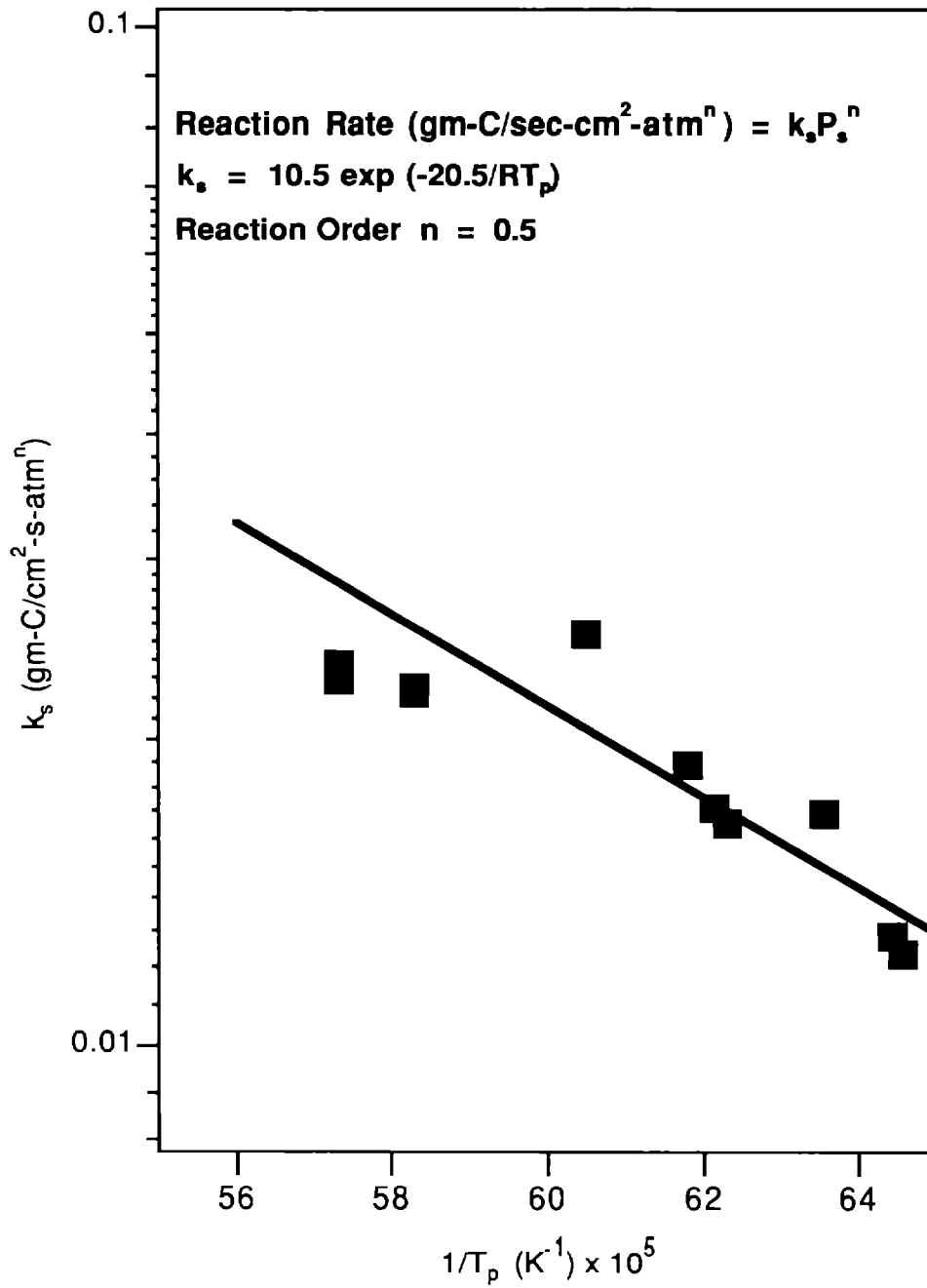


Figure 2.7 Arrhenius diagram and global kinetic parameters for PSOC-1516D, Lower Kittanning coal

Table 2.2
Summary of Combustion Parameters for PSOC-1516D, Lower Kittanning Coal

<p>Char oxidation rate parameters</p> $q = A \exp(-E/RT_p) P^n$	<p>A</p> <p>E</p> <p>n</p>	<p>10.5 gm-C / cm²-s-atmⁿ</p> <p>20.5 kcal / mole</p> <p>0.5 *</p>
<p>Product ratio parameters</p> $CO/CO_2 = A_c \exp(-E_c/RT_p)$	<p>A_c</p> <p>E_c</p>	<p>no carbon dioxide production</p>
<p>Burning mode parameter</p> $\rho/\rho_o = (m/m_o)^\alpha$ $d/d_o = (m/m_o)^{(1-\alpha)/3}$	<p>α</p>	<p>0.0</p>
<p>Char structural parameters</p> $\omega = d_o / d_c$ <p>(linear swelling factor)</p> <p>$\rho_o \equiv \rho$ at $z = 6.5$ cm</p> <p>(Initial char particle density, daf)</p>	<p>ω</p> <p>ρ_{o,daf}</p>	<p>1.27</p> <p>0.455 gm / cm³</p>
<p>As an example, this parameter set yields a combustion rate, <i>q</i>, of 0.0031 gm/sq.cm-s for a 100 μm particle in a gas with T_g = 1600 K containing 6 mole-% oxygen</p> <p>* These particular parameters should be regarded as empirical parameters useful for the prediction of burning rates. They do not necessarily have fundamental significance and /or are not necessarily unique for this data set.</p>		

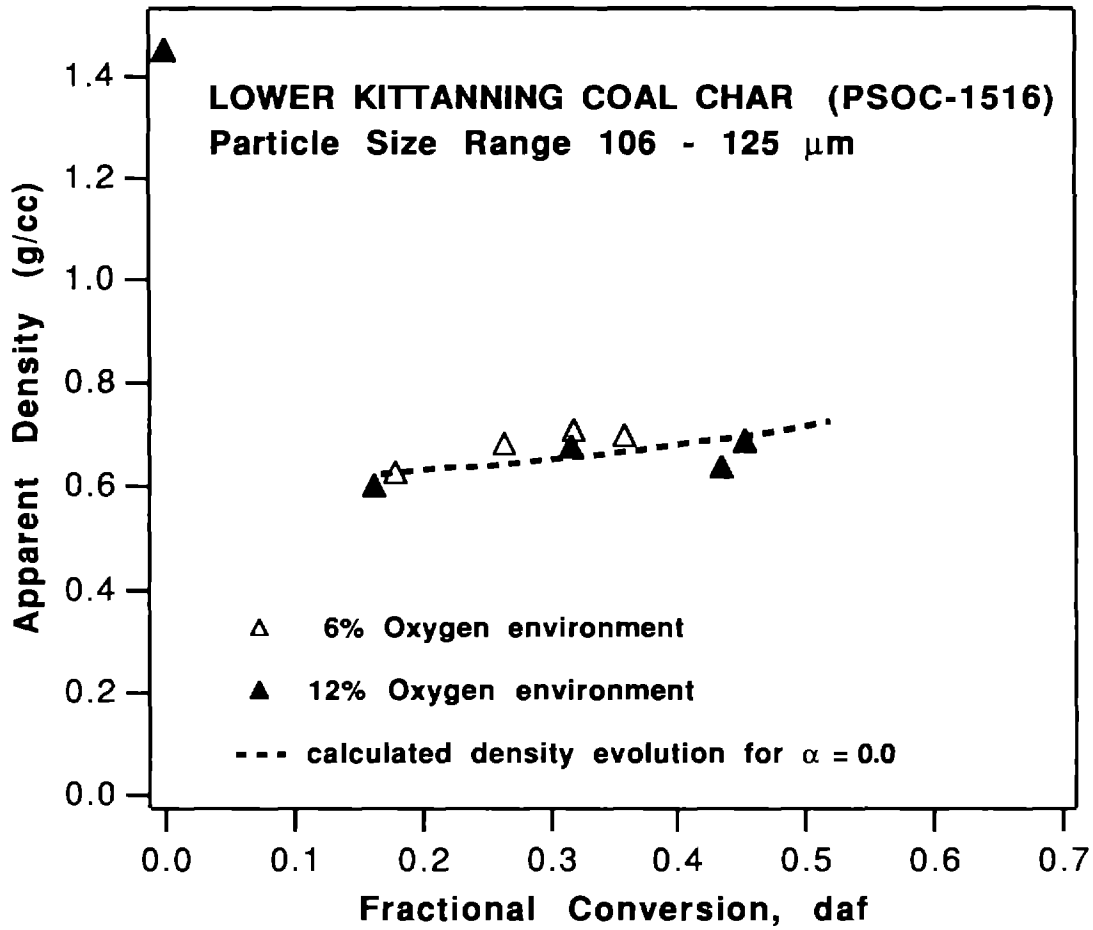


Figure 2.8 Measured (points) and predicted (curve) density evolution for PSOC-1516D, Lower Kittanning coal

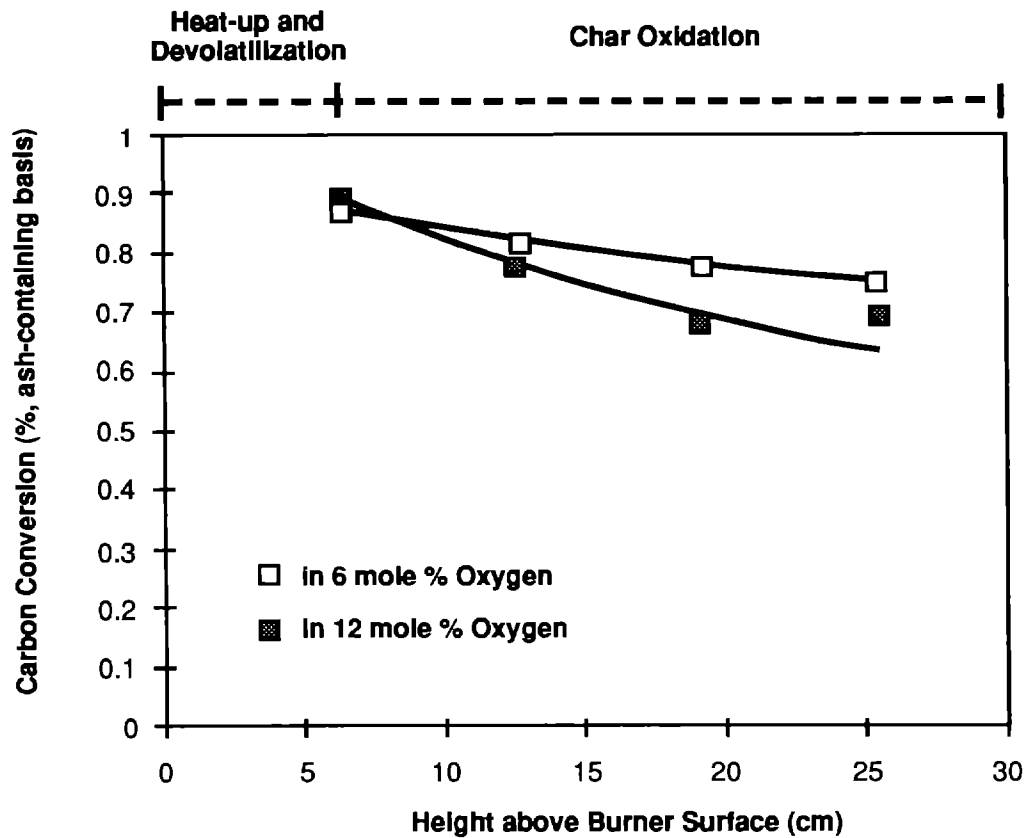


Figure 2.9 Conversion profiles from combustion experiments in the CCL for PSOC-1516D, Lower Kittanning coal. Points are determined by inorganic tracer analysis on extracted samples. Curves are predictions using the rate constants derived from optical measurements.

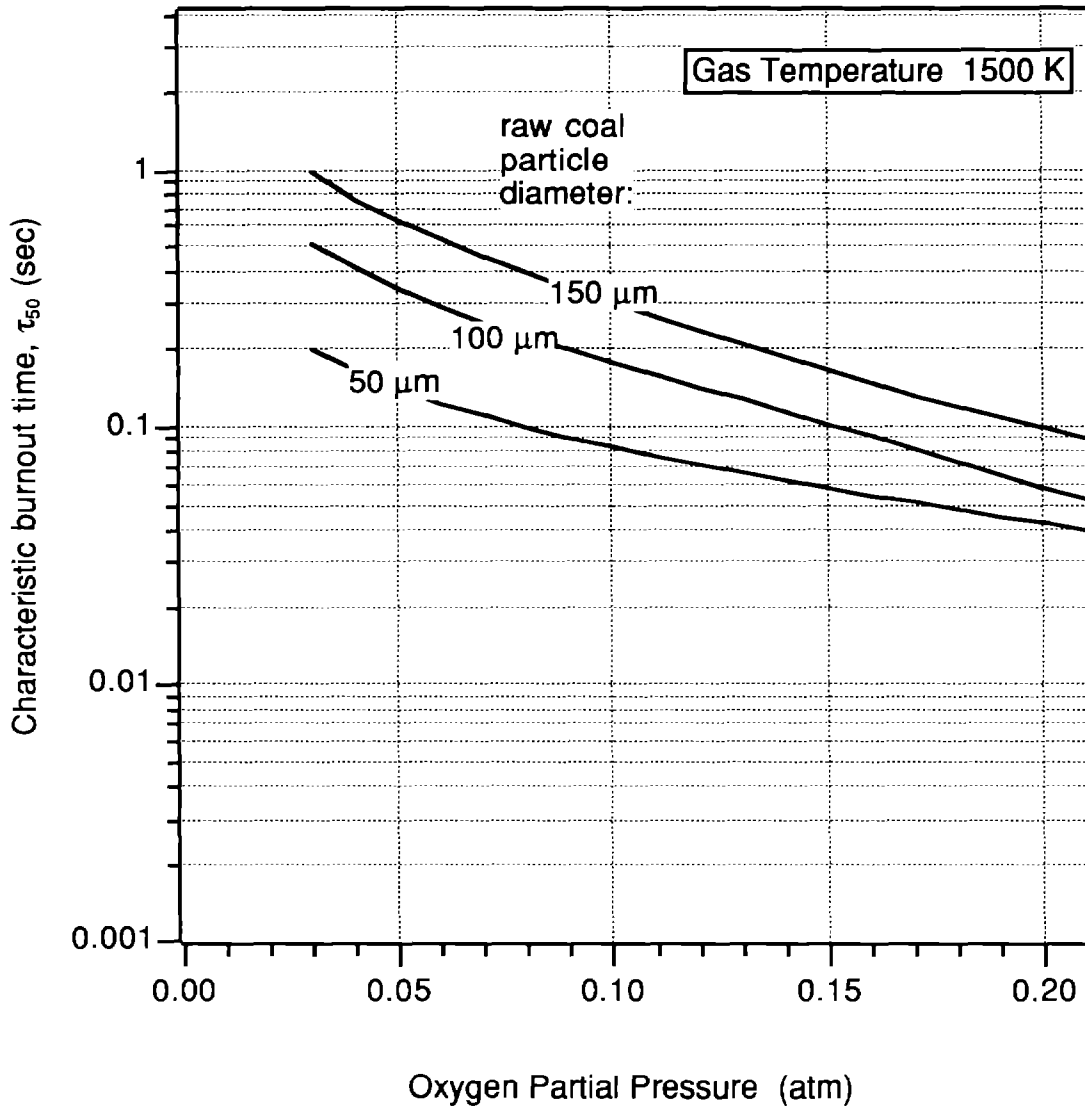


Figure 2.10 Predicted times for 50% completion of char combustion for PSOC-1516D, Lower Kittanning coal at 1500 K gas temperature.

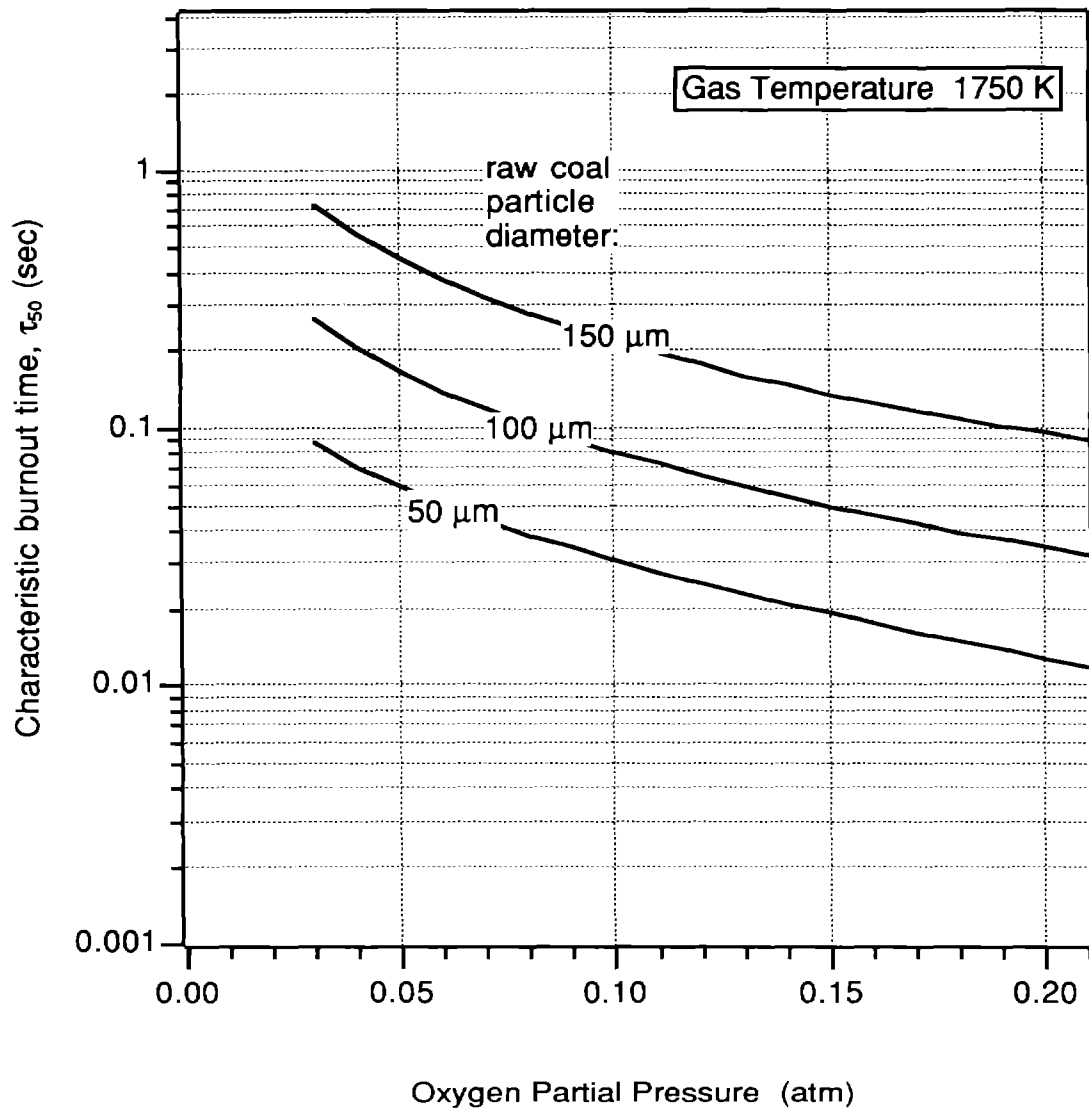


Figure 2.11 Predicted times for 50% completion of char combustion for PSOC-1516D, Lower Kittanning coal at 1750 K gas temperature.

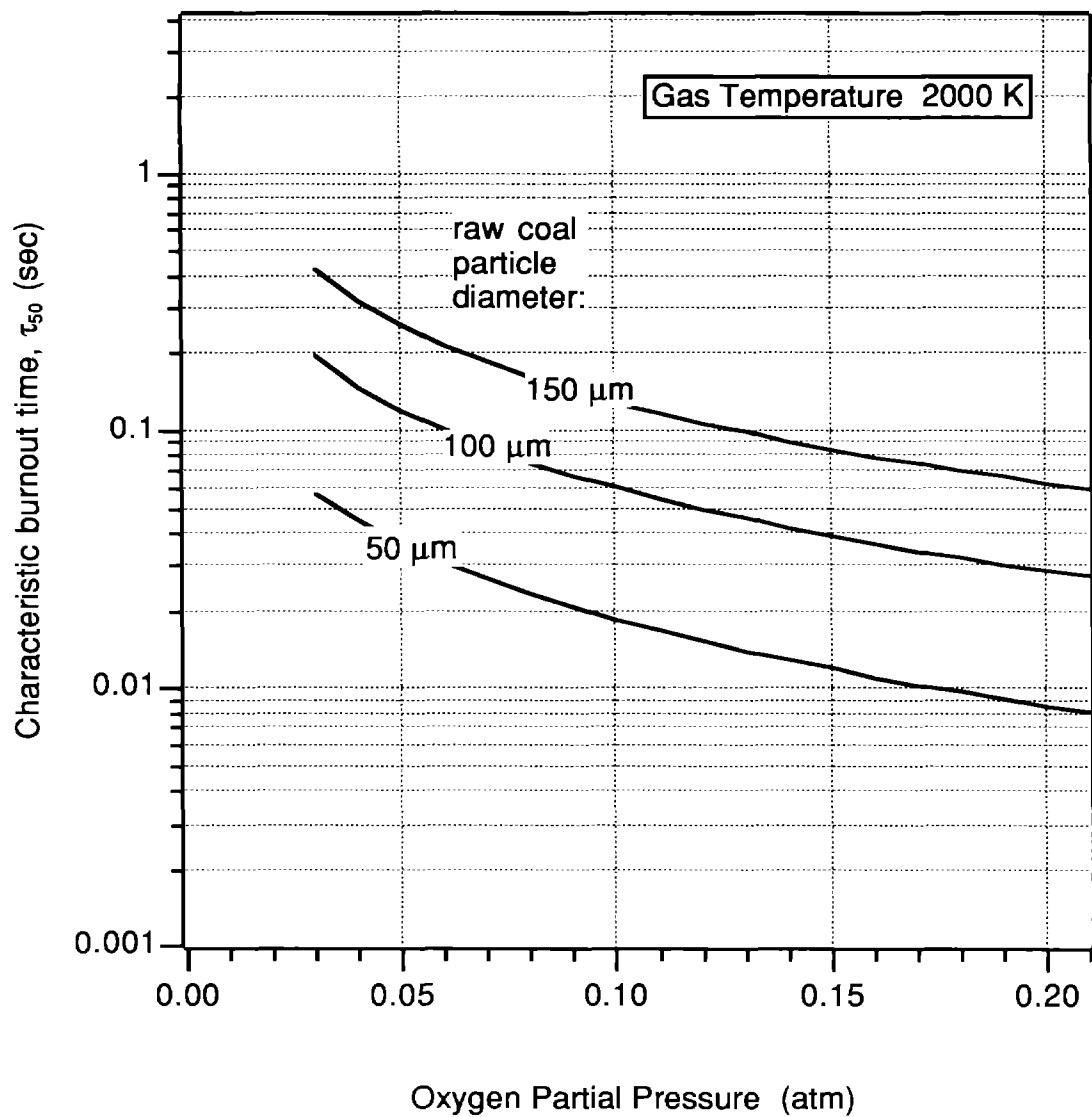


Figure 2.12 Predicted times for 50% completion of char combustion for PSOC-1516D, Lower Kittanning coal at 1750 K gas temperature.

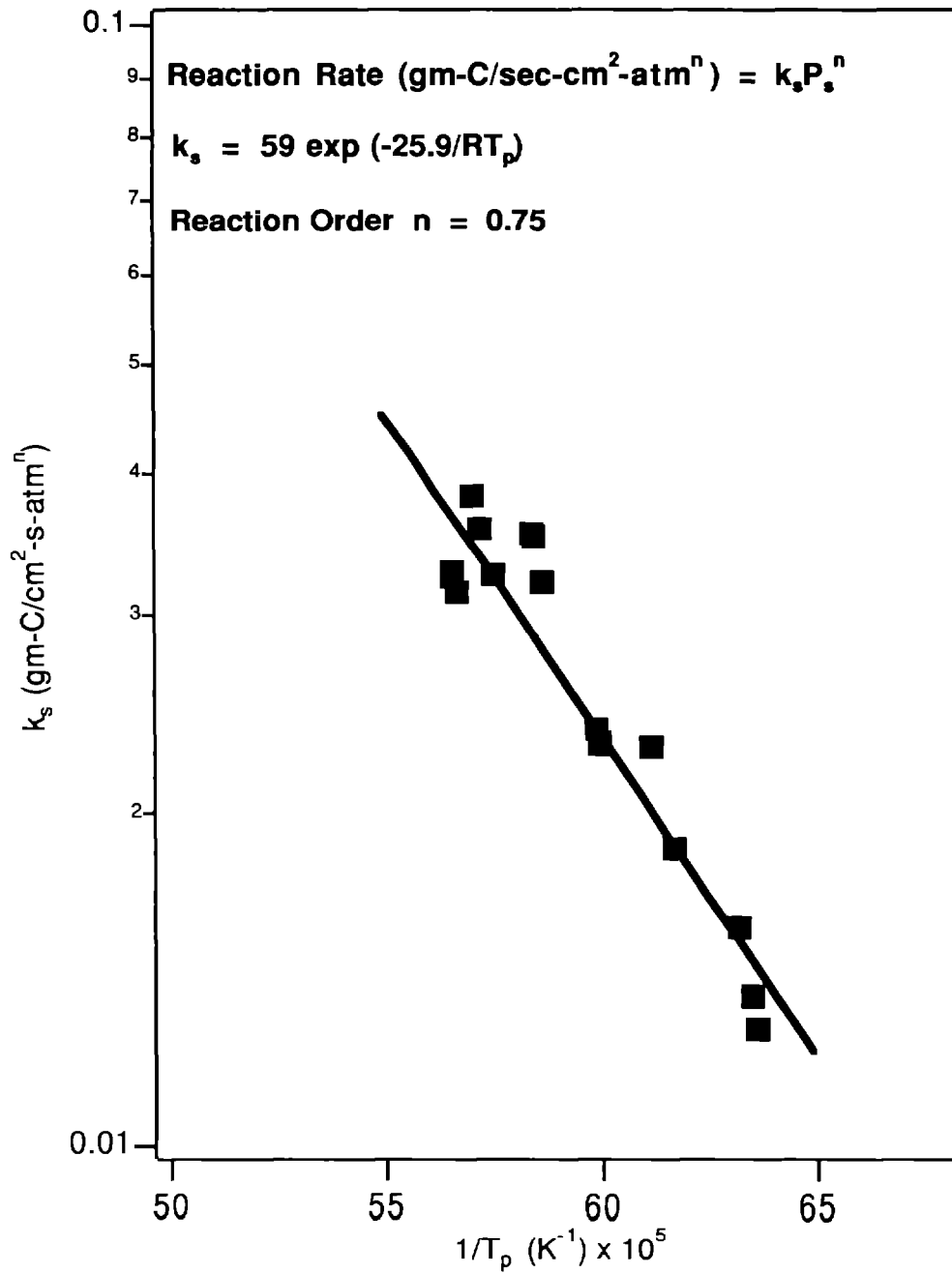


Figure 2.13 Arrhenius diagram and global kinetic parameters for PSOC-1508D, Pocahontas #3 coal

Table 2.3
Summary of Combustion Parameters for PSOC-1508, Pocahontas #3 Coal

<p>Char oxidation rate parameters</p> $q = A \exp(-E/RT_p) P^n$	<p>A</p> <p>E</p> <p>n</p>	<p>59 gm-C / cm²-s-atmⁿ</p> <p>26 kcal / mole</p> <p>0.75</p>
<p>Product ratio parameters</p> $CO/CO_2 = A_c \exp(-E_c/RT_p)$	<p>A_c</p> <p>E_c</p>	<p>3 x 10⁸ *</p> <p>60 * kcal / mole</p>
<p>Burning mode parameter</p> $\rho/\rho_o = (m/m_o)^\alpha$ $d/d_o = (m/m_o)^{(1-\alpha)/3}$	<p>α</p>	<p>0.3</p>
<p>Char structural parameters</p> $\omega = d_o / d_c$ <p>(linear swelling factor)</p> <p>$\rho_o \equiv \rho$ at z = 6.5 cm</p> <p>(Initial char particle density, daf)</p>	<p>ω</p> <p>ρ_{o,daf}</p>	<p>1.21</p> <p>0.613 gm / cm³</p>
<p>As an example, this parameter set yields a combustion rate, q, of 0.00150 gm/sq.cm-s for a 100 μm particle in a gas with T_g = 1600 K containing 6 mole-% oxygen</p> <p>These product ratio parameters yield 3 mole-% carbon dioxide at 1900 K and 15 mole-% carbon dioxide at 1700 K</p> <p>* These particular parameters should be regarded as empirical parameters useful for the prediction of burning rates. They do not necessarily have fundamental significance and/or are not unique for this data set.</p>		

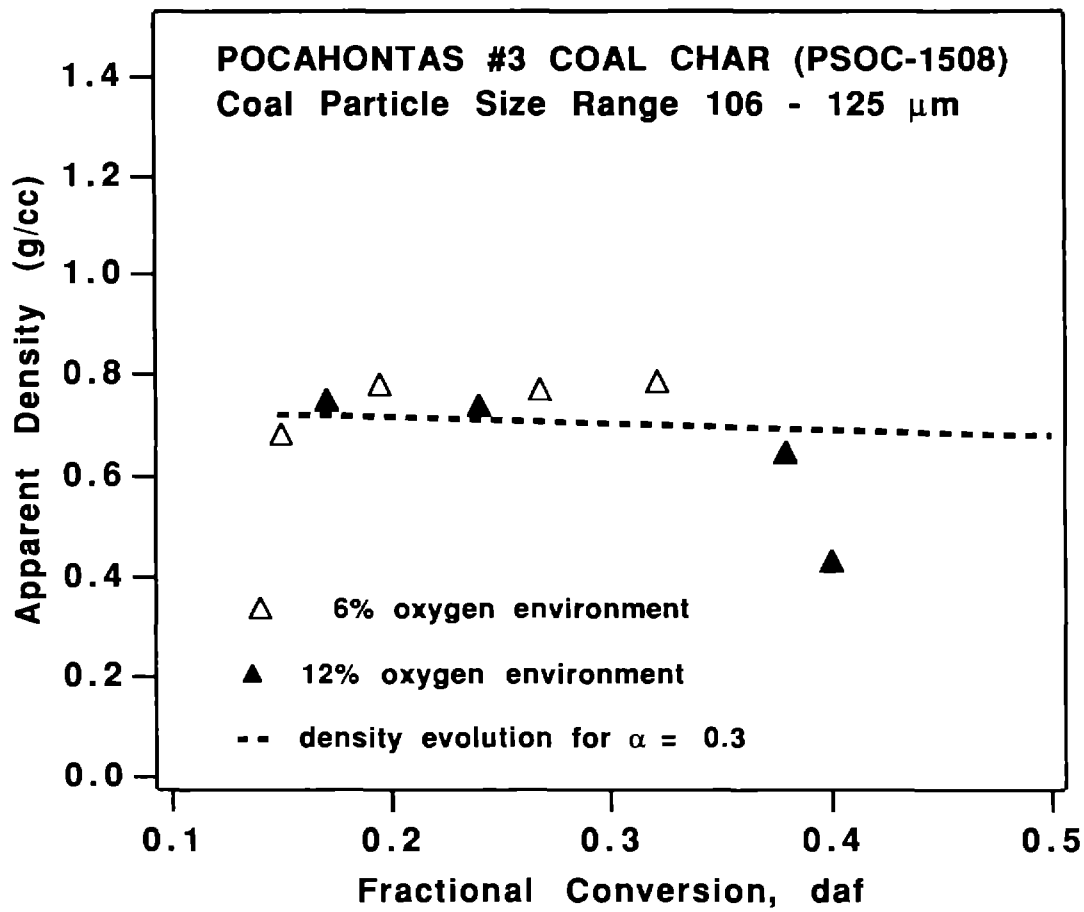


Figure 2.14 Measured (points) and predicted (curve) density evolution for PSOC-1508D, Pocahontas coal

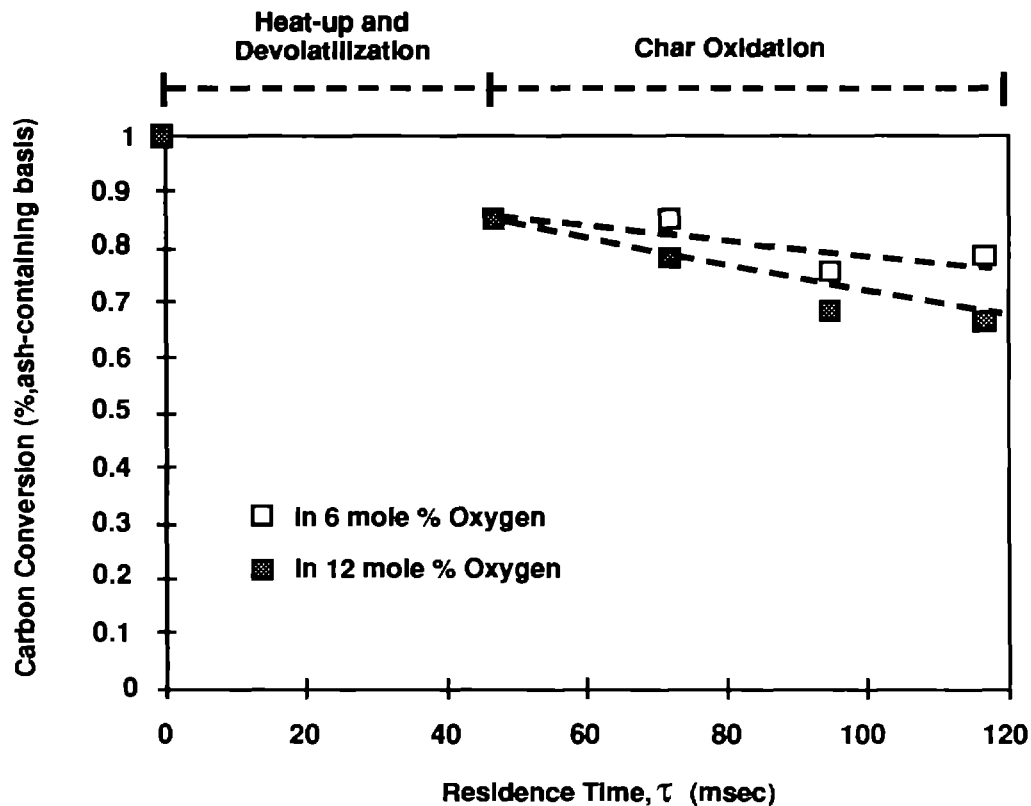


Figure 2.15 Conversion profiles from combustion experiments in the CCL for PSOC-1508D, Pocahontas #3 coal. Points are determined by inorganic tracer analysis on extracted samples. Curves are predictions using the rate constants derived from optical measurements.

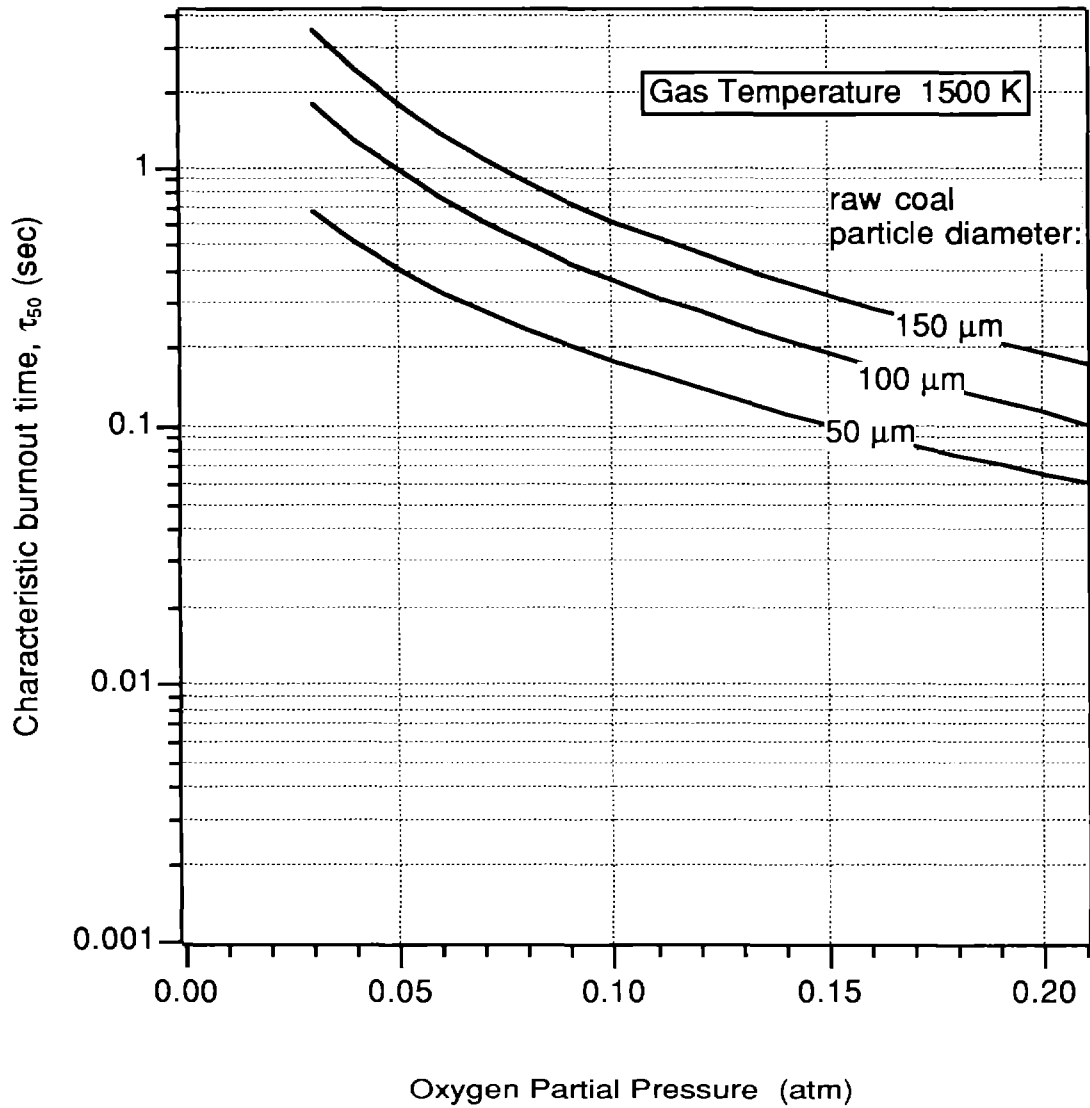


Figure 2.16 Predicted times for 50% completion of char combustion for PSOC-1508D, Pocahontas #3 coal at 1500 K gas temperature.

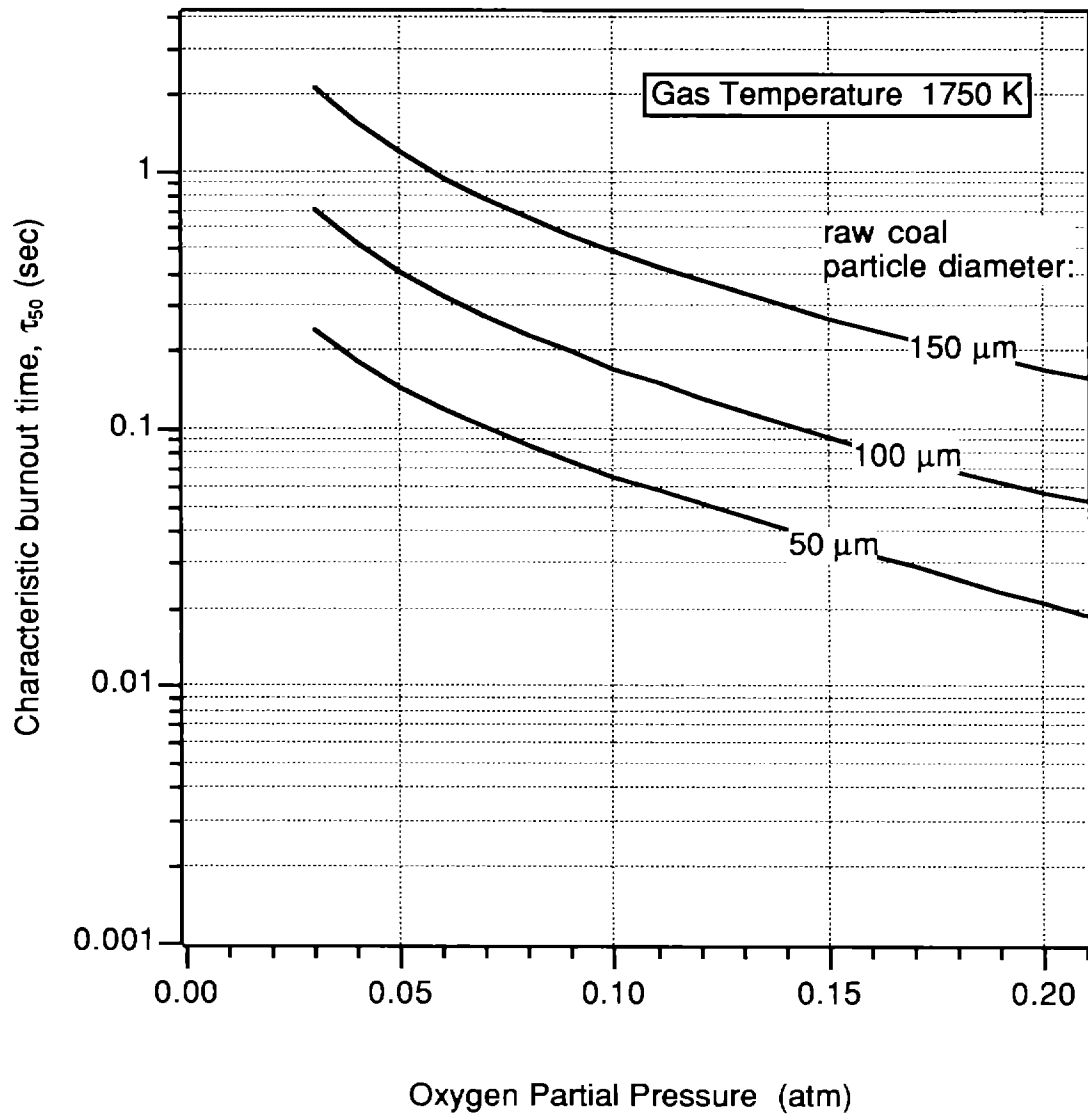


Figure 2.17 Predicted times for 50% completion of char combustion for PSOC-1508D, Pocahontas #3 coal at 1750 K gas temperature.

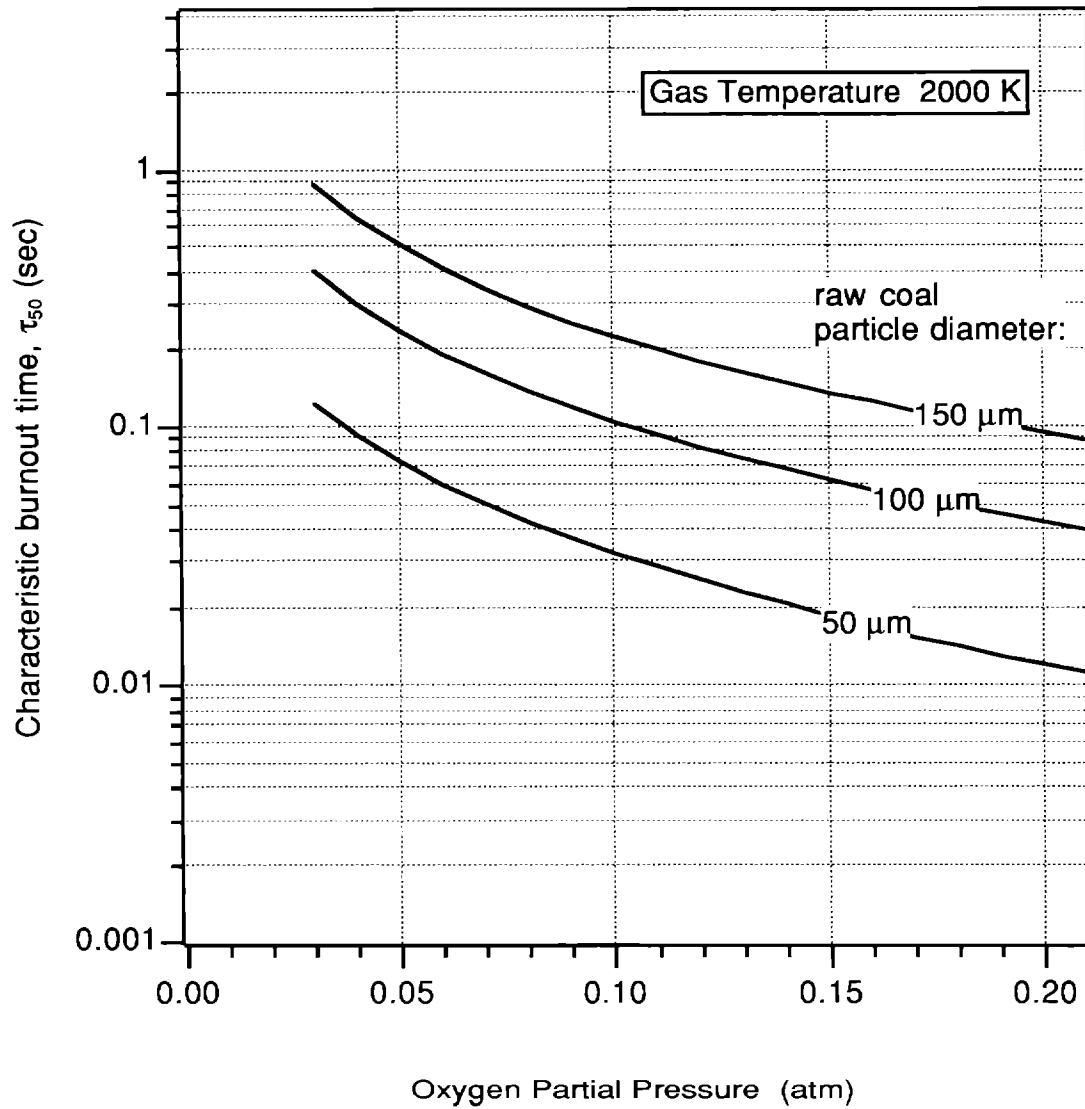


Figure 2.18 Predicted times for 50% completion of char combustion for PSOC-1508D, Pocahontas #3 coal at 2000 K gas temperature.

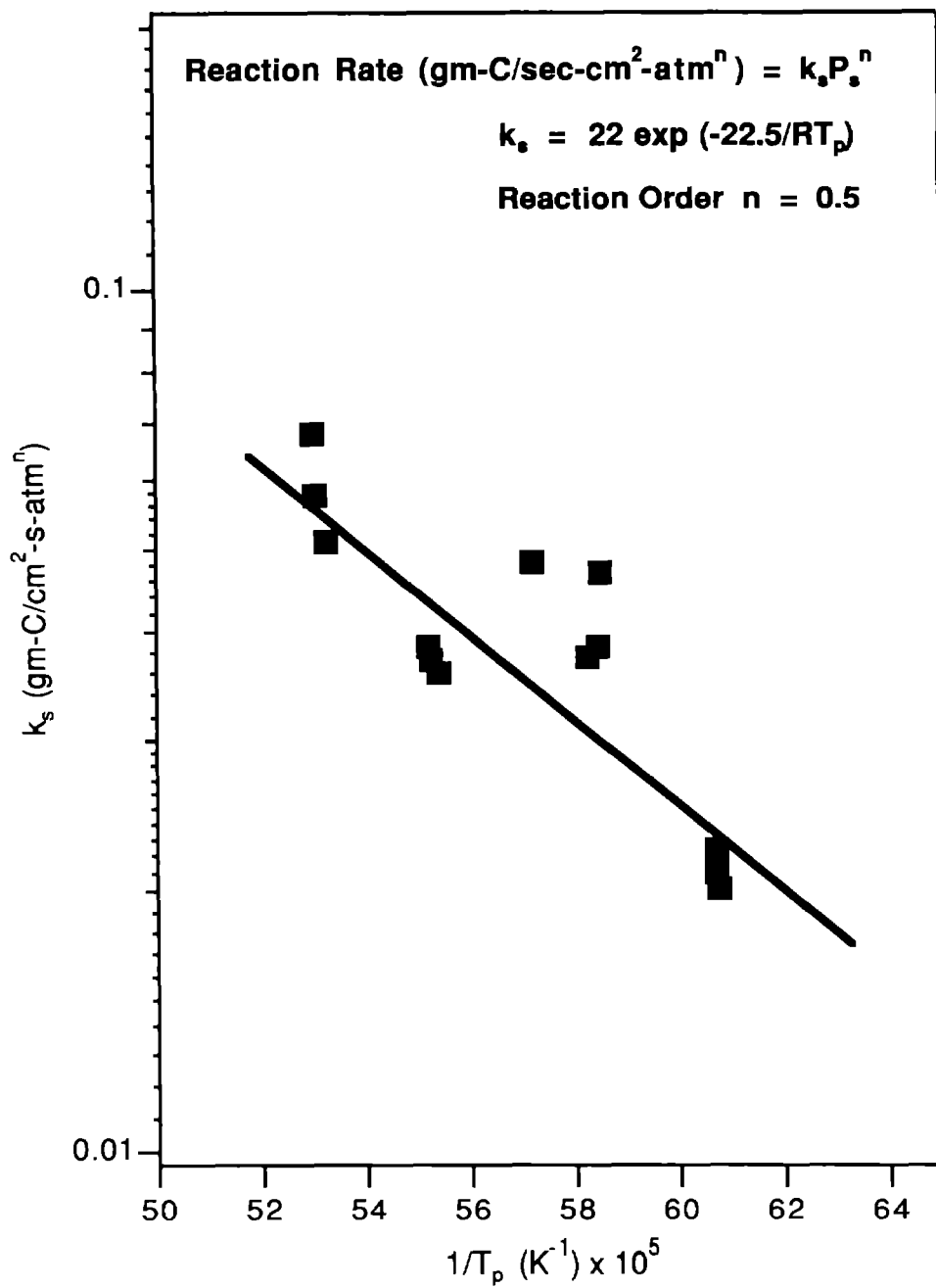


Figure 2.19 Arrhenius diagram and global kinetic parameters for PSOC-1493D, Illinois #6 coal

Table 2.4
Summary of Combustion Parameters for PSOC-1493, Illinois #6 Coal

<p>Char oxidation rate parameters</p> $q = A \exp(-E/RT_p) P^n$	<p>A E n</p>	<p>22.4 gm-C / cm²-s-atmⁿ 22.5 kcal / mole 0.5 *</p>
<p>Product ratio parameters</p> $CO/CO_2 = A_c \exp(-E_c/RT_p)$	<p>A_c E_c</p>	<p>2.5 x 10⁸ * 60 * kcal / mole</p>
<p>Burning mode parameter</p> $\rho/\rho_o = (m/m_o)^\alpha$ $d/d_o = (m/m_o)^{(1-\alpha)/3}$	<p>α</p>	<p>0.45</p>
<p>Char structural parameters</p> $\omega = d_o / d_c$ <p>(linear swelling factor)</p> $\rho_o \equiv \rho \text{ at } z = 6.5 \text{ cm}$ <p>(Initial char particle density, daf)</p>	<p>ω ρ_{o,daf}</p>	<p>1.06 0.385 gm / cm³</p>
<p>As an example, this parameter set yields a combustion rate, <i>q</i>, of 0.0041 gm/sq.cm-s for a 100 μm particle in a gas with T_g = 1600 K containing 6 mole-% oxygen</p> <p>These product ratio parameters yield 3 mole-% carbon dioxide at 1900 K and 17 mole-% carbon dioxide at 1700 K</p> <p>* These particular parameters should be regarded as empirical parameters that are useful for the prediction of burning rates. They do not necessarily have fundamental significance and/or are not necessarily unique for this data set.</p>		

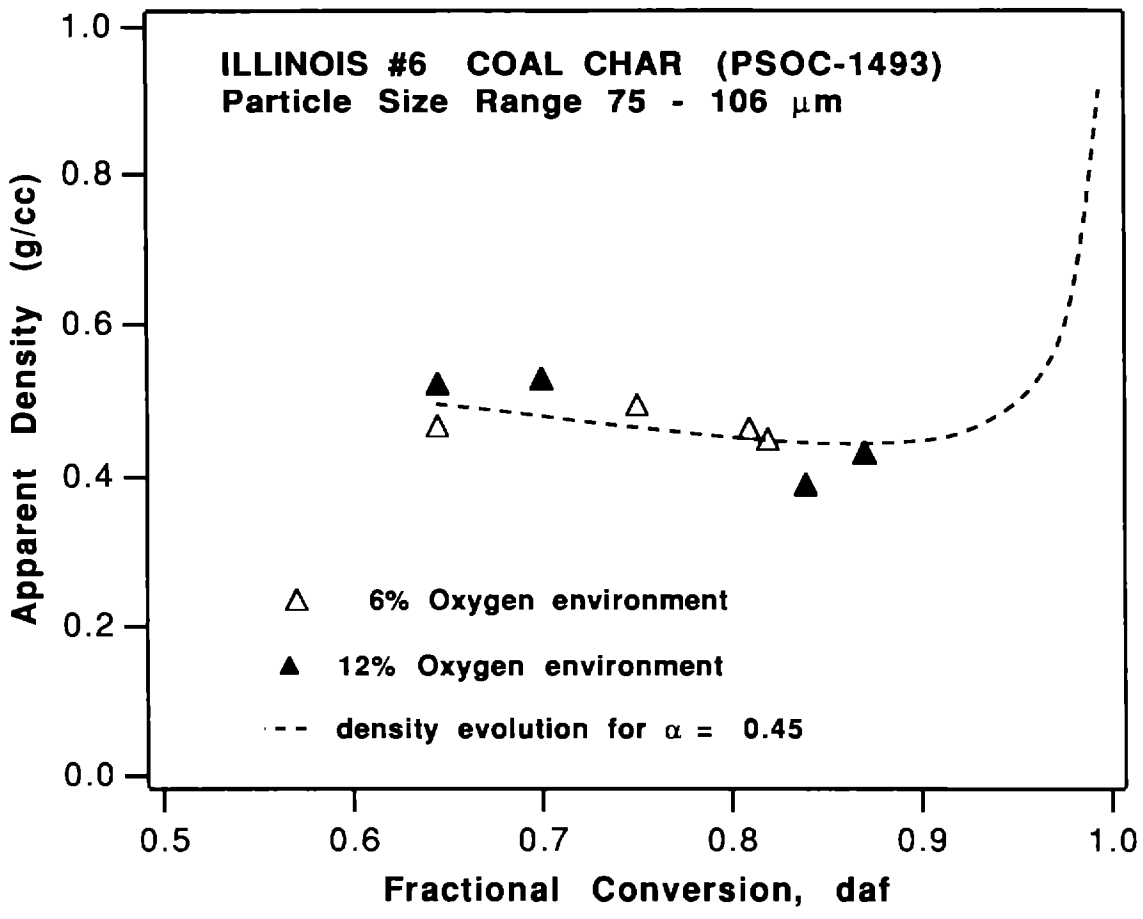


Figure 2.20 Measured (points) and predicted (curve) density evolution for PSOC-1493D, Illinois #6 coal

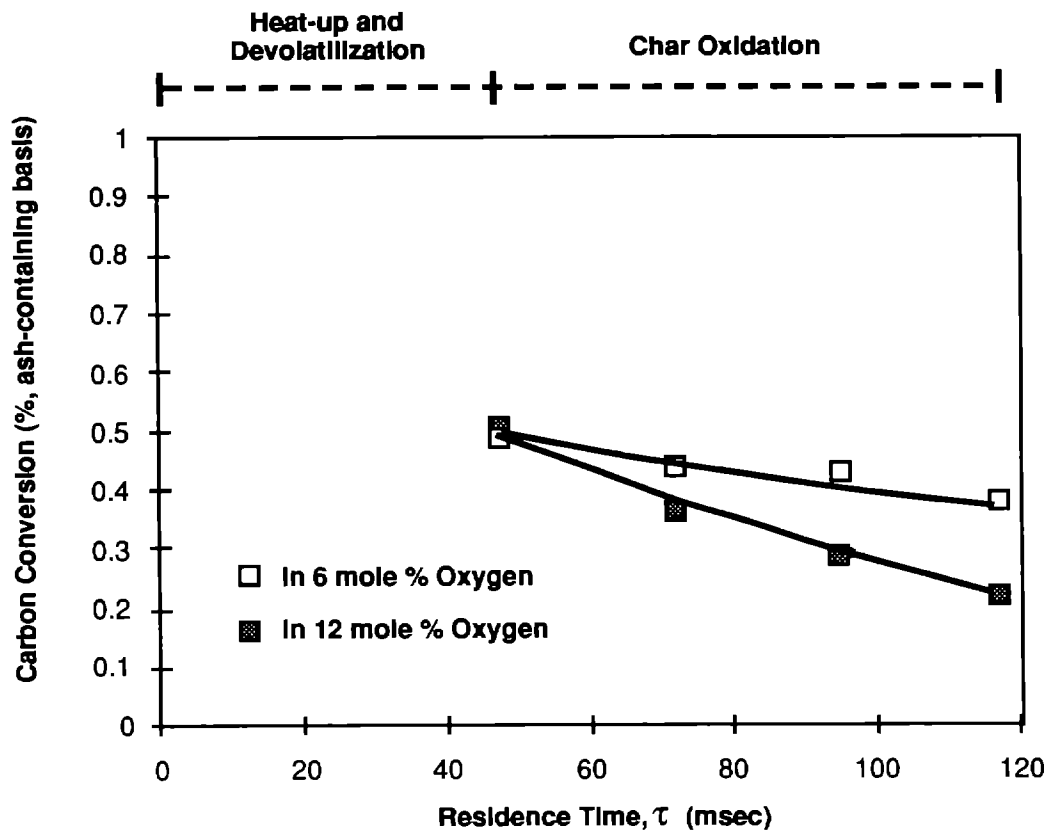


Figure 2.21 Conversion profiles from combustion experiments in the CCL for PSOC-1493D, Illinois #6 coal. Points are determined by inorganic tracer analysis on extracted samples. Curves are predictions using the rate constants derived from optical measurements.

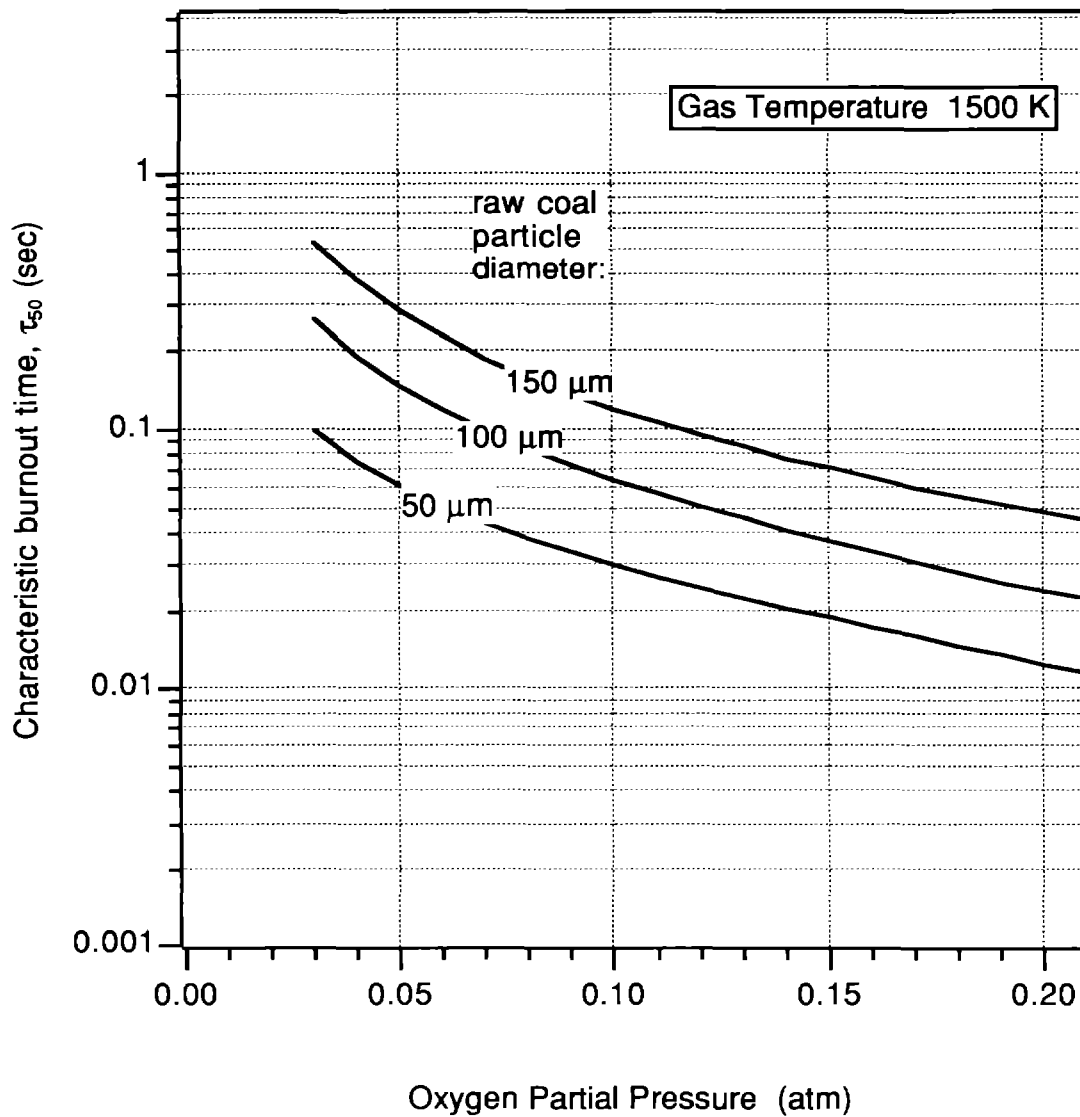


Figure 2.22 Predicted times for 50% completion of char combustion for PSOC-1493D, Illinois #6 coal at 1500 K gas temperature.

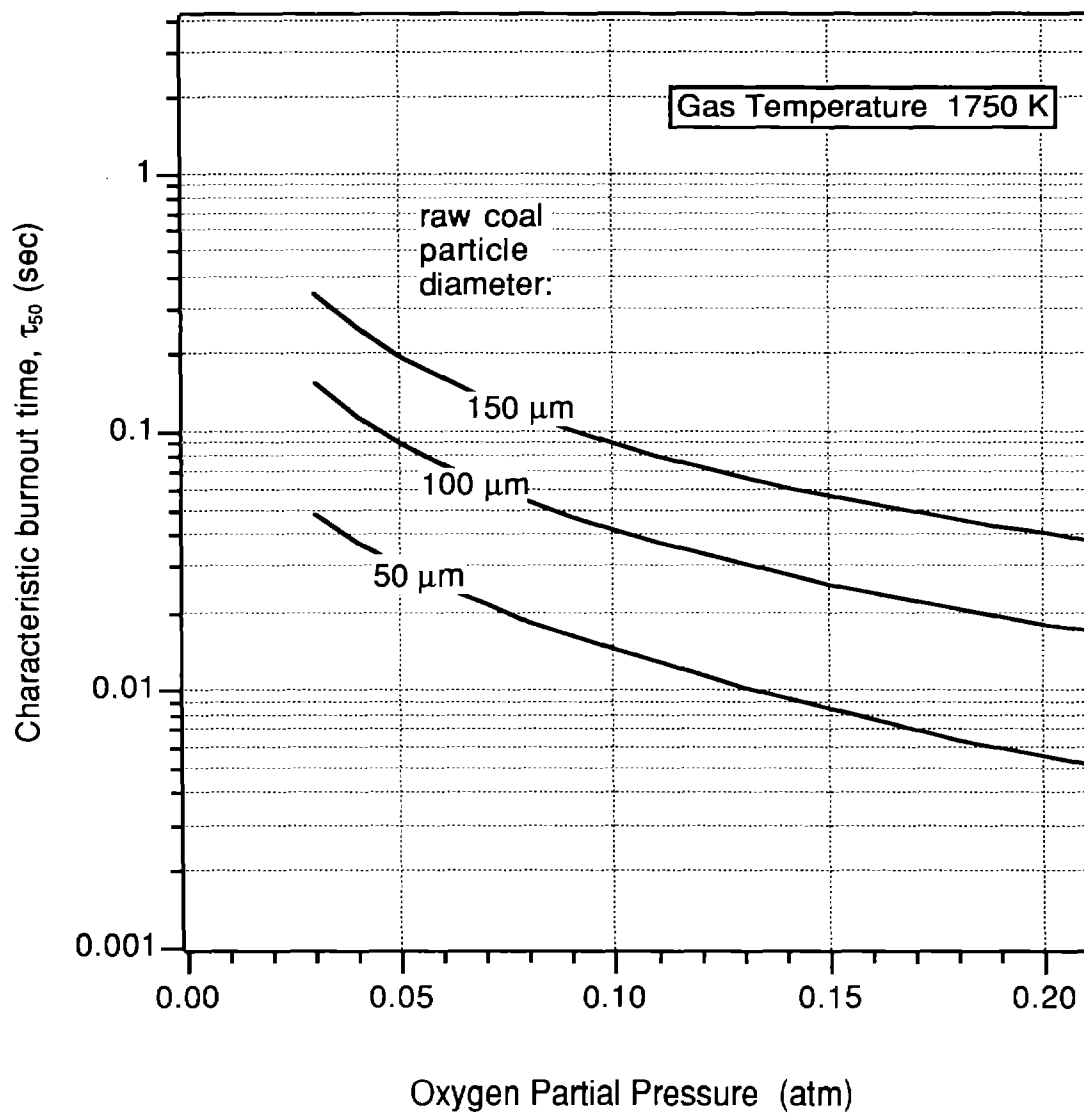


Figure 2.23 Predicted times for 50% completion of char combustion for PSOC-1493D, Illinois #6 coal at 1750 K gas temperature.

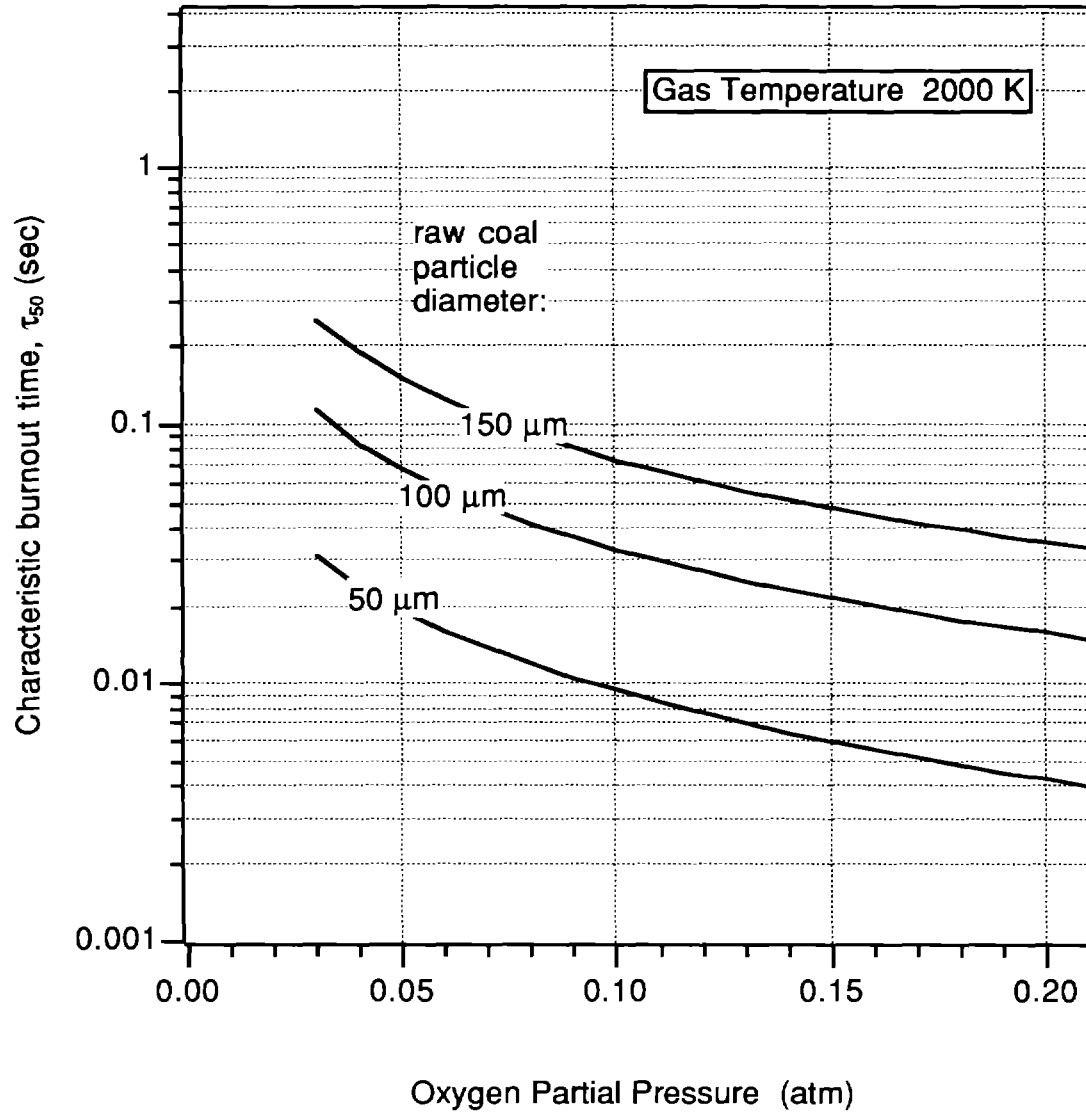


Figure 2.24 Predicted times for 50% completion of char combustion for PSOC-1493D, Illinois #6 coal at 2000 K gas temperature.

Table 2.5
Summary of Combustion Parameters for PSOC-1502, Hiawatha Coal

<p><i>Char oxidation rate parameters</i></p> $q = A \exp(-E/RT_p) P^n$	<p>A E n</p>	<p>chars reacted at their diffusion limited rates in both the 6 and 12 mole-% oxygen environments</p>
<p><i>Product ratio parameters</i></p> $CO/CO_2 = A_c \exp(-E_c/RT_p)$	<p>A_c E_c</p>	<p>3×10^8 * 60 * kcal / mole</p>
<p><i>Burning mode parameter</i></p> $\rho/\rho_o = (m/m_o)^\alpha$ $d/d_o = (m/m_o)^{(1-\alpha)/3}$	<p>α</p>	<p>0.25 in 6 mole-% 0.0 in 12 mole-%</p>
<p><i>Char structural parameters</i></p> $\omega = d_o / d_c$ <p>(linear swelling factor)</p> $\rho_o \equiv \rho \text{ at } z = 6.5 \text{ cm}$ <p>(Initial char particle density, daf)</p>	<p>ω $\rho_{o,daf}$</p>	<p>1.06 0.437 gm / cm³</p>
<p>As an example, this parameter set yields a combustion rate, <i>q</i>, of 0.00704 gm/sq.cm-s for a 100 μm particle in a gas with <i>T_g</i> = 1600 K containing 6 mole-% oxygen</p> <p>These product ratio parameters yield 2.6 mole-% carbon dioxide at 1900 K and 14.7 mole-% carbon dioxide at 1700 K</p> <p>* These particular parameters should be regarded as empirical parameters, useful for the prediction of burning rates. They do not necessarily have fundamental significance and/or are not necessarily unique for this data set.</p>		

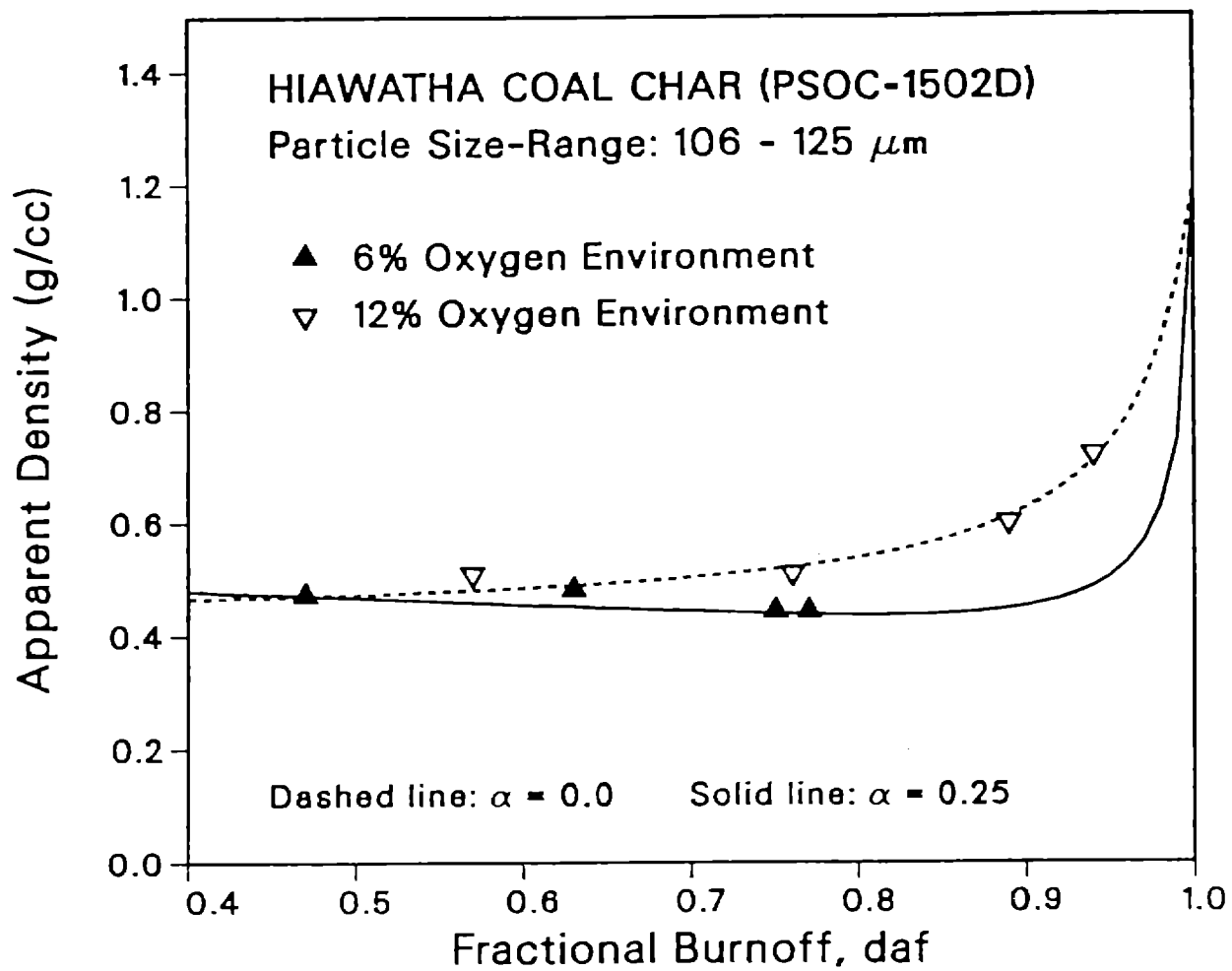


Figure 2.25 Measured (points) and predicted (curve) density evolution for PSOC-1502D, Hiawatha coal

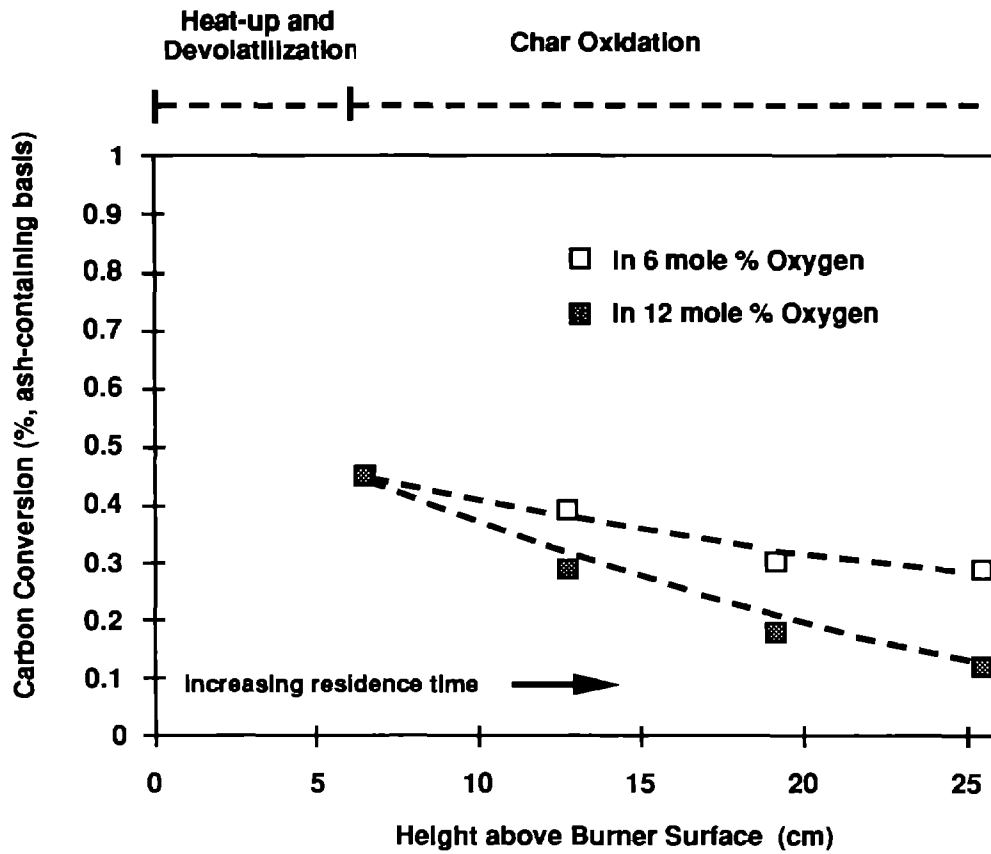


Figure 2.26 Conversion profiles from combustion experiments in the CCL for PSOC-1502D, Hiawatha coal. Points are determined by inorganic tracer analysis on extracted samples. Curves are predictions using the rate constants derived from optical measurements.

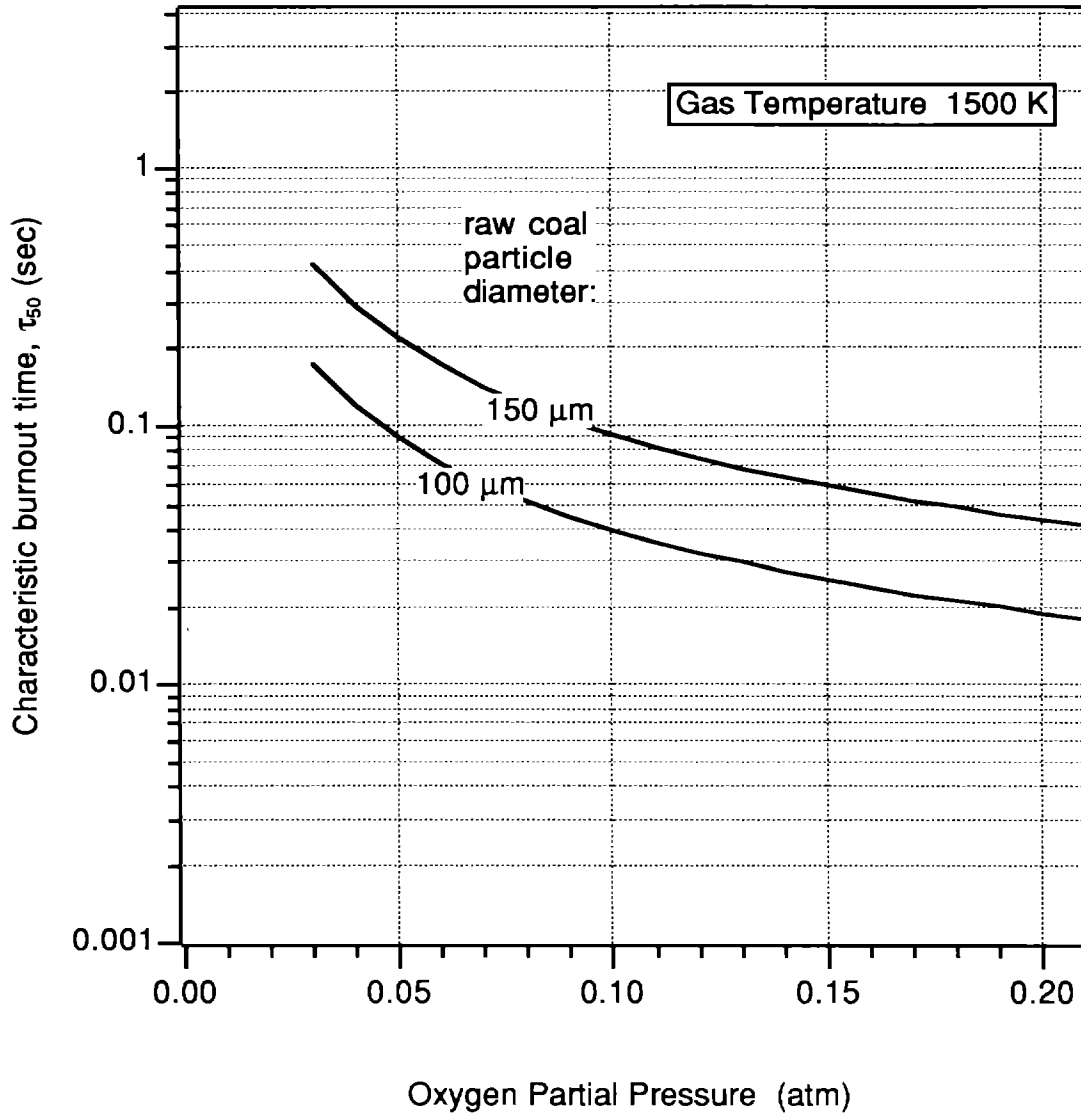


Figure 2.27 Predicted times for 50% completion of char combustion for PSOC-1502D, Hiawatha coal at 1500 K gas temperature.

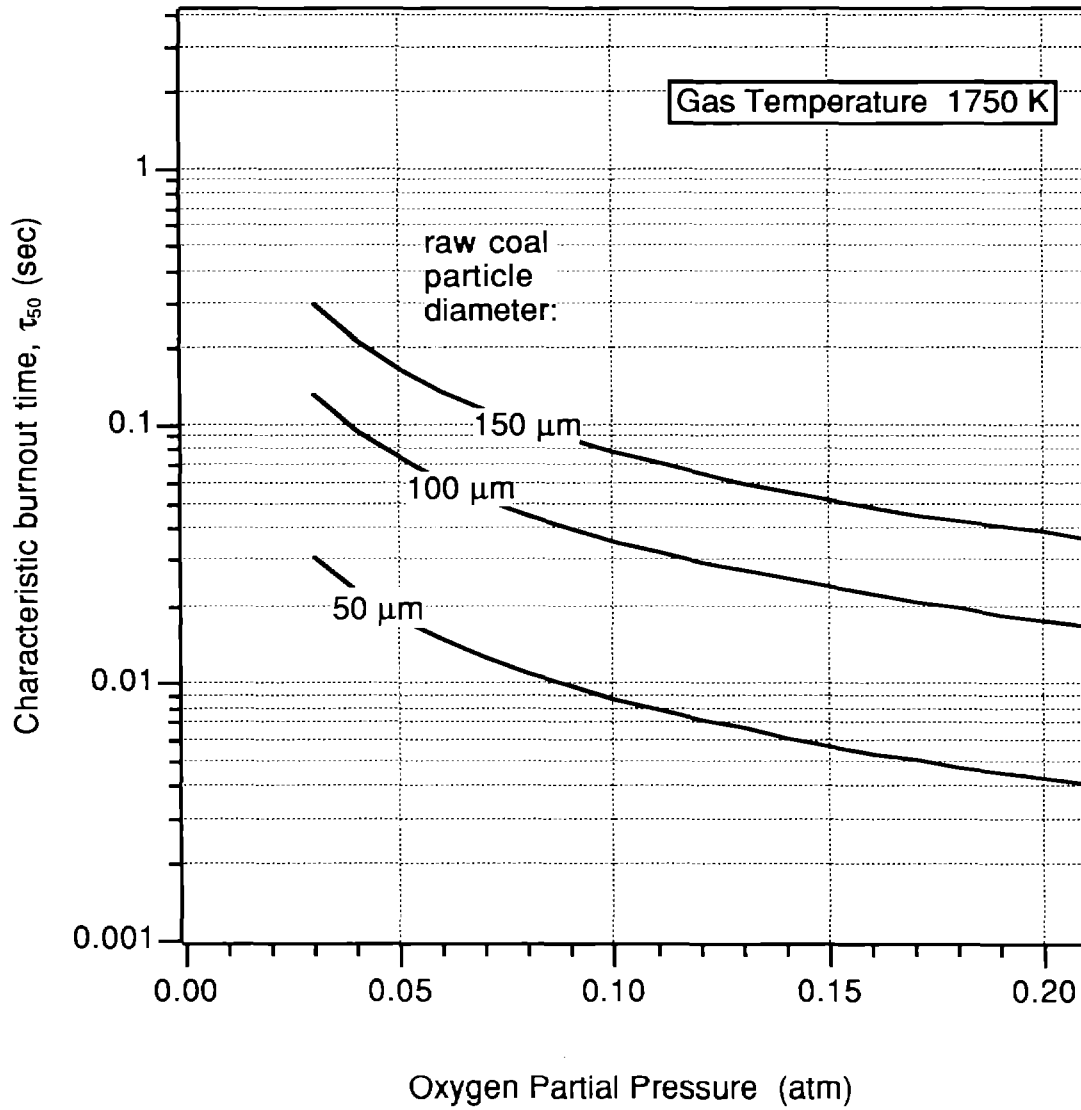


Figure 2.28 Predicted times for 50% completion of char combustion for PSOC-1502D, Hiawatha coal at 1750 K gas temperature.

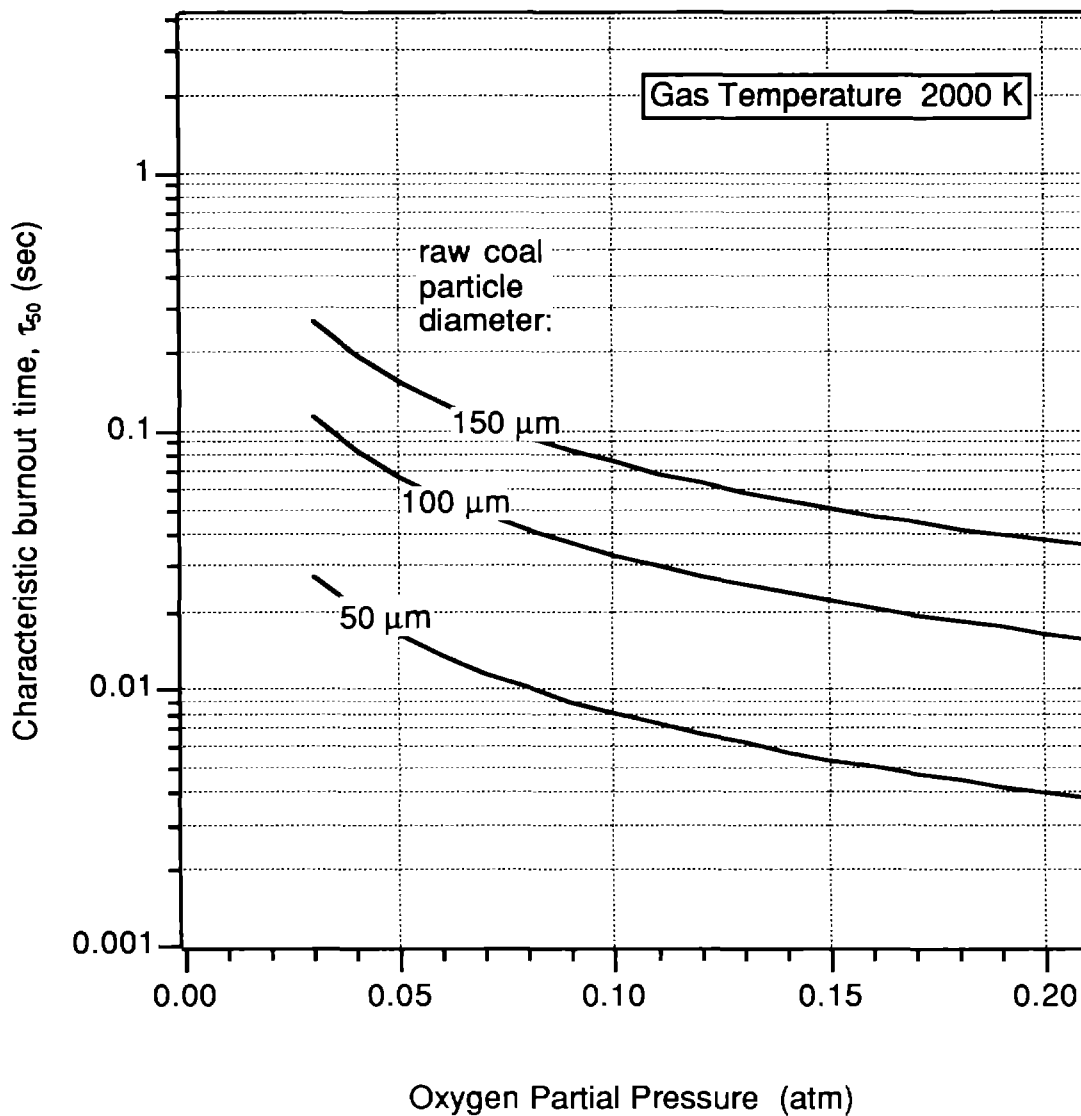


Figure 2.29 Predicted times for 50% completion of char combustion for PSOC-1502D, Hiawatha coal at 2000 K gas temperature.

Table 2.6
Summary of Combustion Parameters for PSOC-1488, Dietz Coal

<p><i>Char oxidation rate parameters</i></p> $q = A \exp(-E/RT_p) P^n$	<p>A E n</p>	<p>Chars burned at their diffusion limited rates (zone 3) in both 6 and 12 mole-% oxygen.</p>
<p><i>Product ratio parameters</i></p> $CO/CO_2 = A_c \exp(-E_c/RT_p)$	<p>A_c E_c</p>	<p>5 x 10⁸ * 60 * kcal / mole</p>
<p><i>Burning mode parameter</i></p> $\rho/\rho_o = (m/m_o)^\alpha$ $d/d_o = (m/m_o)^{(1-\alpha)/3}$	<p>α</p>	<p>0.25</p>
<p><i>Char structural parameters</i></p> $\omega = d_o / d_c$ <p>(linear swelling factor)</p> $\rho_o \equiv \rho \text{ at } z = 6.5 \text{ cm}$ <p>(initial char particle density, daf)</p>	<p>ω ρ_{o,daf}</p>	<p>1.04 0.41 gm / cm³</p>
<p>As an example, this parameter set yields a combustion rate, q, of 0.0072 gm/sq.cm-sec in a gas with a temperature of 1600 K containing 6 mole-% oxygen</p> <p>These product ratio parameters yield an average of 7 mole-% carbon dioxide in the 6 mole-% oxygen environment and 1 mole-% carbon dioxide in the 12 mole-% oxygen environment</p> <p>* These particular parameters should be regarded as empirical parameters, useful for the prediction of burning rates. They do not necessarily have fundamental significance and/or are not necessarily unique for this data set.</p>		

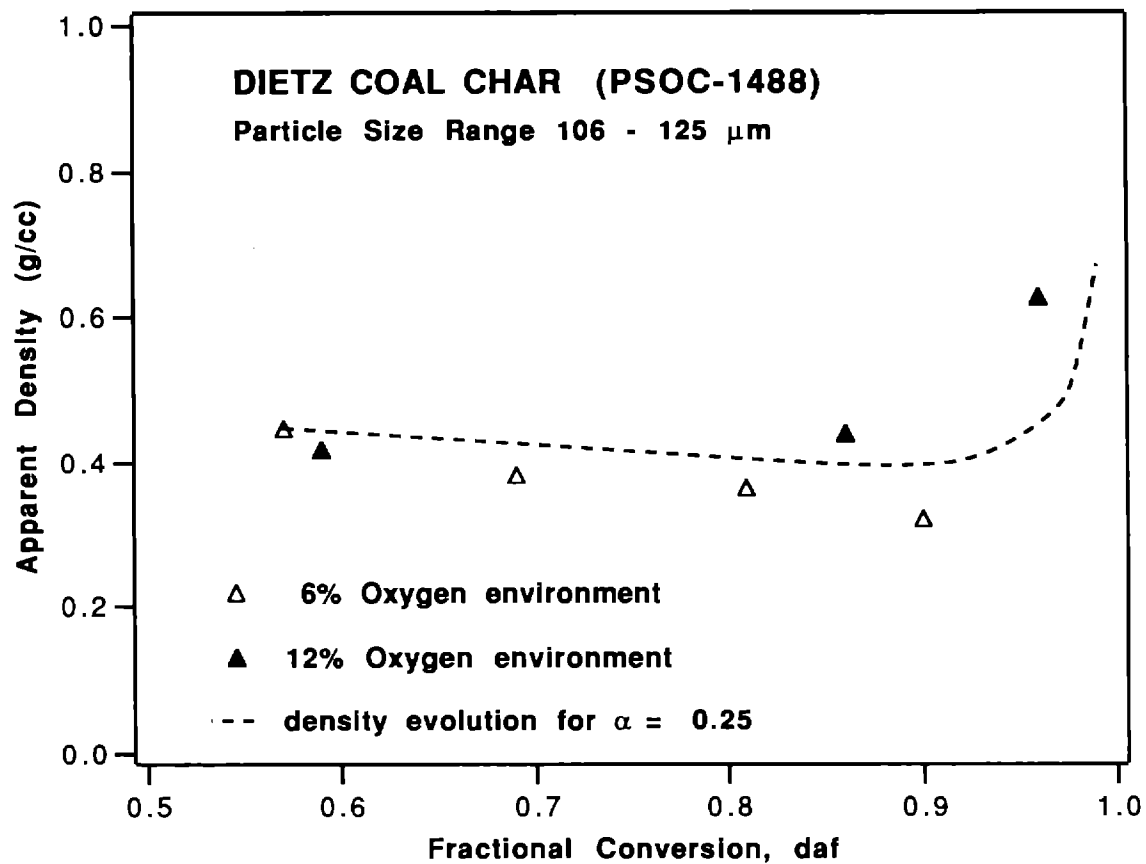


Figure 2.30 Measured (points) and predicted (curve) density evolution for PSOC-1488D, Dietz coal

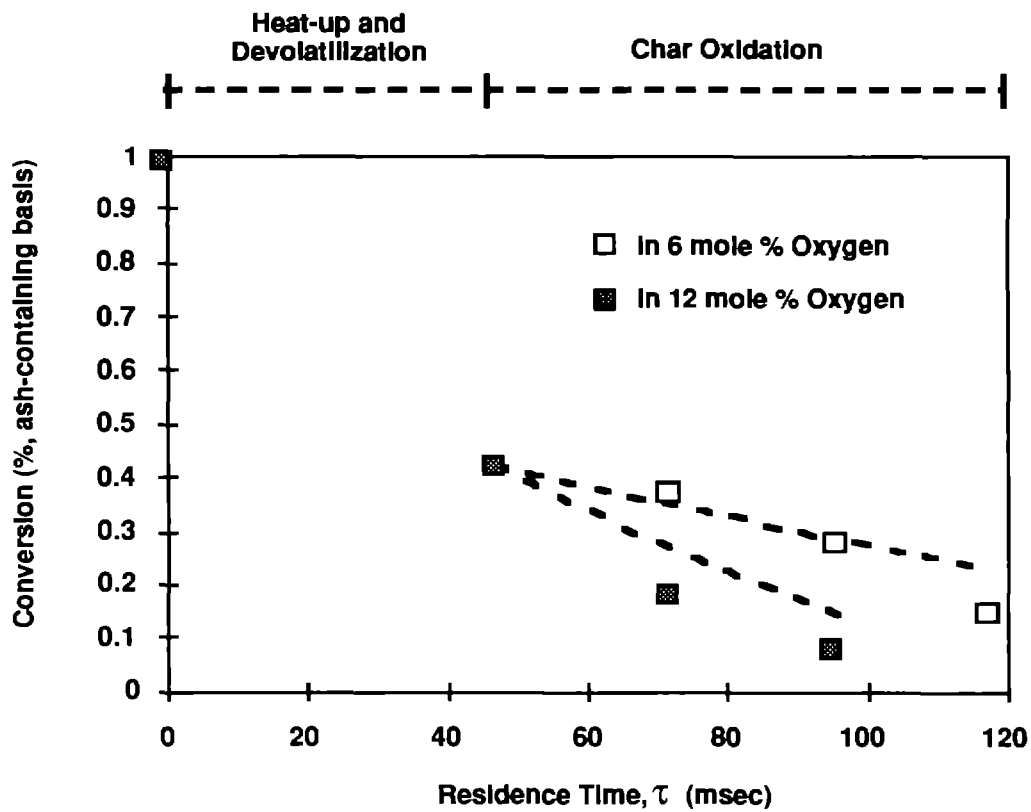


Figure 2.31 Conversion profiles from combustion experiments in the CCL for PSOC-1488D, Dietz coal. Points are determined by inorganic tracer analysis on extracted samples. Curves are predictions using the rate constants derived from optical measurements.

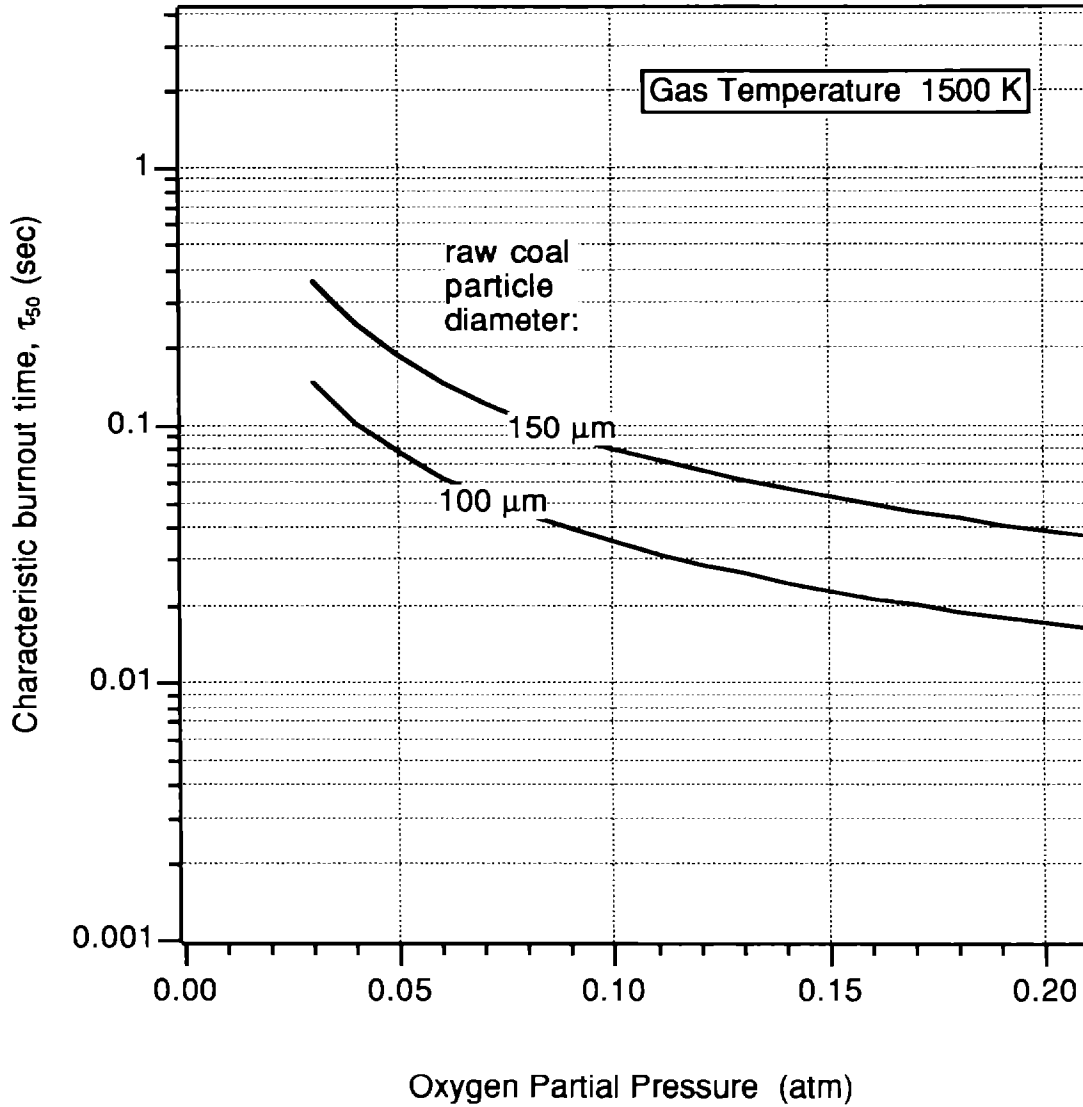


Figure 2.32 Predicted times for 50% completion of char combustion for PSOC-1488D, Dietz coal at 1500 K gas temperature.

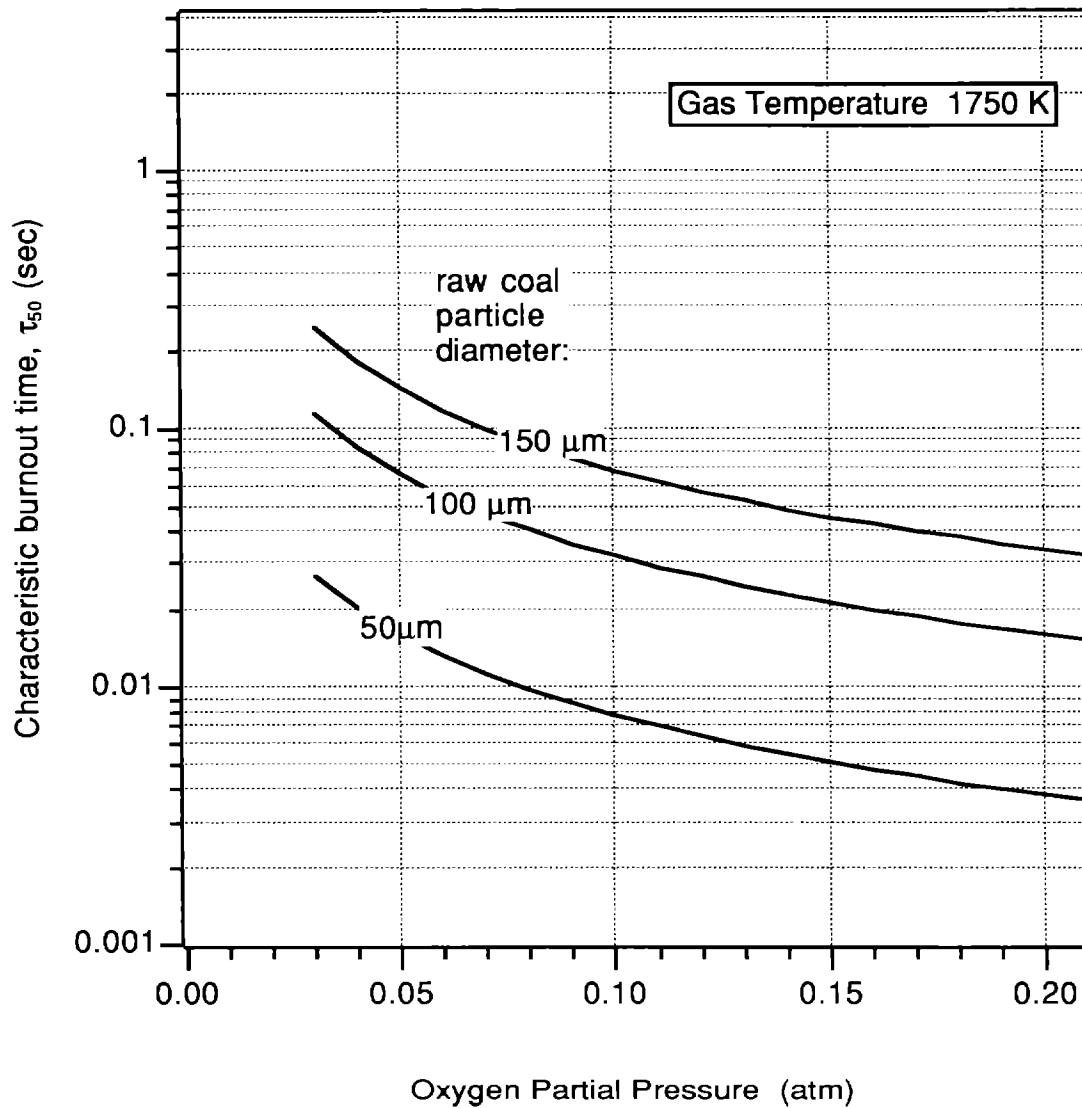


Figure 2.33 Predicted times for 50% completion of char combustion for PSOC-1488D, Dietz coal at 1750 K gas temperature.

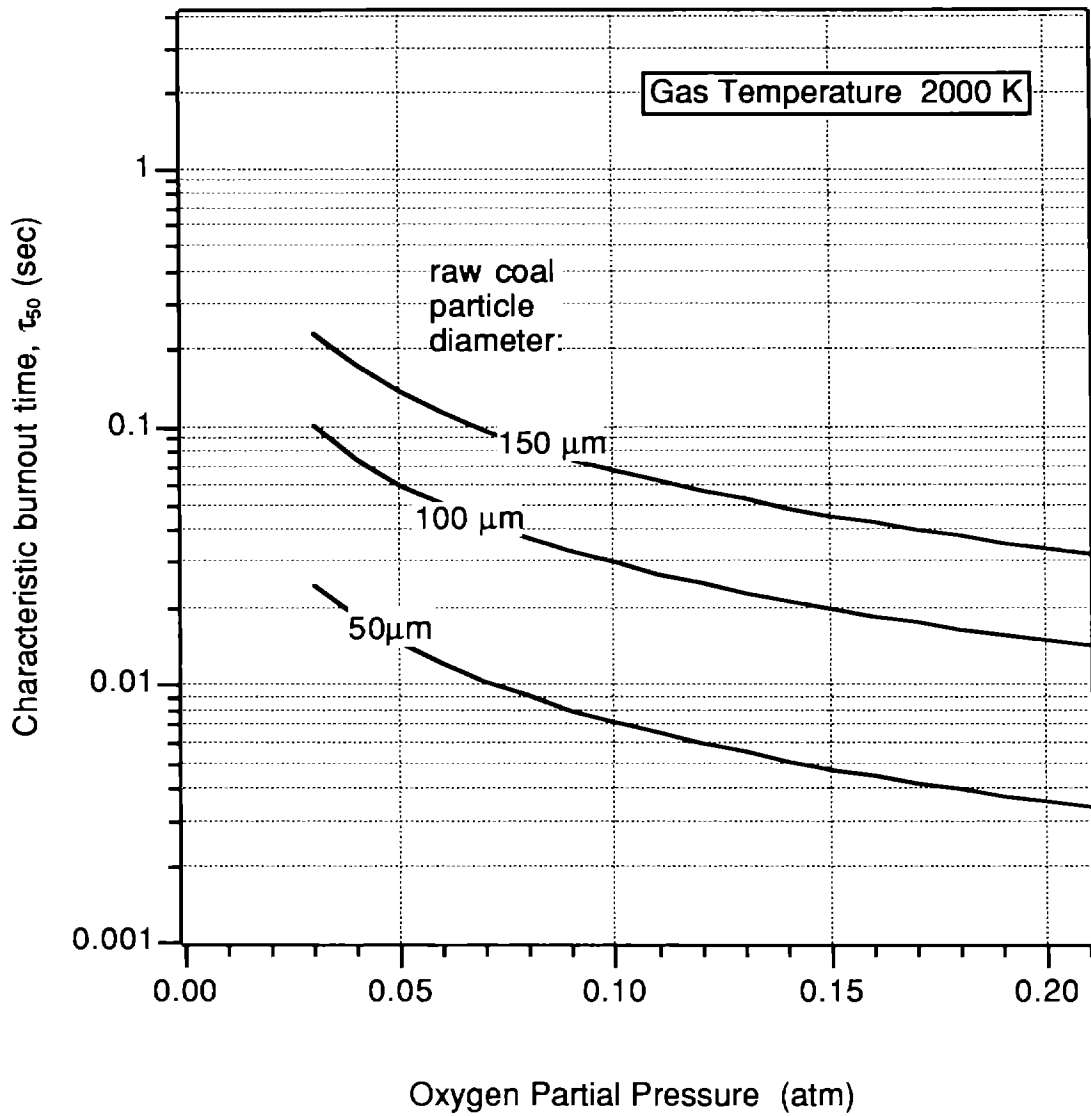


Figure 2.34 Predicted times for 50% completion of char combustion for PSOC-1488D, Dietz coal at 2000 K gas temperature.

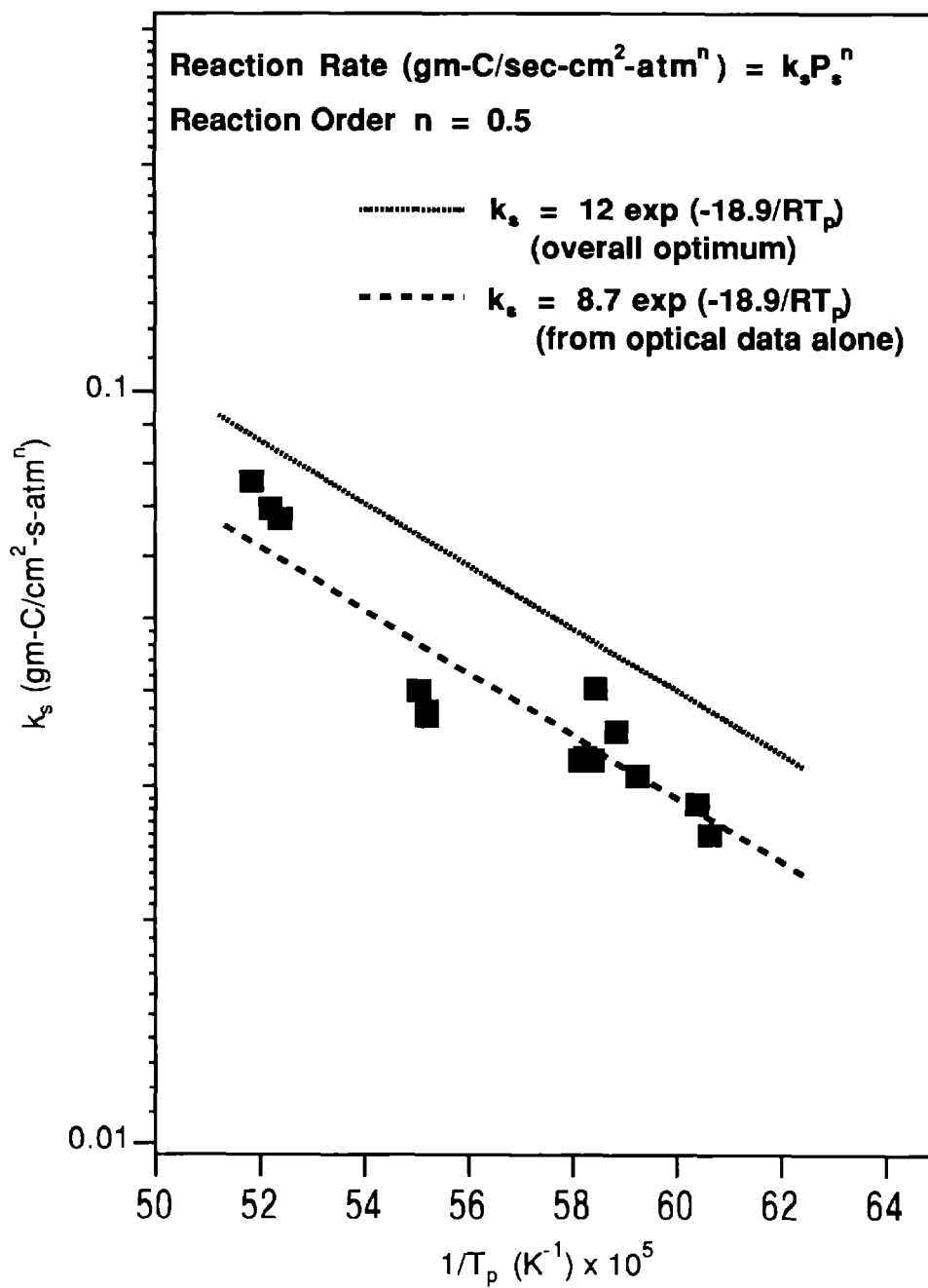


Figure 2.35 Arrhenius diagram and global kinetic parameters for PSOC-1443D Lower Wilcox lignite

Table 2.7
Summary of Combustion Parameters for PSOC-1443, Lower Wilcox Lignite

<p><i>Char oxidation rate parameters</i></p> $q = A \exp(-E/RT_p) P^n$	<p>A</p> <p>E</p> <p>n</p>	<p>12 gm-C / cm²-s-atmⁿ</p> <p>19 kcal / mole</p> <p>0.5 *</p>
<p><i>Product ratio parameters</i></p> $CO/CO_2 = A_c \exp(-E_c/RT_p)$	<p>A_c</p> <p>E_c</p>	<p>5 x 10⁸ *</p> <p>60 * kcal / mole</p>
<p><i>Burning mode parameter</i></p> $\rho/\rho_o = (m/m_o)^\alpha$ $d/d_o = (m/m_o)^{(1-\alpha)/3}$	<p>α</p>	<p>0.3</p>
<p><i>Char structural parameters</i></p> $\omega = d_o / d_c$ <p>(linear swelling factor)</p> <p>$\rho_o \equiv \rho$ at $z = 6.5$ cm</p> <p>(Initial char particle density, daf)</p>	<p>ω</p> <p>ρ_{o,daf}</p>	<p>0.92</p> <p>0.62 gm / cm³</p>
<p>As an example, this parameter set yields a combustion rate, <i>q</i>, of 0.0054 gm/sq.cm-sec for a 100 μm particle in a gas with T_g = 1600 K containing 6 mole-% oxygen</p> <p>These product ratio parameters yield 3 mole-% carbon dioxide at 1900 K and 17 mole-% carbon dioxide at 1700 K</p> <p>* These particular parameters should be regarded as empirical parameters, useful for the prediction of burning rates. They do not necessarily have fundamental significance and/or are not necessarily unique for this data set.</p>		

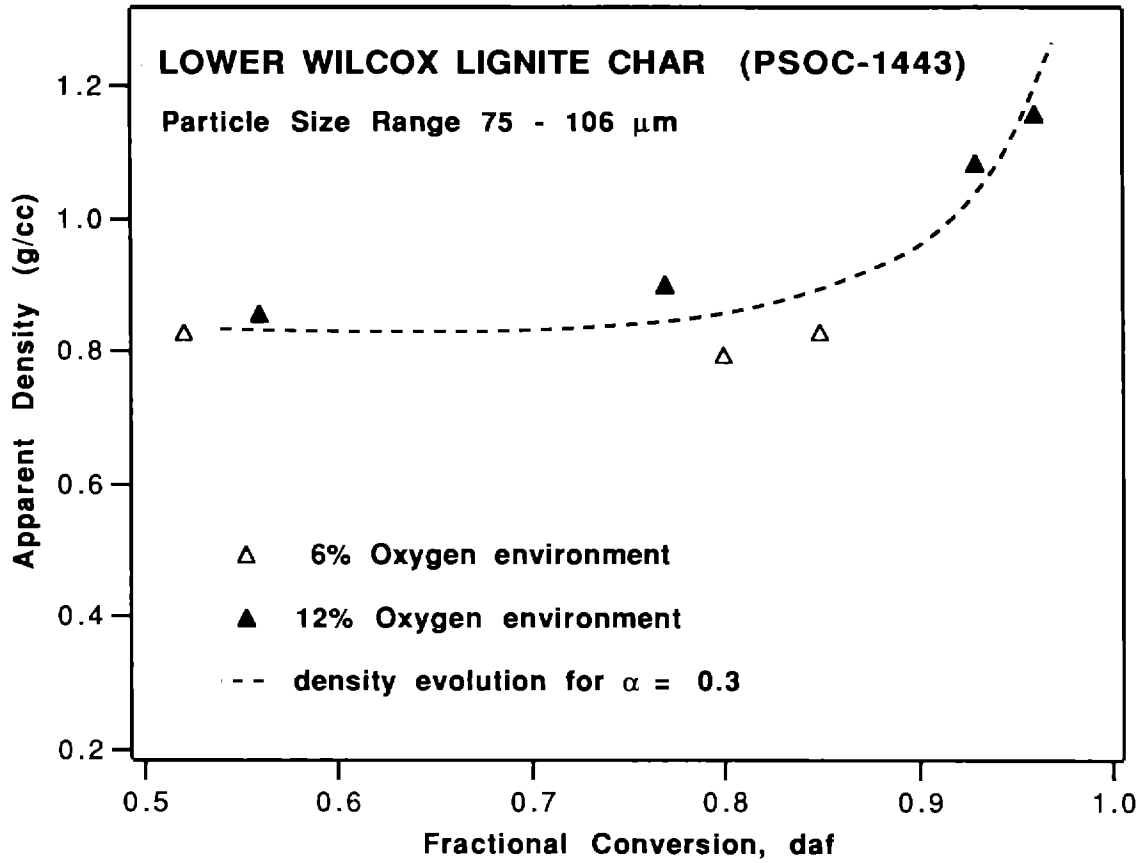


Figure 2.36 Measured (points) and predicted (curve) density evolution for PSOC-1443D, Lower Wilcox lignite

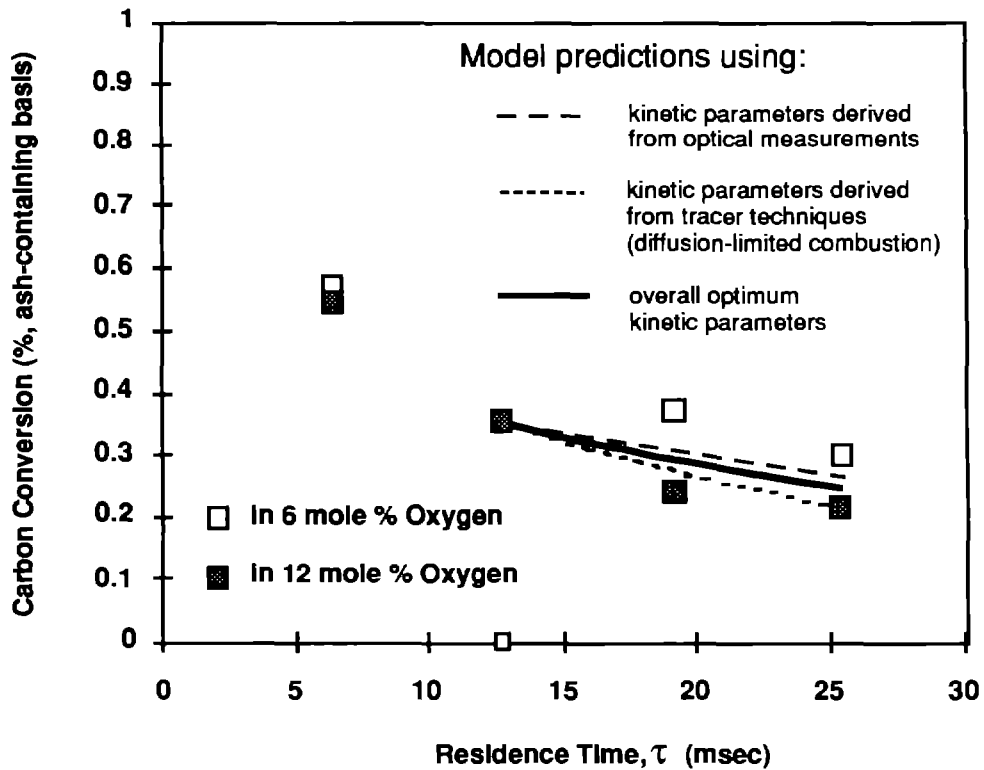


Figure 2.37 Conversion profiles from combustion experiments in the CCL for PSOC-1443D, Lower Wilcox lignite. Points are determined by inorganic tracer analysis on extracted samples. Curves are predictions using the rate constants derived from optical measurements.

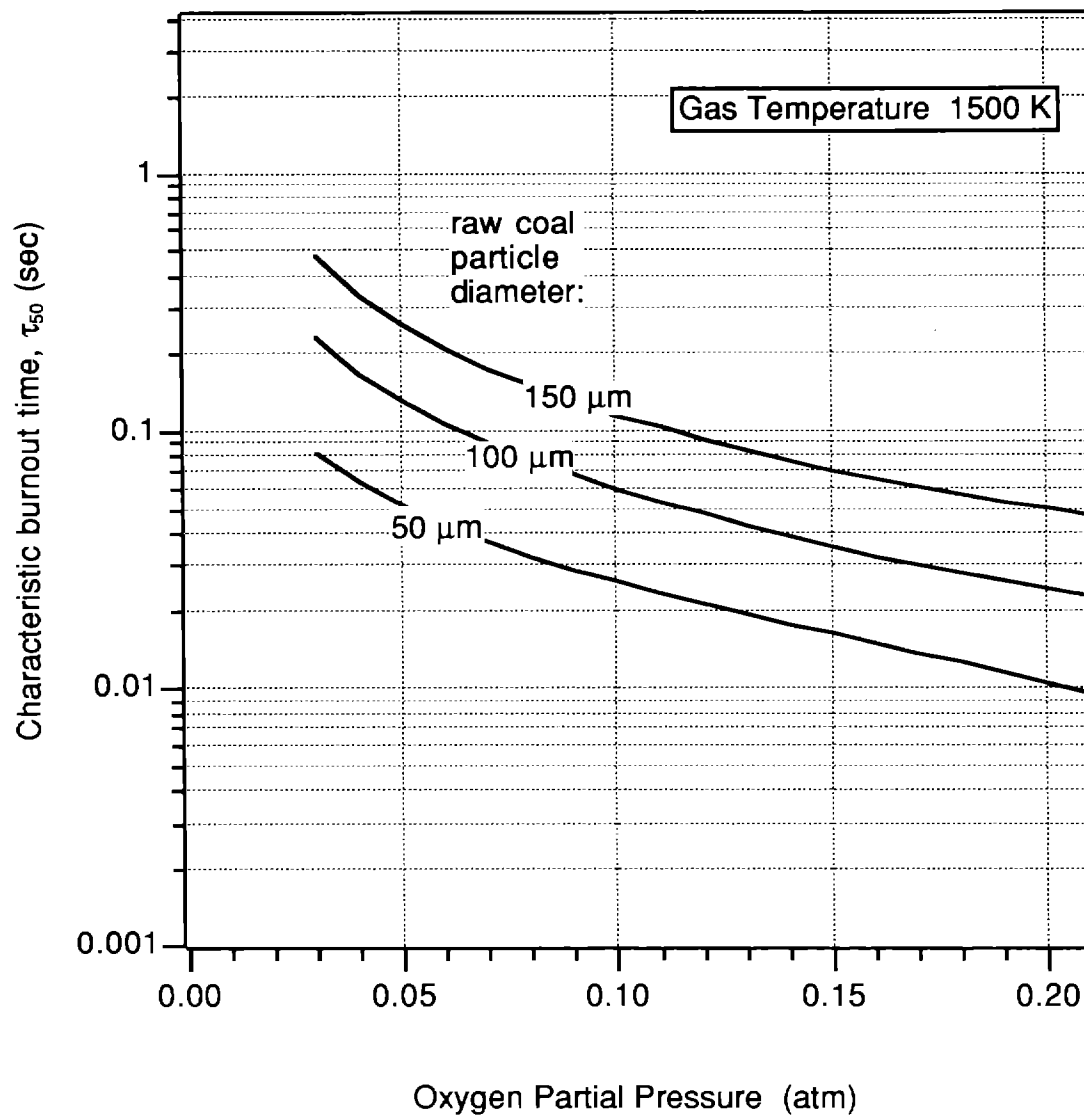


Figure 2.38 Predicted times for 50% completion of char combustion for PSOC-1443D, Lower Wilcox lignite at 1500 K gas temperature.

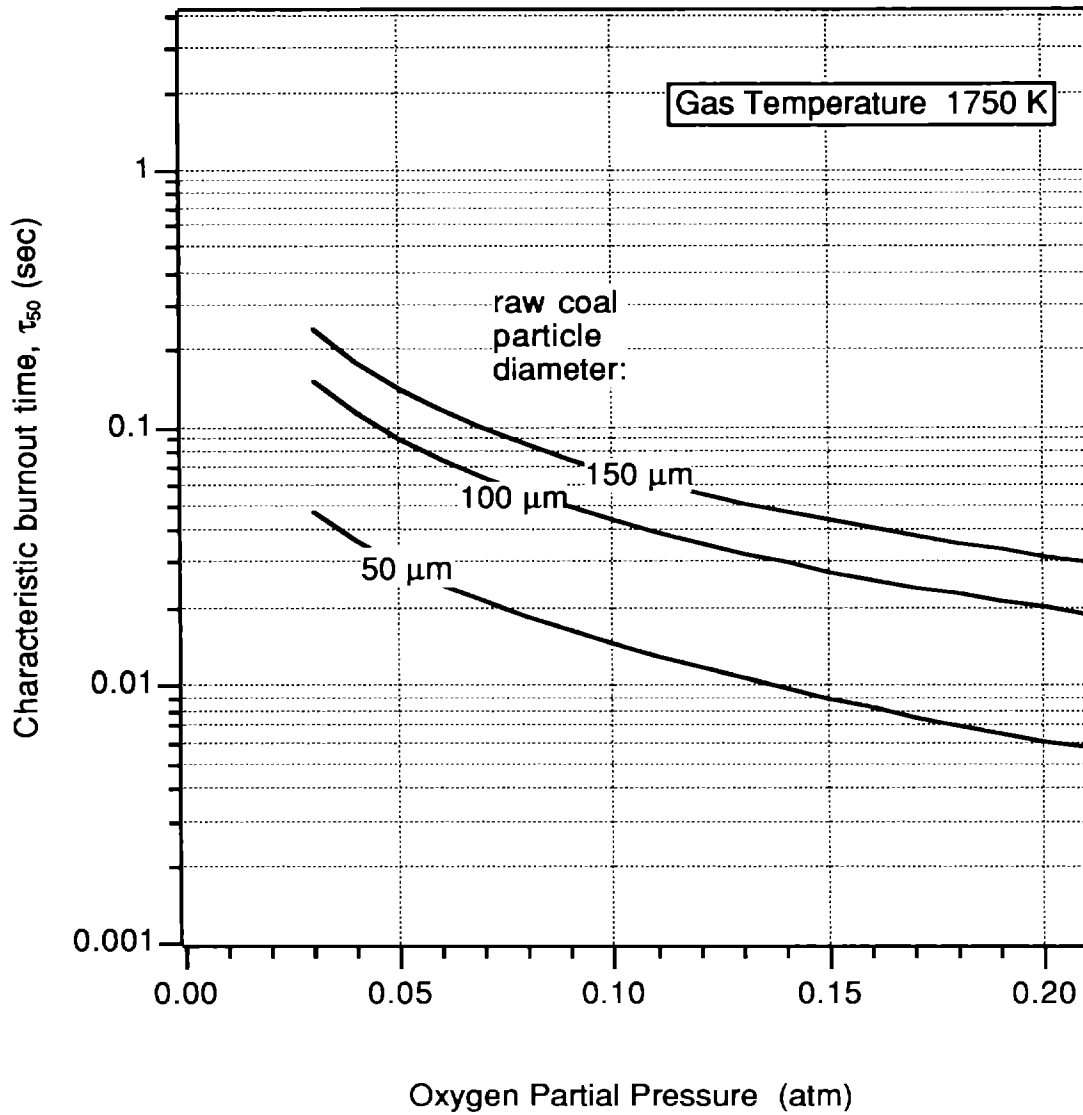


Figure 2.38 Predicted times for 50% completion of char combustion for PSOC-1443D, Lower Wilcox lignite at 1750 K gas temperature.

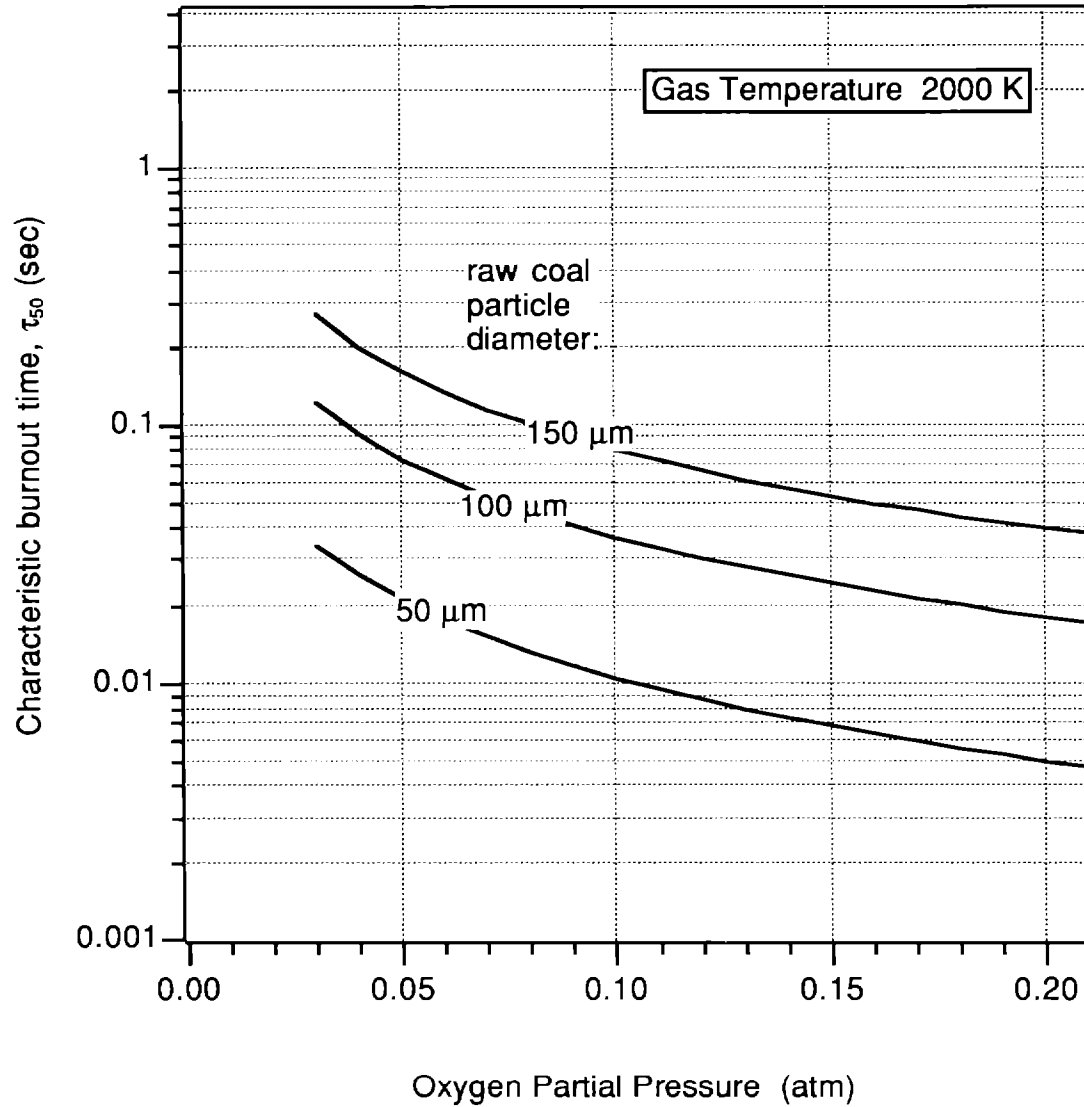


Figure 2.38 Predicted times for 50% completion of char combustion for PSOC-1443D, Lower Wilcox lignite at 2000 K gas temperature.

Discussion

A detailed discussion of the complete data/analysis set, including an identification of reactivity trends, will appear in the next quarterly report. A few important points are made here about the analyses presented to date.

For six of the seven coals investigated, the model of heterogeneous chemical kinetics and transport phenomena adequately describes the data from both the optical technique and from bulk analyses of extracted samples.[†] Two of the coals (PSOC-1502 Hiawatha and PSOC-1488, Dietz) react at or very near their diffusion-limited rates under conditions in the CCL experiments. For these coals, the assumption of diffusion-limited burning is adequate to describe the particle temperatures as well as the mass conversion determined by tracer techniques. No values of A , E , or n can be obtained in these cases. There is nevertheless much information to be extracted from the experimental data in such cases, including burnout time predictions over a wide range of conditions. The burnout time predictions for the diffusion-limited cases are generated based on the following argument.

For PSOC-1502 and PSOC-1488, the CCL experiments established that the combustion rate was within 5% of its diffusion-limit under each experimental condition investigated. Specifically it can be stated for these coals that a 100 μm particle reacts at 95% or greater of its diffusion limited rate at a gas temperature of 1600 K and an oxygen particle pressure of 6 mole-%. If a reaction order of 1/2 and a typical activation energy of 20 kcal/mol are now assumed, a preexponential factor can be computed to arrive at 95% of the diffusion-limited rate under this set of conditions. This set of A , E , and n yield the slowest possible combustion rates under CCL conditions that are still indistinguishable from diffusion-limited burning. Using this parameter set, one can then determine the range of conditions (T_g , P_g , d_p) throughout which the combustion rate is *within 10%* of its diffusion-limited value. Within this range the assumption of diffusion-limited burning will be adequate for these coals and outside of this range no predictions can be made with the information available.

[†] PSOC-1443 Lower Wilcox lignite is an exception, for which the optical data cannot be completely reconciled with the measurements of overall burning rate by tracer techniques. The tracer measurements are consistent with diffusion-limited combustion, while the measured particle temperatures are indicative of somewhat slower combustion and thus finite kinetics. The source of this discrepancy has not been identified. Particle fragmentation or errors in the measurement of particle density are possible explanations. In either case, Lower Wilcox lignite is a reactive, low-rank coal that oxidizes at, or slightly below, its diffusion-limited rate under conditions in the CCL. For the practical goal of predicting combustion rates of chars from this coal, a set of kinetic parameters is presented that best describes the data from both the optical and tracer techniques. This set of kinetic parameters should yield an adequate prediction of the combustion rate for most purposes.

For the non-diffusion-limited cases, burnout time predictions are presented in the parameter range: $0.03 < P_g < 0.21$; $d_p = 50, 100, 150 \mu\text{m}$; and $T_g = 1500, 1750,$ and 2000 K . For the coals whose rates are diffusion-limited in the CCL, the calculation indicates that burnout time predictions are still accurate for this same range with the exclusion of the $50 \mu\text{m}$ diameter prediction at 1500 K . For $50 \mu\text{m}$ particles at 1500 K gas temperature the diffusion-limited assumption may be in error by as much as 20%.

For each of the diffusion-limited coals, therefore, accurate burnout time predictions are presented over the parameter range specified above, with the exclusion of the $50 \mu\text{m}$ diameter prediction at 1500 K . There is, clearly, much information contained in the single observation that a given coal reacts at its diffusion-limit during conditions present in CCL experiments.

In most cases the inclusion of limited CO_2 formation at the lower temperatures found in the 6 mole-% O_2 environment results in an improved fit to the data. For some applications, a kinetic expression may be required that does not account for CO_2 production. In such cases it is recommended that the same reported values of A , E , and n be used. Sample calculations were performed which indicate that this approach yields a reasonable approximation for the overall burning rate under conditions present in CCL experiments. The particle temperatures do, however, tend to be underpredicted when CO_2 formation is neglected.

SUBTASK 2.3 CHAR REACTIVITY AT HIGH CARBON CONVERSION

During this quarter, the literature was reviewed on the topic of unburned carbon in fly ash and on the evolution of carbon properties and reactivity during the combustion process. Several experiments were also performed to identify the origin of the broad distribution of single-particle temperatures observed at any one measurement location. The goal of these experiments is to understand the relative contributions of: (a) temperature measurement errors, (b) variations in physical properties, and (c) variations in reactivity to the observed distributions of particle temperatures.

Char particles from PSOC-1508D Pocahontas #3 coal were injected into a 0% oxygen environment and the distributions of (nonburning) particle temperatures were measured. The particle temperatures in 0% O_2 are *not* affected by reactivity differences and can thus be used, in connection with our model of particle-gas transport to calculate the particle-to-particle variability in physical properties. Having thus characterized the variability in physical properties, the data in oxidizing environments can be reanalyzed to quantify the particle-to-particle variability in *reactivity*. The data taken to date suggest that variations in reactivity are responsible for much of the distribution of particle temperatures observed at low-to-intermediate carbon conversion. At high carbon conversion, in contrast, much of the distribution is believed to be attributable to the presence of extinguished or nearly-extinguished, high-ash content particles near burnout (Mitchell, 1990). It is anticipated that the observed particle-to-particle variations in reactivity have an important influence on

carbon reactivity at high conversion. Kinetic rate expressions that account for the particle-to-particle variations in reactivity are likely needed to accurately predict the carbon content in fly ash samples from laboratory or commercial combustors. Future work will need to carefully consider the connection between heterogeneity in the particle population and unburned carbon content in fly ash.

PLANS FOR NEXT QUARTER

During the next quarter, kinetic parameters will be determined for the remaining three coals in the PSOC suite and the data compilation will be completed. Under subtask 2.2, reactivity measurements will be performed on chars previously collected from the CCL under various devolatilization conditions. Under subtask 2.3, results of the literature search and scoping experiments will be used to formulate a research plan on the topic of carbon reactivity at high conversions. The plan will identify research priorities on both the fundamental and applied aspects of this problem and will serve to define and delineate the related PETC and EPRI programs for FY92.

Reactivity measurements will also be performed on another proprietary coal-derived product and the results will be reported to PETC under separate cover.

NOMENCLATURE

A	preexponential factor
A_c	preexponential factor in the correlation for CO/CO ₂ ratio
d_o, d_c	particle diameter or unreacted char, coal
E	activation energy for the combustion reaction
E_c	activation energy in the correlation for CO/CO ₂ ratio
k_s	rate constant
m_p, m_c	mass of particle, mass of carbonaceous material in particle
n	reaction order
P_g	partial pressure of oxygen in the bulk gas
q	combustion rate (g C/s-m ² -external surface)
R	gas constant
T_g	gas temperature
T_p	particle temperature
z	height above burner

Greek symbols

α	mode of burning parameter
ρ_o, ρ_c	particle density of unreacted char, coal
$\rho_{o,daf}$	dry ash-free particle density,
$\rho_{o,daf}$	initial daf char density corrected for swelling
τ_{50}	characteristic time for 50% carbon conversion
ω	swelling factor

REFERENCES

Hurt, R. H., and D. R. Hardesty, "Task 2: Rates and Mechanisms of Coal Char Combustion," in Coal Combustion Science--Quarterly Progress Report, Hardesty, D. R. (ed.), Sandia Report SAND91-8217 (1991).

Hurt, R. H., D. R. Dudek, J. P. Longwell, and A. F. Sarofim, *Carbon* **26**:4 433 (1988)

Mitchell, R. E. *Twenty-Second Symp. (Int.) on Comb.*, The Combustion Institute, Pittsburgh, Pennsylvania, P. 69 (1988)

Mitchell, R. E. *Twenty-Third Symp. (Int.) on Comb.* The Combustion Institute, Pittsburgh, Pennsylvania, (1990)

PUBLICATIONS, PAPERS, AND PRESENTATIONS

A manuscript entitled: "On the Combustion Kinetics of Heterogeneous Char Particle Populations" by R. H. Hurt and R. E. Mitchell was submitted to the American Chemical Society Fuel Chemistry Division in May. The manuscript will appear as a preprint for the ACS meeting in New York, N.Y. in August 1991.

An article entitled "Role of Microporous Surface Area in Uncatalyzed Carbon Gasification," by R. H. Hurt, A. F. Sarofim (MIT), and J. P. Longwell (MIT) appeared this quarter in *Energy and Fuels*, **5**:2, 290 (1991).

PROJECT TITLE: COAL COMBUSTION SCIENCE
TASK 3: THE FATE OF MINERAL MATTER

ORGANIZATION: Sandia National Laboratories, Livermore

CONTRACT: FWP 0709

REPORTING PERIOD: April 1, 1991 - June 30, 1991

REPORTED BY: L. L. Baxter and D. R. Hardesty
Phone: FTS 234-2862 and 234-2321

OBJECTIVES FOR TASK 3

The long-term objective of this task is to gain quantitative understanding of the rates and mechanisms of selected aspects of mineral matter evolution, transport and deposition under conditions relevant to pulverized coal combustion. These selected aspects of mineral matter evolution include: (1) release of inorganic material from coal particles during reactions of the organic and inorganic portions of the particle and by vaporization; (2) changes in mineral matter composition during combustion; (3) size distributions of fly ash formed during coal combustion; and (4) deposition of mineral matter on surfaces. These aspects of mineral matter evolution will be studied as a function of coal and mineral type, total ash loading, rate of organic and inorganic reaction, local gas conditions, and time.

The focus of research during FY91 is on (i) the release of inorganic material during coal devolatilization, (ii) the evolution of particle and fly ash size distributions, and (iii) theoretical and experimental studies of ash deposition. Three subtasks are defined to address these issues.

SUBTASK 3.1 RELEASE OF INORGANIC MATERIAL DURING COAL DEVOLATILIZATION AND CHAR OXIDATION

The goal of this subtask is to test the hypothesis that some inorganic species are released from coal particles during coal devolatilization and char oxidation. Particular focus is on mechanisms of release other than ash vaporization. Material release effected by coal devolatilization involves the small-grained and organically-associated minerals, many of which are strongly implicated in deposit formation in commercial-scale boilers. Mineral release associated with inorganic reactivity includes thermally unstable or chemically reactive material such as pyrite and calcite, both of which play significant roles

in deposit formation and properties. This subtask uses data collected in each of the three coal reactors at Sandia and tests several ranks of coal at several rates of devolatilization.

SUBTASK 3.2 THE EVOLUTION OF PARTICLE AND FLY ASH SIZE DISTRIBUTIONS

The goal of this subtask is to determine the extent of char fragmentation during pulverized coal combustion. This is accomplished by measuring the particle size distributions of the char and fly ash and relating these through a mathematical model. The model indicates the number of fly ash particles generated per original char particle, both for the overall fuel and as a function of size. These results are collected as a function of coal rank and of ash loading. Also reported under this subtask is progress in evaluating and improving the accuracy and precision of the computer-controlled scanning electron microscope (CCSEM) technique for measuring mineral grain size and composition. CCSEM is the basis of a great deal of current coal and fly ash characterization research in the US and has the potential of providing unique and valuable insights into the evolution of particle and fly ash size distributions.

SUBTASK 3.3 THEORETICAL AND EXPERIMENTAL STUDIES OF ASH DEPOSITION

Theoretical and experimental investigations of ash deposition are being conducted to determine the elemental composition of deposits as a function of coal type, boiler operating conditions, and deposit location within a boiler. The effect of deposit formation on heat transfer efficiency through simulated boiler tubes and waterwalls is also being studied. The mechanisms of deposit formation are being combined into an engineering model that predicts elemental deposit composition.

SUMMARY OF TECHNICAL PROGRESS DURING THIS QUARTER

During this quarter, analyses of elemental release rates from a spherical oil agglomerate product (SOAP) were conducted in the CCL. This work was done in cooperation with R. H. Hurt. Overall mass loss is determined as a function of residence time within approximately 10 relative percent. From these data, the release of inorganic and organic constituents of the SOAP are determined.

Of the eight major inorganic components of SOAP, only two were found to be released to the gas phase in appreciable concentrations during combustion. These are sodium and potassium, both alkali metals. At the latest stage of combustion monitored during these tests (95 ms), approximately 35 and 50 percent of these elements, respectively, is released.

Elemental release rates of the organic constituents is also presented. Hydrogen and oxygen were found to leave the SOAP rapidly during devolatilization, leaving much smaller fractions of the original mass of these elements in the char than of any other elements. During char combustion, hydrogen and oxygen continue to leave the char and continue to be the most highly depleted components of the original coal. Sulfur behaved

similarly, although the preferential loss of sulfur is significantly lower than that for either hydrogen or nitrogen. Fractional loss of nitrogen only slightly exceeds that of overall mass. Carbon loss is slightly less than that of overall mass. These results are consistent with similar calculations for pulverized coal under similar conditions.

Also during this quarter, analyses of char fragmentation were completed for coals with a broad variation in rank, geographic origin, ash loading, and ash type. Results indicate that the extent of fragmentation increases with increasing initial char diameter, decreases with increasing ash loading, increases with increasing rank, and is sensitive to mineral grain size distribution. These results are consistent with results reported earlier for a smaller suite of coals.

SUBTASK 3.1 RELEASE OF INORGANIC MATERIAL DURING COAL DEVOLATILIZATION AND CHAR OXIDATION

During this quarter, elemental release rates of organic and inorganic constituents of the Spherical Oil Agglomerate Product (SOAP) prepared from an Illinois #6 coal were completed. Release rates of the major organic and inorganic constituents were determined for three samples of size-classified particles introduced into the laminar flow reactor of the Char Combustion Laboratory (CCL). The samples were exposed to a vitiated flow at approximately 1700 K containing 12 % O₂ for residence times of 47, 72, and 95 ms, respectively. Overall residual mass is determined by using silicon, aluminum, and titanium as tracers. The tracer values are found to be consistent with one another but, in the SOAP experiments, to differ systematically from the ratio of the coal fed to the mass collected on the filter, with the latter being as much 50 % lower than the tracer techniques. Therefore, the mass balance numbers are not used in the analysis.

Size-classified (106-125 μm) samples of SOAP are used in this study. The samples are derived from a drum of SOAP pellets shipped to Sandia by Asea Brown Boveri-Combustion Engineering (CE) by way of PSI Technology Co. The elemental composition of the size classified sample is indicated in Table 3.1. The composition of this size classified sample is similar to that reported by CE for the overall sample with the exception of the iron content. The CE results are also included in Table 3.1 for comparison. The most probable explanation for the difference in iron content is that pyrite (or other iron-containing minerals) is concentrated in the relatively large 106-125 μm size fraction of the ground SOAP. (This postulate is supported by the sulfur analyses that will be discussed later).

Figure 3.1 illustrates the residual particle mass as a function of time for this coal-derived product. Results are presented on both a total mass and a dry ash free (daf) basis. The error bars for the overall residual mass data indicate 95 percent confidence intervals in the data as determined by comparing results from several independently measured tracer concentrations (Si, Al, and Ti) and applying standard statistical techniques. Typically, the overall mass loss is determined within 10 relative percent.

These mass loss data allow calculation of the fractional elemental loss of the components of the particle. Results from these calculations are indicated in Figure 3.2. Figure 3.2a

indicates inorganic materials that did not leave the coal in appreciable quantities. This includes six of the eight major inorganic components indicated in Table 3.1. The elemental composition of the raw material was measured only once and no experiments were repeated. This prevents calculation of error bars for the elemental mass loss data by normal procedures. This probably also accounts for the small but nearly constant deviation of some of the elemental release data from the zero baseline. That is, a small error in the original concentration of one of these components will produce such results (SiO₂ and TiO₂ are examples in these data).

Table 3.1

Analysis of the inorganic components of the 106-125 μm size fraction of SOAP (Sandia results) compared with an analysis of the overall composition of the inorganic components of SOAP [Nsakala et al., 1991]

Oxide	Sandia Results		CE Results	
	% of Dry Coal	% of Ash	% of Dry Coal	% of Ash
SiO ₂	1.600	33.4	1.73	41.1
Al ₂ O ₃	0.775	16.2	0.85	20.3
TiO ₂	0.102	2.1	0.11	2.56
Fe ₂ O ₃	2.040	42.5	1.10	26.2
CaO	0.142	3.0	0.15	3.47
Na ₂ O	0.055	1.1	0.10	2.35
K ₂ O	0.062	1.3	0.10	2.45
MgO	0.052	1.1	0.060	1.43
Sum of Oxides	4.8	100.7	4.20	99.9
Total Ash	4.8	100	4.21	100

Sodium and potassium, the only alkali metals whose concentrations are monitored, are observed to leave the particles in significant quantities, as illustrated in Figure 3.2b. During the first 100 ms of combustion, approximately 50 percent of the potassium and 35 percent of the sodium escapes the reacting samples. The mechanism by which these elements leave the SOAP is probably associated with convective transport by coal volatiles and tar during the first 50 ms, but is most likely a vaporization process thereafter.

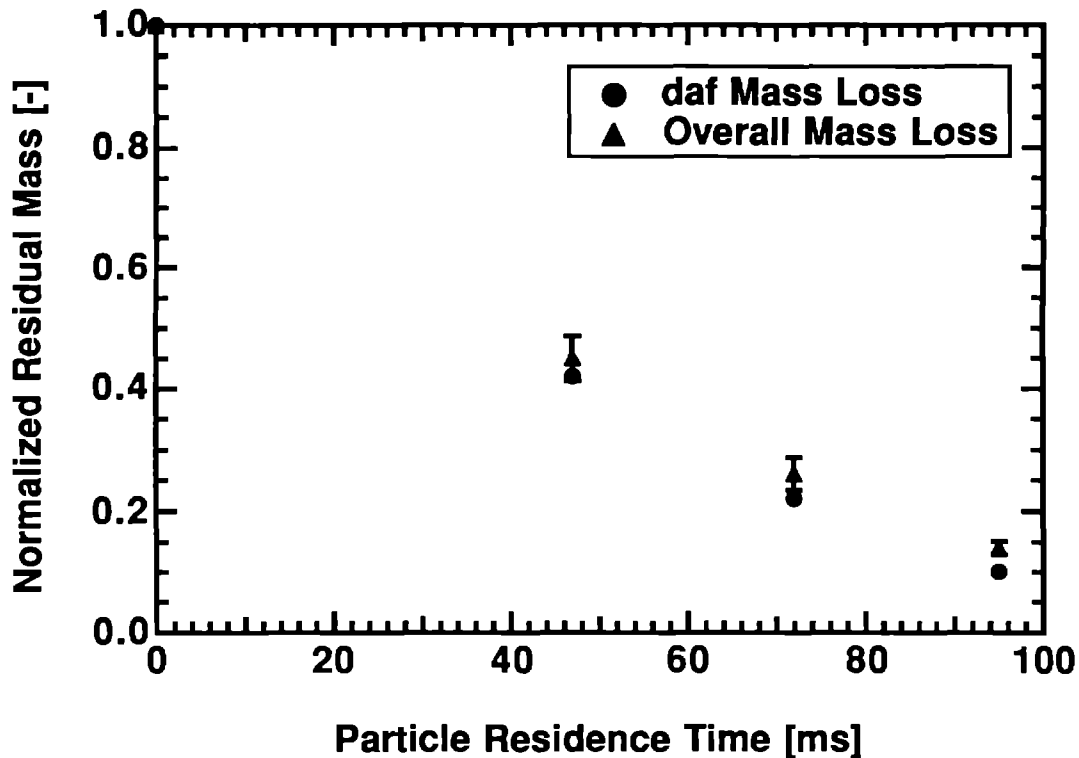


Figure 3.1 Mass loss data for a 106-125 μm size fraction of the spherical oil agglomerate product (SOAP) in the CCL in a 12 mole percent oxygen environment.

The elemental release rates of the remaining components of the SOAP during combustion are illustrated in Figure 3.3, where the fractional mass loss is plotted against total overall daf mass loss. An indication of the initial amounts of each of these elements, for both the 106-125 μm size fraction and for the unclassified product, is included in Table 3.2. Note that the sulfur determination in the Sandia results is not done by difference as is common in many analyses. Therefore, the sum of the elemental analysis does not equal 100 percent. The significantly higher sulfur content in the Sandia sample is consistent with the indication from the inorganic analysis that the coal contains a higher pyritic iron fraction. The higher oxygen content of the Sandia sample probably is an indication of weathering. Otherwise, the two samples are quite similar.

The data indicate that the total amount of hydrogen and oxygen released from the coal particle at the indicated stages of overall burnout is significantly higher than the overall mass. Similarly, total sulfur release is somewhat higher and total nitrogen release slightly higher than overall mass at these stages of combustion. Total carbon release is

slightly lower than overall mass release. In each case, these data are consistent with similar data collected in the CCL for coal particles.

In summary, the combustion behavior of SOAP appears similar to that of pulverized coal when viewed from the perspective of elemental release rates of the inorganic and organic constituents.

Data packages summarizing other work performed in the CCL in support of this subtask are being prepared. These packages include the complete statistical analyses of the release rates of the organic and inorganic species as a function of particle residence time, local oxygen concentration, and coal rank. These data packages are discussed in more detail under Task 2 of this report.

Table 3.2

Analysis of the organic components of the 106-125 μm size fraction of SOAP (Sandia results) compared with an analysis of the overall composition of the organic components of SOAP [Nsakala et al., 1991]

Oxide	Sandia Results		CE Results	
	As Received	Dry Ash-Free	% Dry Coal	Dry Ash-Free
C	72.4	77.33	75.7	79.10
H	4.42	4.72	5.8	6.06
O	12.97	13.85	9.9	10.34
N	1.4	1.50	1.5	1.57
S	3.26	3.48	2.8	2.93
Moisture	1.57			
Ash	4.80		4.3	
Total	100.82	100.88	100.0	100.0

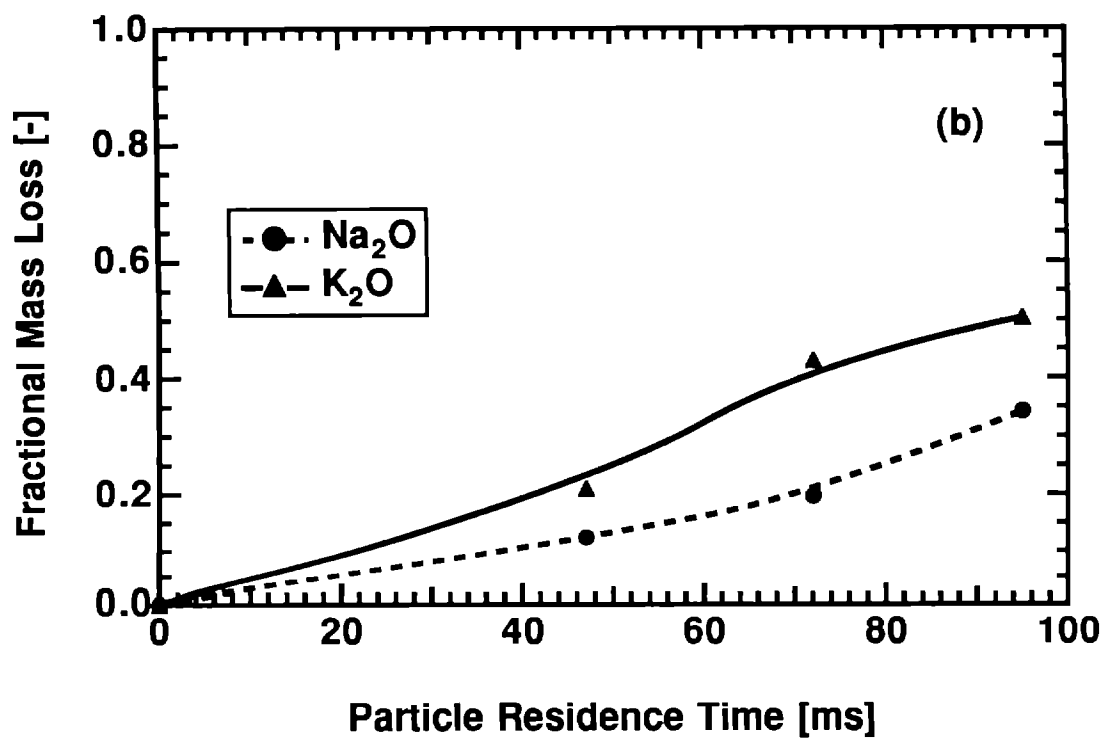
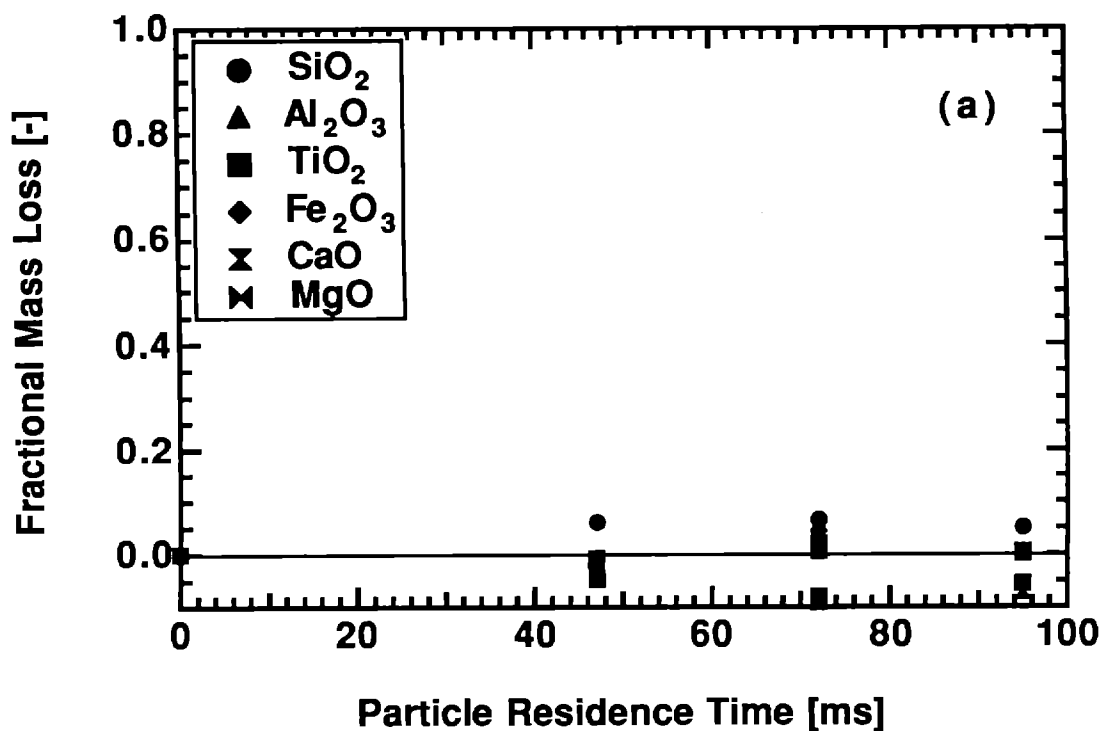


Figure 3.2 Elemental release rates of the inorganic components of SOAP. Only the alkali metals are observed to leave the coal particles in significant quantities.

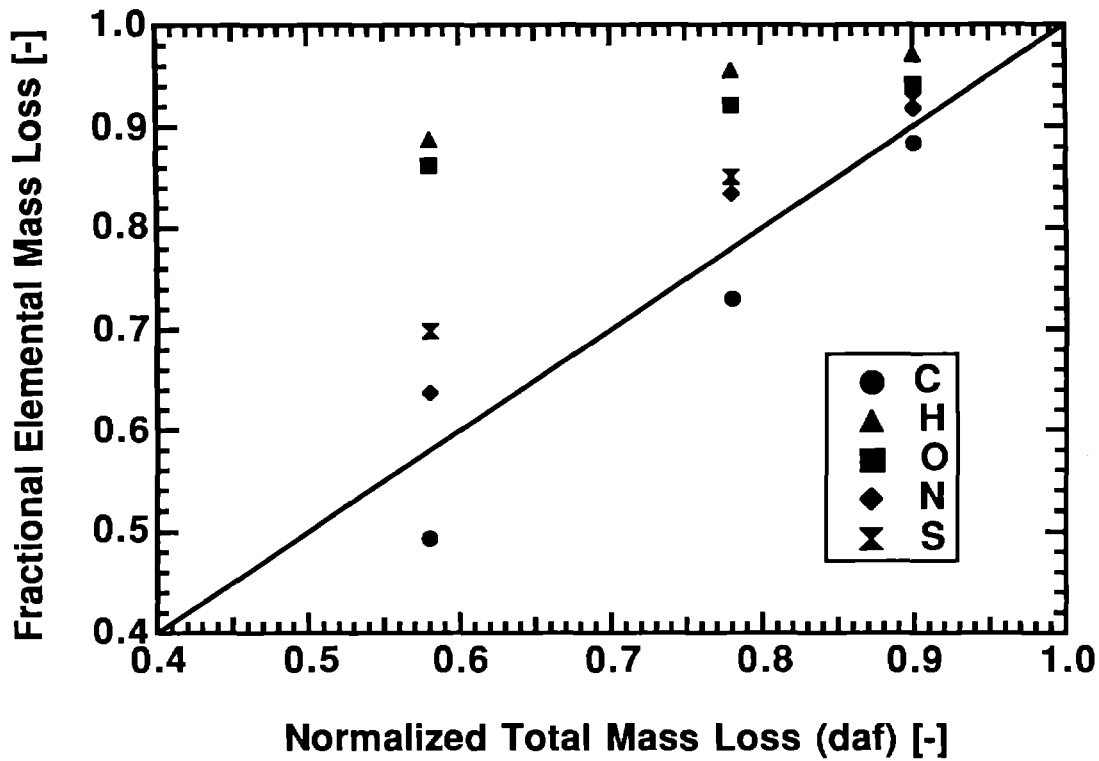


Figure 3.3 Fractional elemental mass loss as a function of normalized total mass loss (daf) for the SOAP particles.

SUBTASK 3.2 THE EVOLUTION OF PARTICLE AND FLY ASH SIZE DISTRIBUTIONS

During this quarter, work continued to determine the extent of char fragmentation and the resulting fly ash size distribution for several coals and coal blends. To date, the total number of coals investigated is ten. Coals used in the study range in rank from lignites to bituminous, and range in ash content from 5 to 22 %.

One of the unique aspects of these investigations is the use of the same *in situ* sizing technique to determine both char and fly ash particle sizes. Experiments are conducted in the Multifuel Combustor (MFC) using utility-grind, pulverized coal in an environment simulating that of a utility-scale boiler. Size distributions are measured immediately after coal devolatilization and at the end of char combustion (greater than 99% daf burnout as determined from tracer analysis of solid samples).

The extent of char fragmentation, as indicated by the number of fly ash particles formed per char particle, is found to depend on (in order of importance): (1) char structure, (2)

initial char particle size, (3) ash content, and (4) mineral grain size distribution. The first three dependencies are clearly indicated by existing data. The fourth is postulated pending further investigation of mineral grain size distributions in these coal samples.

The analysis of the data collected from the MFC is similar to a previously published model of char fragmentation [Baxter, 1991; Baxter, 1990a]. This analysis is briefly reviewed here. The experimental design is also briefly reviewed. The bulk of the discussion centers on the results and their implications.

Theoretical Analysis

The fragmentation model described below relates the initial char (not coal) feedstock and final fly ash size distributions. The model is written in terms that are convenient for laboratory analyses. That is, the char particles have physical properties that can vary as a function of size but, at a given size, are described by a single-valued function. Particle-to-particle variations in physical properties *at a given size* are neglected. Also, transient developments in particle size distributions, as discussed by many of the previously cited authors, are neglected. Size distributions of the initial char and final fly ash can be related, in general, through a particle number balance.

$$\int_{d_{a1}}^{d_a} n'_a(x) dx = \int_{d_c=0}^{d_c=\infty} \int_{d_{a1}}^{d_a} g(x|y) dx n'_c(y) dy \quad (3.1)$$

The functions n'_a and n'_c represent particle concentration density functions for fly ash and char, respectively, with typical units of particles/(m³ μm). Dummy variables x and y are used in the integrands to represent fly ash (d_a) and char (d_c) particle diameters, respectively. Integration of n' with respect to particle diameter represents the cumulative concentration of particles with sizes between the limits of integration. Thus, the integral on the left represents the total concentration of fly ash particles with diameters larger than d_{a1} and smaller than d_a .

The function $g(x|y)$ is a conditional fly ash particle size distribution (psd); It indicates the *ultimate* size distribution of fly ash particles formed from a char particle with *initial* size y . This represents the only portion of the above equation that is not determined experimentally in this investigation.

Several published theoretical and experimental results suggest general forms of the function. One example [Quann and Sarofim, 1986] provides data from which $g(x|y)$ can be determined for one char particle size. In that study, coal particles were mechanically sieved to a 140 μm nominal diameter and combusted at a particle temperature of about 2000 K in a 20 % O₂ environment. The number of fly ash particles generated was deduced as a function of fly ash particle size.

The function $g(x|y)$ for the data of Quann and Sarofim [1986] can be generated by differentiating the cumulative size distribution with respect to particle size. This is illustrated in Figure 3.4. The linearity of the data when plotted in this way suggests that the data follow a power-law distribution, i.e.,

$$g(x|y) = \begin{cases} a(y) x^b & \text{for } x_1(y) \leq x \leq x_2(y) \\ 0 & \text{otherwise} \end{cases} \quad (3.2)$$

where x_1 and x_2 represent the diameters of the smallest and largest fly ash particle generated, respectively. This conditional psd describes a power-law size distribution between the limits x_1 and x_2 for fly ash particles generated from each char particle of size y . Note that this functional form can only describe the results from an ensemble of initial char particles with size y . The functional form of g for a single char particle is series of Dirac delta functions.

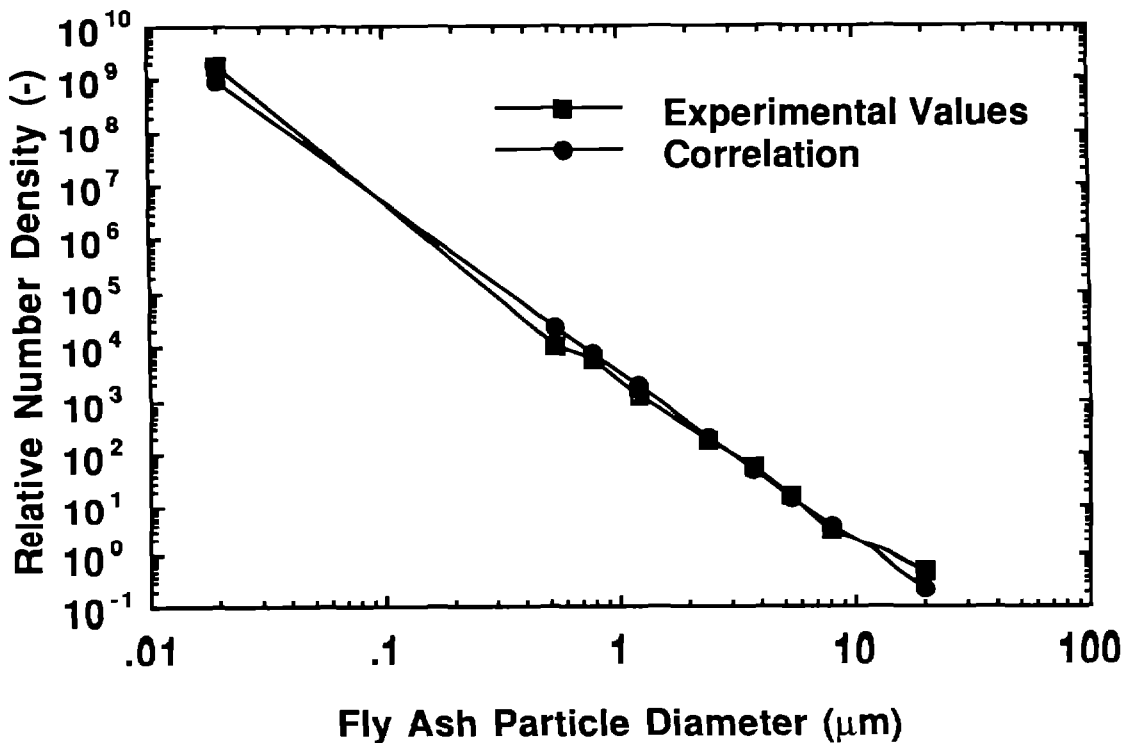


Figure 3.4 Power law function $g(x|y)$ correlated with the power-law size distribution. Original data are from Quann and Sarofim [1986].

Values for a and b of 3260 and -3.21, respectively, fit the data of Quann and Sarofim [1986] with a coefficient of determination [Canavos, 1984] (r^2) greater than 0.99 (in logarithmic coordinates with x expressed in microns). The original data of Quann and Sarofim have been recast in number density form, and this correlation is compared with these recast data in Figure 3.4. The authors state that the smallest particles (those smaller than about 0.6 μm) are generated by vaporization-recondensation mechanisms, whereas the larger particles are believed to be generated by surface drop shedding or disintegration of char structures. If the data at sizes smaller than 0.6 μm are eliminated, values for a and b of 2370 and -2.95, respectively, fit the remaining data, also with a coefficient of determination greater than 0.99. Therefore, the functional form for $g(x|y)$ given by Eq. 3.2 represents at least this set of data regardless of the mechanism of fragmentation and the value of b used in the conditional psd can be assumed to be approximately -3.

Results of a percolation model of char fragmentation [Dunn-Rankin and Kerstein, 1988] provide further theoretical motivation for this functional form of this conditional pdf. This formulation has been used in other theoretical studies of the transient evolution of char particle size distributions [Kerstein and Edwards, 1987].

A mass balance on the fly ash determines the function $a(y)$, as follows:

$$m_a(y) = \int_0^{\infty} \frac{\pi}{6} \rho_a x^3 g(x|y) dx = \frac{\pi}{6} \rho_a a(y) \Delta x(y) = \omega_a(y) m_c = \omega_a(y) \frac{\pi}{6} \rho_c y^3 \quad (3.3)$$

where ρ represents density, ω represents ash mass fraction, and Δx represents $x_2 - x_1$. Note that the density of the *initial* char particle (ρ_c) represents the density of the total particle, not just the organic portion. Also, the density of the *final* ash particle and the ash mass fraction in the char particle (ρ_a and ω_a , respectively) represent values of *ash*, as opposed to the mineral matter from which the ash is formed. It follows from Eq. 3.3 that,

$$a(y) = \frac{\omega_a(y) \rho_c y^3}{\rho_a \Delta x(y)} \quad (3.4)$$

For convenience in determining the upper and lower bounds of g , a parametric function $f(y)$ is designated the *fragmentation factor* and is defined as follows:

$$f(y) \equiv \frac{\left(\frac{\omega_a \rho_c}{\rho_a}\right)^{1/3} y}{x_2} \quad (3.5)$$

The numerator represents the size of the fly ash particle that obtains when all of the ash in a char particle coalesces, i.e., no fragmentation occurs. The function f equals the ratio of this hypothetical size to the size of the largest fragment actually generated from a char particle (x_2); f increases with an increase in the *extent* of fragmentation. In the limit of no fragmentation, f is unity, independent of either initial char particle size (y) or char size dependencies in either ρ or ω . (This statement may appear to contradict the explicit

dependence of f on y indicated in Eq. 3.3. However, in the case of no fragmentation, this explicit dependence cancels with the implied dependence of x_2 and of the physical properties on y .) In general, f is expected to be greater than or equal to 1. The parameter f indicates the extent of fragmentation in that it increases as the extent of fragmentation increases. If char were to produce a monodispersion of fly ash particles as a consequence of fragmentation, the total number of fragments produced would be equal to f^3 .

A second function $s(y)$, designated the *fragment size ratio*, is defined as

$$s(y) \equiv \frac{x_1(y)}{x_2(y)} \quad (3.6)$$

and represents the *mode* of fragmentation in the sense that s decreases as the range of fragment sizes produced from a char particle increases. If there is no fragmentation, both f and s are unity. As s decreases from unity toward zero, the range of sizes of fragments produced from a single char particle increases.

Equation 3.2 can be written in terms of the parameters f and s as

$$g(x|y) = \begin{cases} \frac{\omega_a \rho_c y^3}{\rho_a \Delta x} x^{-3} = \frac{f^3 x_2^3}{\Delta x} x^{-3} & \text{for } x_1(y) \leq x \leq x_2(y) \\ 0 & \text{otherwise} \end{cases} \quad (3.7)$$

yielding

$$\int_{d_{a1}}^{d_a} g(x|y) dx = \frac{f^3}{2} \left(\frac{1-s^2}{s^2 - s^3} \right) + \min \left\{ \frac{f^3}{2(1-s)} \left[\left(\frac{x_2}{\min(x_2, d_{a1})} \right)^2 - \left(\frac{1}{s} \right)^2 \right], 0 \right\} + \min \left\{ \frac{f^3}{2(1-s)} \left[1 - \left(\frac{x_2}{\max(x_1, d_a)} \right)^2 \right], 0 \right\} \quad (3.8)$$

where s , f and x_2 depend on y . The second term on the right side is negative for all y where $d_{a1} > x_1$ and the third term is negative for $d_a < x_2$. Otherwise, both terms are zero. If all particle sizes are included in the integration ($d_{a1} = 0$ and d_a larger than the largest char or fly ash particle in the stream), the only nonzero term on the right side of the equation is the first term, which represents the ratio of the total numbers of fly ash and char particles.

In general, both f and s depend on initial char particle size y . However, the qualitative relationship between initial char and fly ash particle size distributions is conveniently illustrated by assuming that f , s and the ratio $(\omega_a \rho_c) / \rho_a$ are independent of initial char particle size and can be treated with average values. This means the char particles are homogeneous, or size-invariant, with respect to both their physical properties and their fragmentation properties and that the behavior of particles in a given size range can be represented by statistical averages of properties. Under these assumptions,

$$x_2 = \left(\frac{\omega_a \rho_c}{\rho_a} \right)^{1/3} \frac{y}{f} \equiv py \quad (3.9)$$

and

$$x_1 = s x_2 = p s y \quad (3.10)$$

where p is independent of y and typically has a value of order 0.5 or less. This allows the integral of the conditional psd to be expressed analytically in terms of y only. If all ash particles are included in the integration ($d_{a1} = 0$), the relationship between char and fly ash concentration distributions can be written as

$$\int_0^{d_a} n'_a(x) dx = \int_0^{d_a/(ps)} n'_c(y) \frac{f^3}{2} \left(\frac{1-s^2}{s^2-s^3} \right) dy + \int_{d_a/p}^{d_a/(ps)} n'_c(y) \frac{f^3}{2(1-s)} \left[1 - \left(\frac{py}{d_a} \right)^2 \right] dy \quad (3.11)$$

A linear transformation of this equation relates directly to the experimentally measured cumulative particle size distributions reported later. This transformed expression is

$$K_a(d) \equiv \int_d^\infty n'_a(x) dx = \int_0^\infty n'_a(x) dx - \int_0^d n'_a(x) dx \quad (3.12)$$

where the integral from 0 to ∞ is a constant (independent of d_a). A similar expression defines the function K_c for the char particles.

$$K_c(d) \equiv \int_d^\infty n'_c(y) dy = \int_0^\infty n'_c(y) dy - \int_0^d n'_c(y) dy \quad (3.13)$$

These cumulative distributions will be used in the discussion of the experiments that follows.

Dependence of the fly ash psd on the extent of fragmentation (f) under these assumptions is straightforward; the ratio n'_a/f^3 is independent of f when plotted as a function of the dimensionless size pd_a . Dependence on mode of fragmentation (s) is more complex. This is discussed in more detail elsewhere [Baxter, 1991; Baxter, 1990].

Limiting forms of Eq. 3.1 other than Eq. 3.11, are useful to consider. If the initial char particles are monodisperse (n'_c is a Dirac delta function), the integral on the left represents the total number of fly ash particles produced per char particle. Assuming Eq. 3.2 as the appropriate description for g , the total number of fly ash particles generated per char particle becomes

$$g = \frac{f^3}{2} \left(\frac{1+s}{s^2} \right) \quad (3.14)$$

Eq. 3.14 indicates the dependence of the number of fly ash particles on the parameters f and s . For a given value of f , the number of fly ash particles increases dramatically as s decreases. (Recall that s is always less than or equal to 1). Similarly, as f increases for a given value of s , the total number of fly ash particles increases as f^3 .

The valid range of the functions f and s illustrate that this theoretical approach is applicable only to ensembles of particles, not to individual particles. For example, when the ash *in an individual particle* coalesces to form a single fly ash particle ($f = 1$), there is only one size fly ash particle produced ($s = 1$). However, only a fraction of the particles in an ensemble of nominally identical char particles may behave this way. Therefore, f can assume a value of unity for the ensemble without limiting the range of values s can assume. In the application of this theory in this paper, the only theoretical limitations on these two parameters are that $f \geq 1$ and $s \leq 1$. The functions are independent of each other.

Experimental Conditions

The Multifuel Combustor (MFC) and a Particle Counter Sizer Velocimeter (PCSV) are the primary experimental facility and diagnostic, respectively, used in this examination. The MFC provides careful control of gas temperature and composition in a long-residence-time facility. The MFC was operated at a firing rate of 0.07 MBtu/hr with overall oxygen concentrations varying from 5 to 3 mole % during char oxidation, conditions similar to commercial-scale boiler operation. Particle residence time is varied by moving the location of the coal injection lance to various ports along the length of the combustor.

The PCSV performs *in situ* measurements of particle frequency (count), size and speed at the base of the combustor. The PCSV is based on near-forward light scattering from laser beams focused at the center of the reactor flow. Two laser beams are used, one for large particles ($> 3 \mu\text{m}$) and the second for small particles. The measurements are based on individual particles passing through an approximately ellipsoidal diagnostic volume with a major axis of about 1 mm and minor axes of approximately 300 μm for one beam and 50 μm for the second. The diagnostic is discussed more fully in the literature [Holve 1983].

We determined the accuracy of the instrument by passing monosized standards through the diagnostic volume and comparing the measured particle sizes with the known actual sizes. Standards used included glass beads entrained in air and transparent discs etched in an opaque reticule. The standards varied from 0.6 to 60 μm and indicate that the PCSV reports particle sizes within one size bin or 0.1 μm of the correct size, whichever is larger.

The precision of the data is determined by repeating measurements of coal and fly ash in the MFC under nominally identical conditions and computing coefficients of variation from the results. At least five and as many as twelve replicate experiments were performed for each coal at each sampling height. The coefficient of variation thus determined includes experimental uncertainty as well as actual fluctuations due, for example, to turbulent fluctuations and variations in coal feed rates. The impact of such fluctuations on

the data can be minimized by computing the total mass flowrate from the measured particle concentrations and normalizing all the results to this value. Confidence intervals presented below are based on these measured coefficients of variation and standard statistical techniques.

The upper and lower detection limits of the PCSV are determined in these experiments by the points at which the agreement among the repeated tests becomes poor, as indicated by the statistical confidence intervals. The lower limit is 0.4 - 0.7 μm and is controlled primarily by signal-to-noise levels in the detector. The upper limit is controlled by sampling statistics in this experiment. Approximately 160,000 individual particles were sampled per measurement, and each measurement was repeated 5 to 12 times. Under these conditions, the upper detection limit is about 100 μm .

Reasonably complete analyses of the coals used in these experiments are included in the appendix. The data in the appendix include all of the coals used in the program to date. There are several samples of coal with the same name. These are distinguished by numbers, for example, Illinois #6 (2) is a different coal sample than Illinois #6 (1).

The nominal conditions under which these experiments were conducted are summarized in Table 3.3. Under these experimental conditions, the particles form a dilute phase in the gas, with the total particle volume fraction far less than one percent of the overall gas volume. Consequentially, the probability of particle-with-particle collisions producing agglomerated fly ash is vanishingly small.

Table 3.3

Typical Local Gas and Particle Properties in the MFC at the Initial Char and the Fly Ash Measurement Locations

Property	Initial Char	Fly Ash
Gas temperature ($^{\circ}\text{C}$)	1100	900
Oxygen mole fraction	0.06	0.04
Particle residence time τ (s)	0.2	2.1
Particle burnout (daf)	0.65	0.99+
Particle temperature ($^{\circ}\text{C}$)	1250	900

Coals and Coal Properties Studied

Analyses of all of the raw coals used in this study were completed this quarter. (These analyses are recorded in the appendix and were performed as a contribution in support of this research by Consol, as described in more detail in the Technology Exchange section of this report. These analyses include (where relevant): (1) moisture content; (2) proximate analysis; (3) ultimate analysis; (4) ash chemistry; (5) ash fusion temperatures under reducing and oxidizing environments; (6) sulfur forms; (7) particle size distributions determined by sieves; and (8) particle size distributions determined by Malvern optical analyses. In virtually all cases, the data are averages of several replicated measurements. The statistical analysis of the data is completed but is not presented in the appendix. The statistical certainty with which the chemical and physical properties of the raw coal are known are used in determining error bars for experiments and, in the future, for predictions.

The range of coals and coal properties indicated in the appendix covers the range of commercially significant steam coals rather thoroughly. Coals from essentially every major coal producing region of the US are represented. There are no samples of very high rank (low volatile bituminous coals or anthracites) among the coals indicated in the appendix.

Fragmentation data have yet to be collected for a few of the coals in the appendix. However, data have been collected for representative coals of every major rank and field and these are presented below.

Experimental Results and Discussion

Data derived from many coals are presented below. The discussion will first contrast a typical swelling coal (Pittsburgh #8) and a non-swelling coal (Roland coal). Results from the remainder of the coals will be presented in the context of the results from these two coals and will be shown to be consistent in their interpretation.

Cumulative size distributions for char and fly ash particles generated from the Pittsburgh #8 (2) coal are illustrated in of Figure 3.5a. The mean value of the several measured distributions is indicated together with 95% confidence intervals. The coefficients of variation (standard deviation divided by mean) used in computing the confidence intervals are illustrated as a function of particle size in Figure 3.5b. These experimentally determined coefficients of variation are largest at small particle sizes. Light scattering intensity is lowest for small particles and is most influenced by experimental error (detector noise, beam steering, etc.), giving rise to higher coefficients of variation.

The data illustrated in Figure 3.5 are representative of all of the coals studied. Only the final results of the fragmentation analysis will be presented for the remainder of the coals studied.

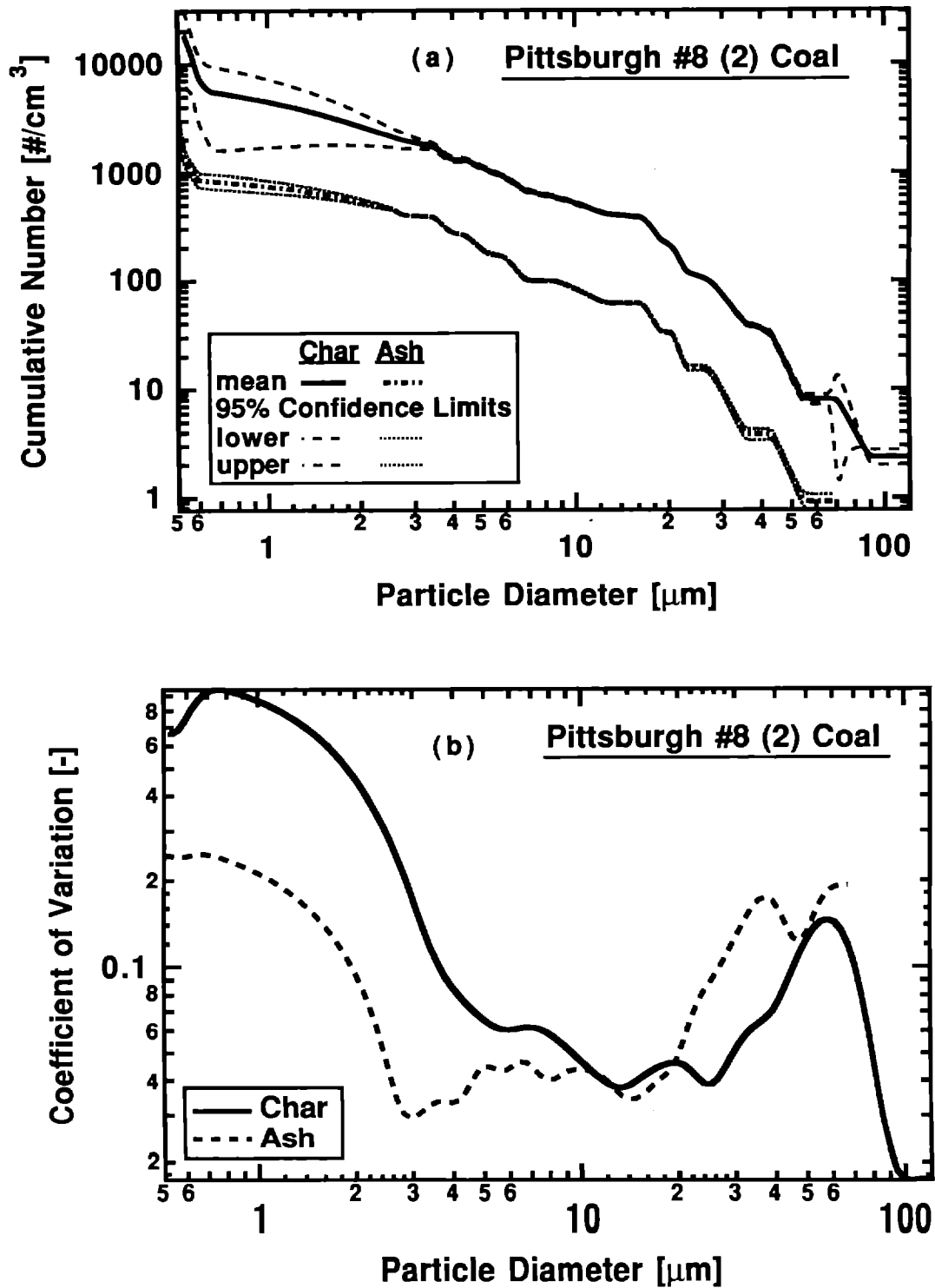


Figure 3.5 Cumulative particle size distributions and statistics for char and fly ash generated from the Pittsburgh #8 (2) hv A bituminous coal.

The confidence intervals are largest for the submicron-sized char particles. These, however, are of little consequence to the analysis since they form fly ash particles too small to reliably detect with this technique. Over the range of char and fly ash particle sizes of interest in this study, the size distributions are determined within approximately ± 20 relative percent accuracy. The confidence intervals are much smaller over most of the range of interest.

Using these data, the fragmentation factor f is computed according to the equations indicated in the preceding discussion. The only quantity not determined from the measurements is s . Figure 3.5a illustrates the computed value of f for an assumed value of s of unity. This is equivalent to assuming that equal-sized fly ash particles form from a char particle of a given initial size. While this assumption is probably not realistic, it is convenient for engineering models (such as ADLVIC) that incorporate fragmentation behavior.

As is illustrated in Panel (a) of Figure 3.5, the value of the fragmentation factor significantly exceeds unity only at initial char particle sizes larger than $30\ \mu\text{m}$. The size of fragments generated by the fragmentation of these large particles is indicated by the second abscissa at the top of the figure. Fly ash particles generated through fragmentation are concentrated in the $10\ \mu\text{m}$ size range.

The fragmentation factor should range from 1 to larger values, as can be seen from its definition (Eq. 3.5). The experimental measurements indicate a fragmentation factor as low as 0.7 in some regions of char and fly ash sizes. This is probably associated with variations in the char density and ash mass fraction and the fly ash density as a function of particle size. Reliable information concerning the particle size variation of these physical properties is not available for this coal. Therefore, the properties were assumed to be equal to their average values at all particle sizes. Considering that the fragmentation factor is derived entirely from experimental data, this small deviation of the experimental value below its theoretical limit is viewed as only a minor concern in these results.

Results from similar measurements and analyses for a Roland-seam coal are illustrated in Figure 3.6. The ordinates of the two panels in Figure 3.7 are scaled the same as those in Figure 3.6 to allow a direct comparison. The lower-rank Roland coal is seen to fragment less extensively than the Pittsburgh #8 bituminous coal. This is consistent with our previous results and with the postulate that fragmentation is strongly influenced by char structure [Baxter, 1991]. Coals that form chars that are cenospheres or 'mesospheres' (have very large voids) are more likely to fragment because they have inherently unstable structures as they burn out. Such is the case with high volatile bituminous coals. Chars that do not form cenospheres, such as the Roland coal, are stable as the char particles burn out. The fragmentation data reflect the stability of the char structure in that there are few fragments formed per original char particle.

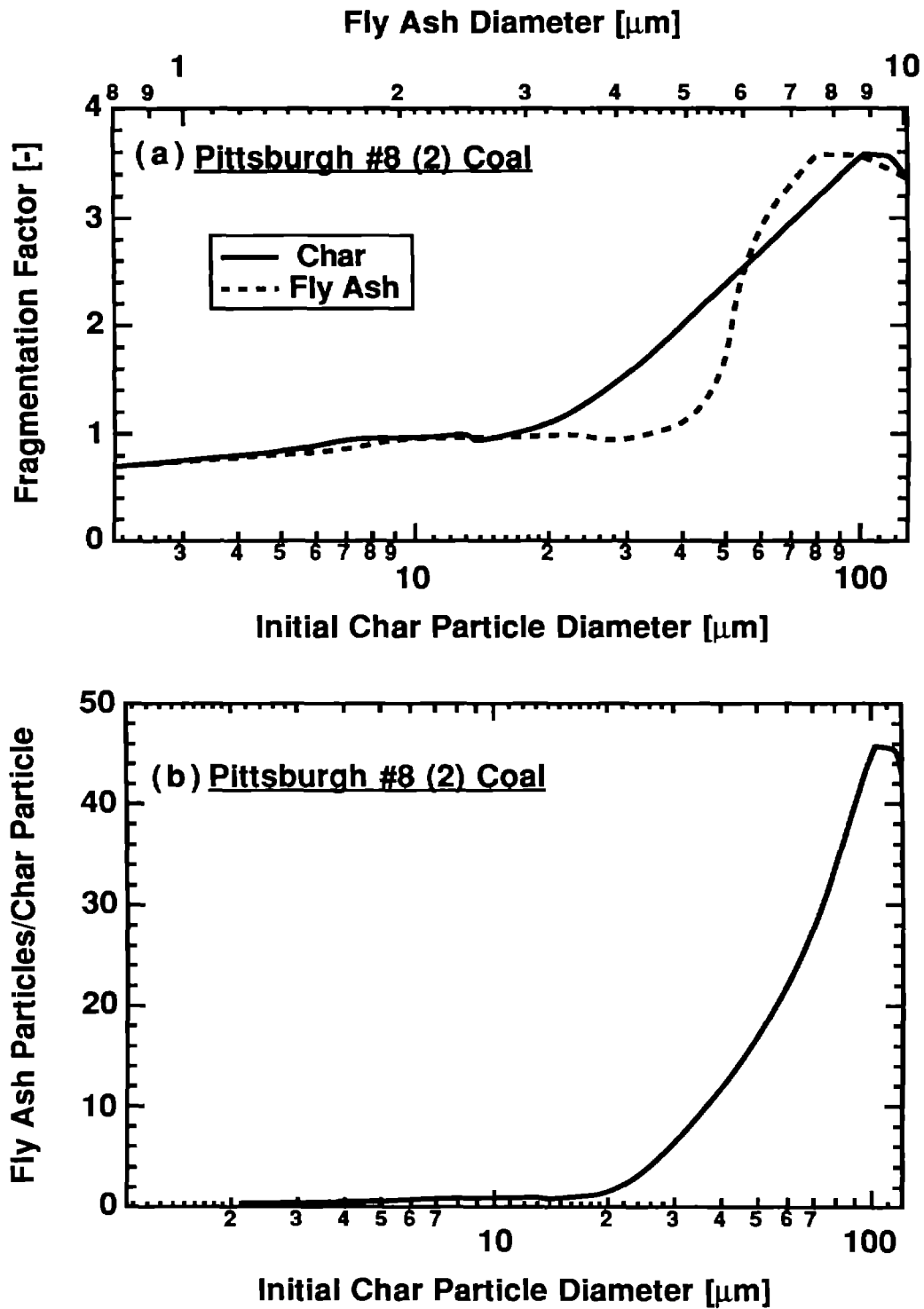


Figure 3.6 Variation of the fragmentation factor with initial char particle size and fly ash size (a) and the number of fly ash particles formed per char particle as a function of initial char particle size (b) for the Pittsburgh #8 hv A bituminous coal.

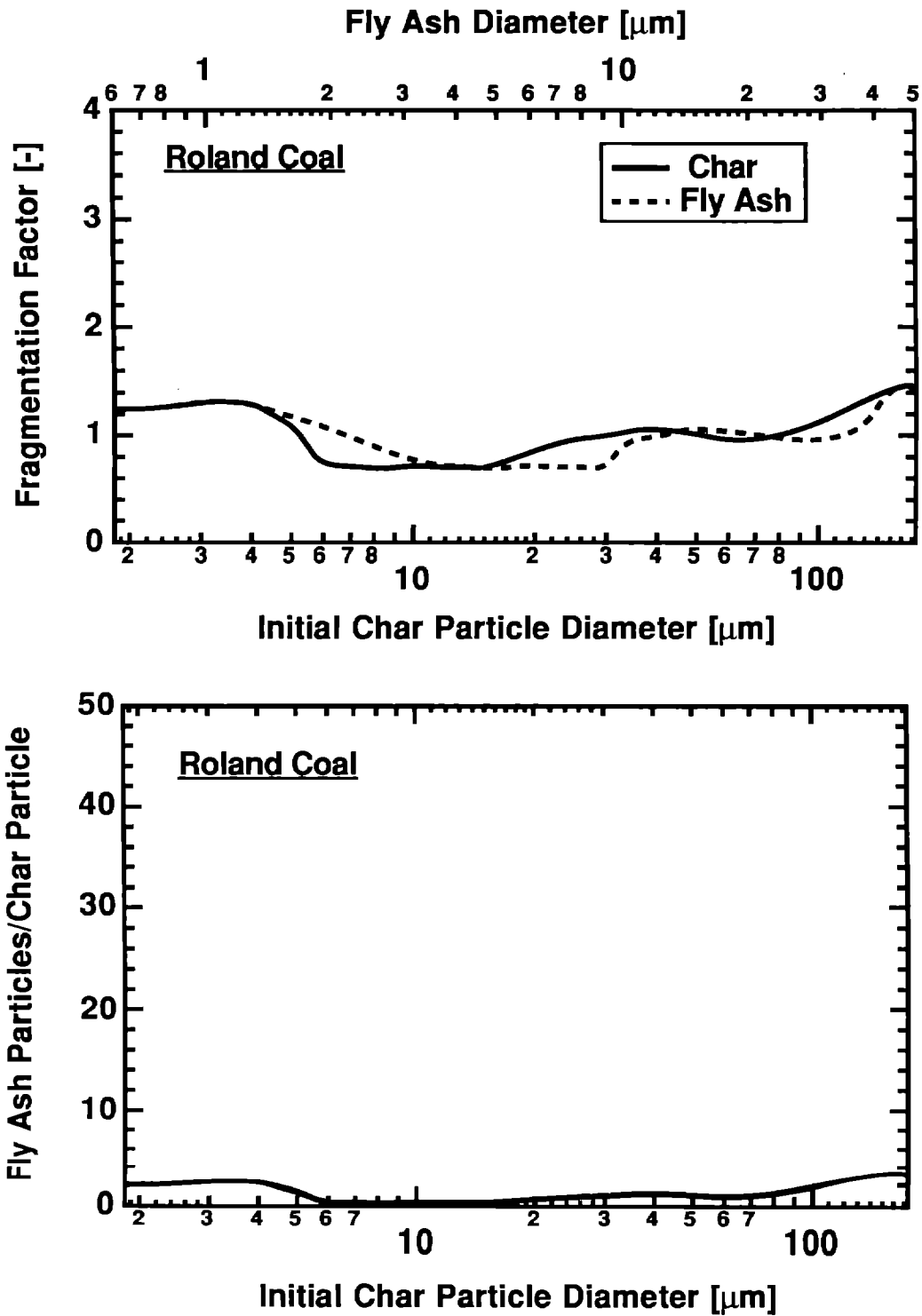


Figure 3.7 Variation of the fragmentation factor as a function of initial char and final fly ash particles sizes (a) and of the number of fly ash particles produced per char particle as a function of initial char particle size (b) for a Roland-seam subbituminous coal.

The comparison of the Pittsburgh #8 and Roland coals is representative of the remainder of the coals we have studied. Data for additional coals and coal blends are illustrated in Figures 3.8 through 3.11. These data are consistent with earlier observations, i.e., the extent of fragmentation generally increases with increasing char particle size, is greater for chars that are cenospheres than for more dense chars, and decreases with increasing ash loading. These general characteristics are consistent among all of the data. However, there are details of the data that need further explanation.

Data for the Utah Blind Canyon coal, which is is borderline between hv A and hv B bituminous, indicate little fragmentation at any particle size, much the same as the Roland and other subbituminous coals and lignites studied thus far. When compared to the other bituminous coals, the behavior of the Blind Canyon coal appears anomalous. This is only an apparent anomaly, as can be verified by a more detailed investigation of the chemistry of the Utah Blind Canyon coal.

Figure 3.12 indicates the detailed chemical structure of coals from many of the same seams studied in this experiment, including the Blind Canyon coal. These data are taken from published NMR spectroscopy results [Solum et al., 1989] and are from the Argonne premium coal bank, not the samples of the coals we studied here. The Blind Canyon coal in the Argonne coal bank is chemically more similar to the lower-rank subbituminous coals and lignite than it is to even to the hv B bituminous samples. There are no samples of hv C available for comparison in these data. We postulate this chemical difference is the reason for the different fragmentation behavior. Coal rank is based solely on heating value and moisture content for these coals (as determined by ASTM D388-36) and is only a crude indicator of the actual chemical structure of the raw coal.

The influence of ash loading on fragmentation behavior can be seen by comparing the Illinois #6 (2) coal with the Illinois #6 (1) coal results. The latter results were reported earlier and are repeated with the Kentucky #9 and Beulah lignite results in Figures 3.13 and 3.14 for comparison. Note that the same trends with respect to rank and ash loading are observed in the two sets of data.

There are several details of the fragmentation behavior that have yet to be satisfactorily explained. For example, our earlier work showed a strong correlation between the size of the mineral grains in the coal and the fly ash sizes at which fragments were generated. The detailed CCSEM characterizations for the coals whose behavior is recorded in Figures 3.4 through 3.11 has yet to be completed. At this point we can only hypothesize that the details of the fragmentation behavior in, for example, the Decker coal are related to the size distribution of the mineral grains. This may also be the explanation why the highest rank, lowest ash coal (Pittsburgh #8), shows less extensive fragmentation behavior than some of the higher ash bituminous coals.

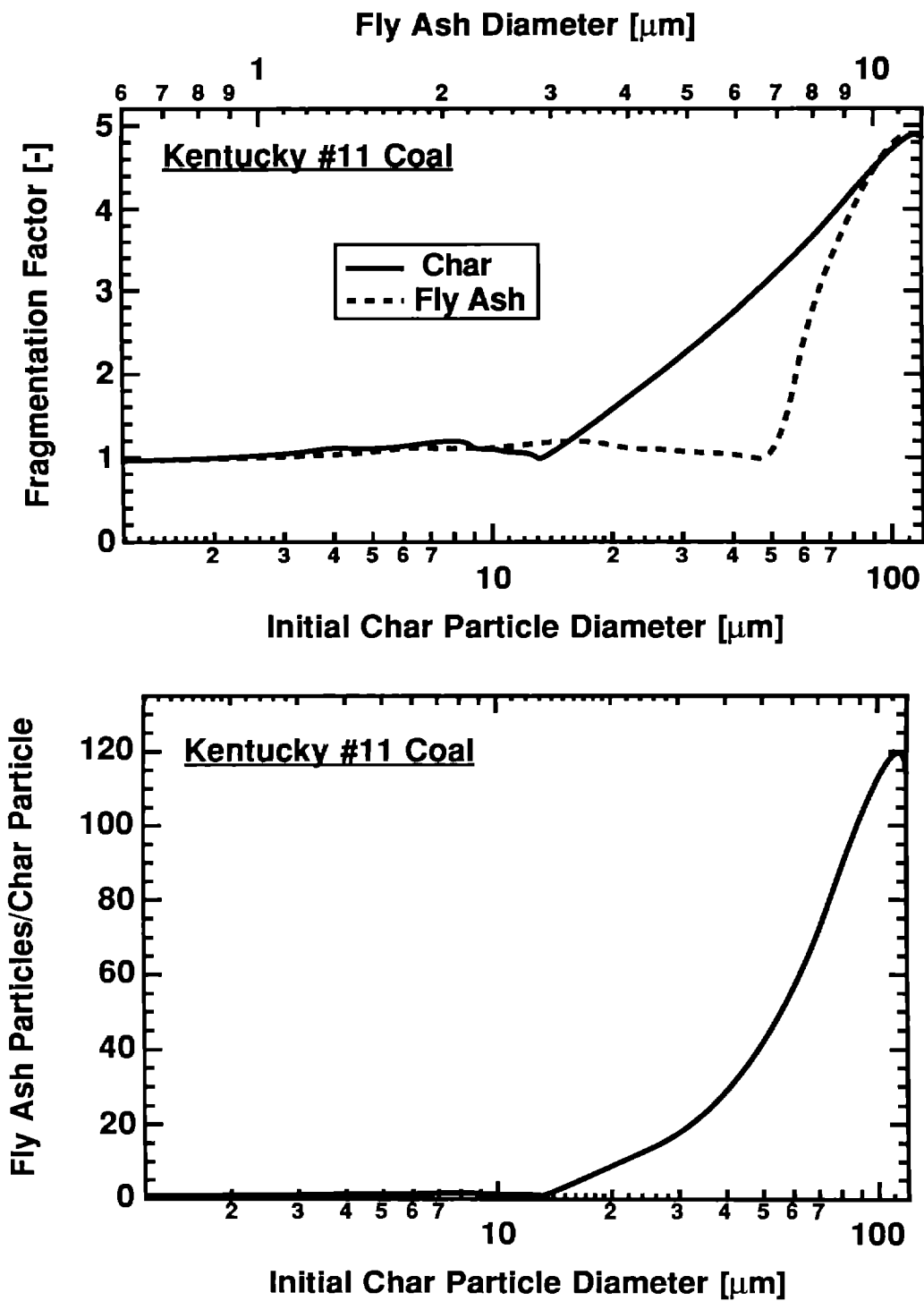


Figure 3.8 Variation of the fragmentation factor as a function of initial char and final fly ash particle sizes (a) and of the number of fly ash particles produced per char particle as a function of initial char particle size (b) for a Kentucky #11 hv B bituminous coal.

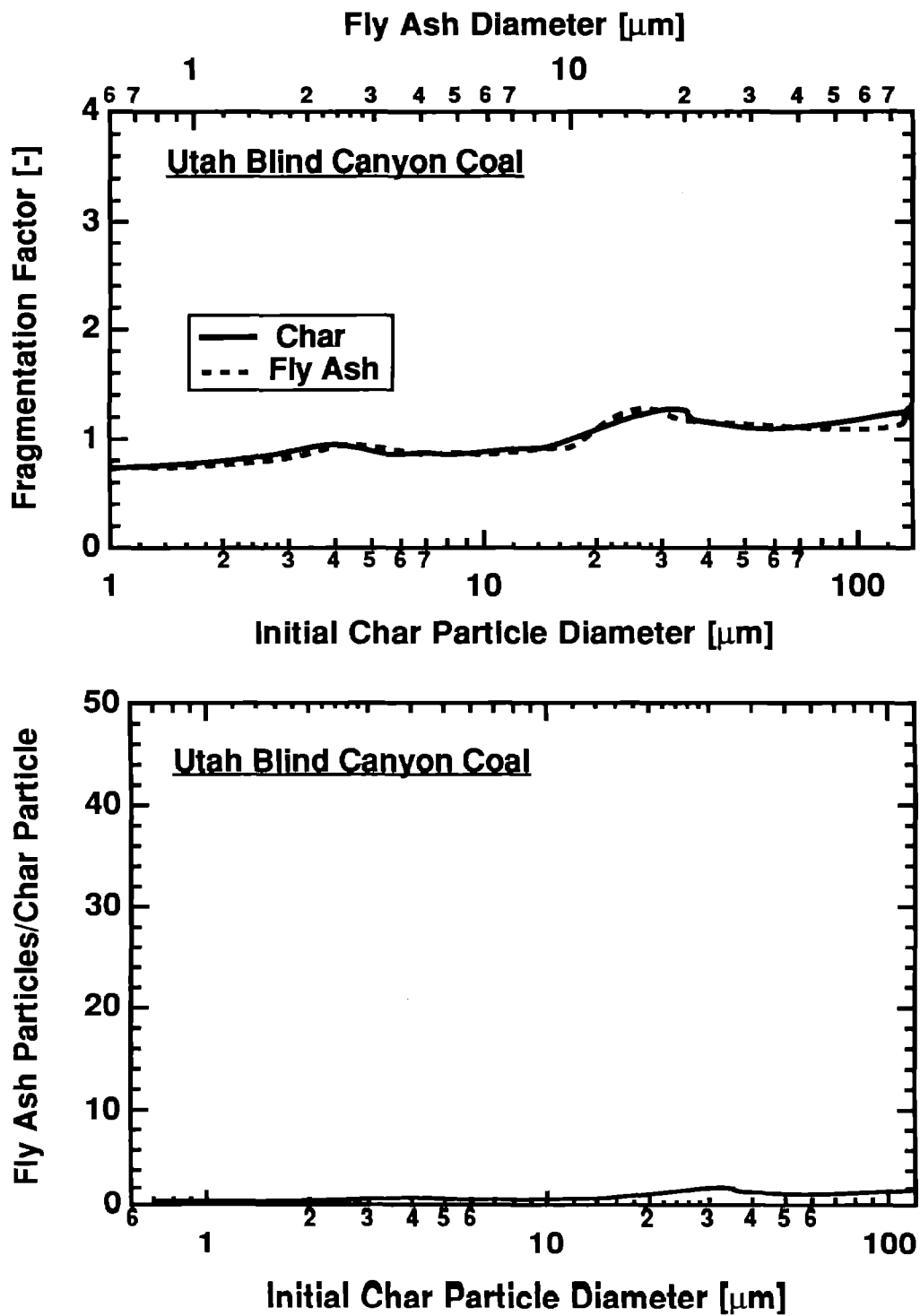


Figure 3.9 Variation of the fragmentation factor as a function of initial char and final fly ash particle sizes (a) and of the number of fly ash particles produced per char particle as a function of initial char particle size (b) for a Utah Blind Canyon hv A bituminous coal.

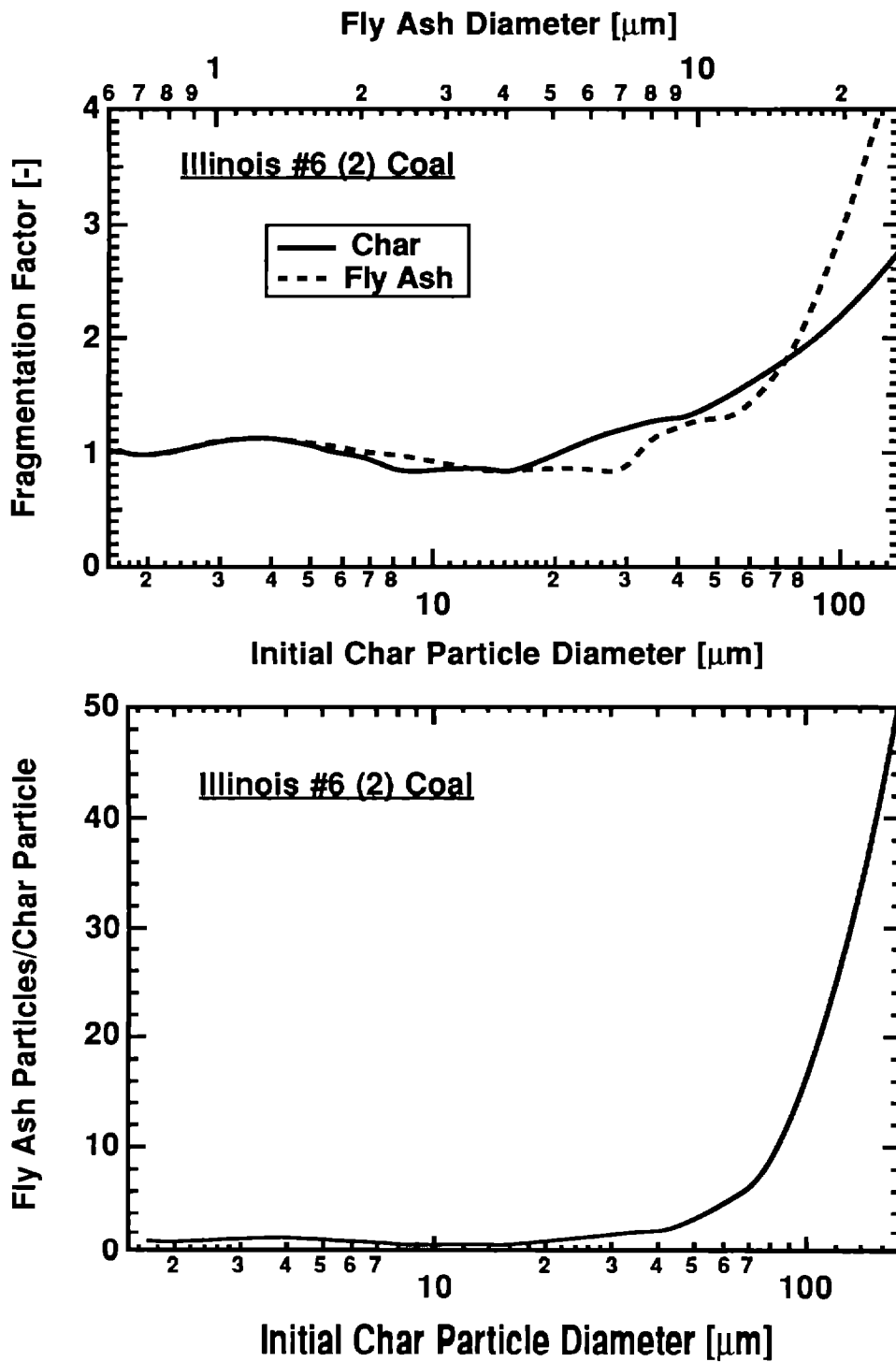


Figure 3.9 Variation of the fragmentation factor as a function of initial char and final fly ash particle sizes (a) and of the number of fly ash particles produced per char particle as a function of initial char particle size (b) for the Illinois #6 (2) hv B bituminous coal.

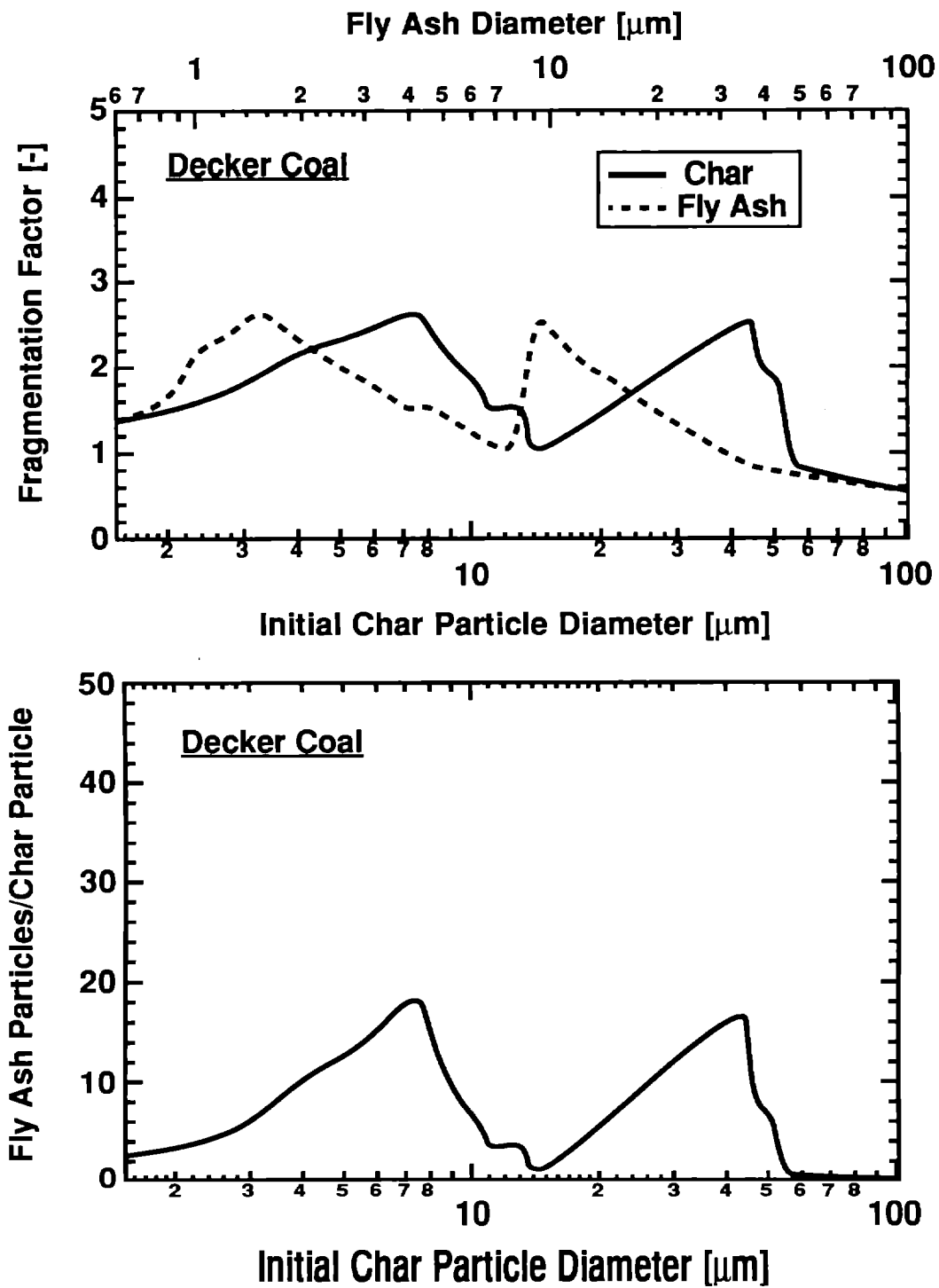


Figure 3.10 Variation of the fragmentation factor as a function of initial char and final fly ash particle sizes (a) and of the number of fly ash particles produced per char particle as a function of initial char particle size (b) for a Decker subbituminous A coal.

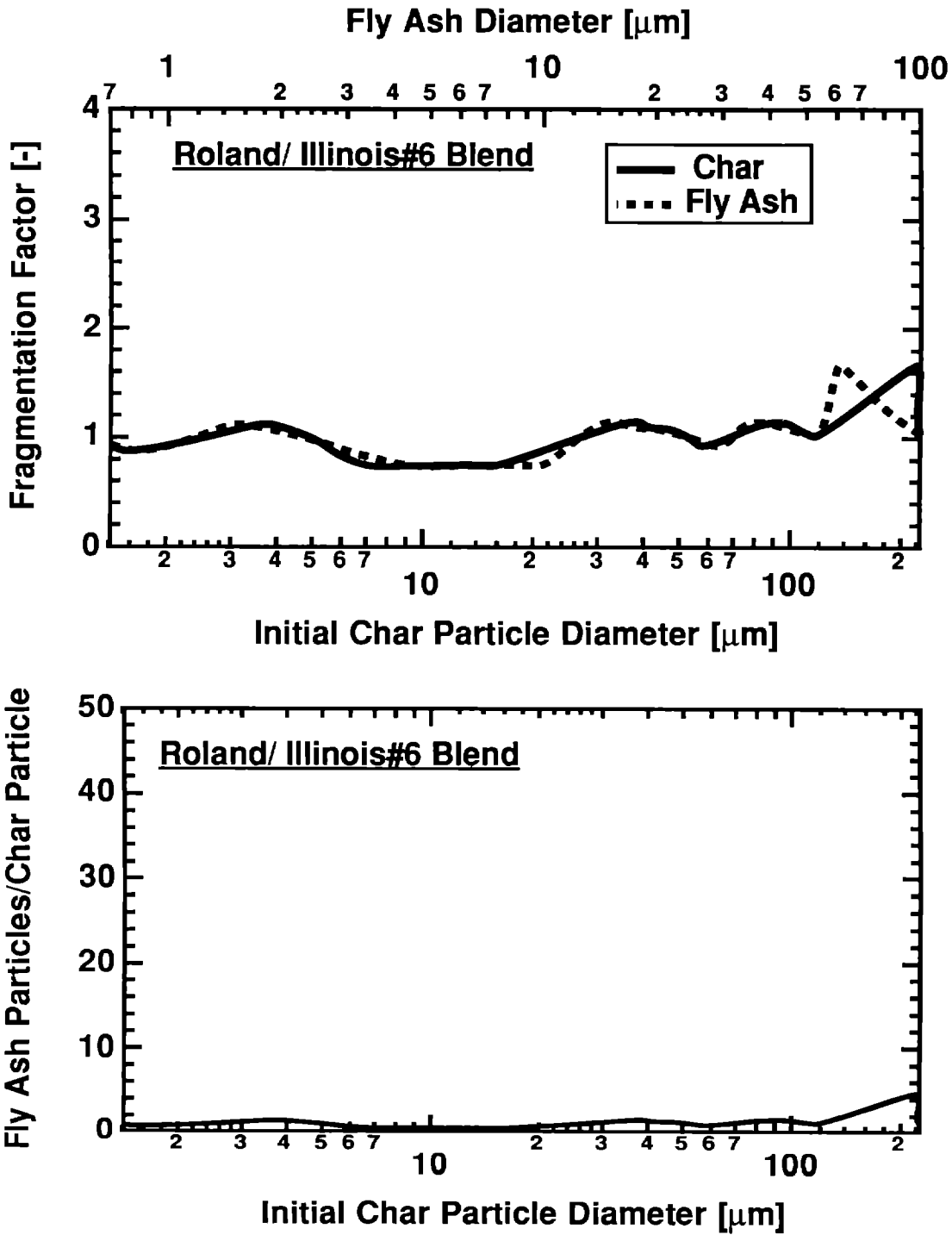


Figure 3.11 Variation of the fragmentation factor as a function of initial char and final fly ash particle sizes (a) and of the number of fly ash particles produced per char particle as a function of initial char particle size (b) for a blend of 70 % Roland and 30 % Illinois # 6 (2) coals.

Summary

The fragmentation data investigated thus far show consistent trends in that: (1) large char particles produce far more fly ash particles than small char particles; (2) the extent of fragmentation tends to increase with increasing coal rank through hv bituminous; (3) the extent of fragmentation tends to decrease with increasing ash loading; and (4) in all cases studied thus far, the total increase in the number of particles greater than 0.6 μm in diameter by char fragmentation is less than a factor of two.

These general trends have been established for a significant number of coals over a broad range of rank, ash loading, and particle size. These results indicate substantial agreement between experimental results previously thought to be in disagreement. A mechanistic description has been presented that successfully anticipates the trends in the data. Significant additional work needs to be performed to establish quantitative relationships between fly ash chemistry and size and mineral grain size distributions.

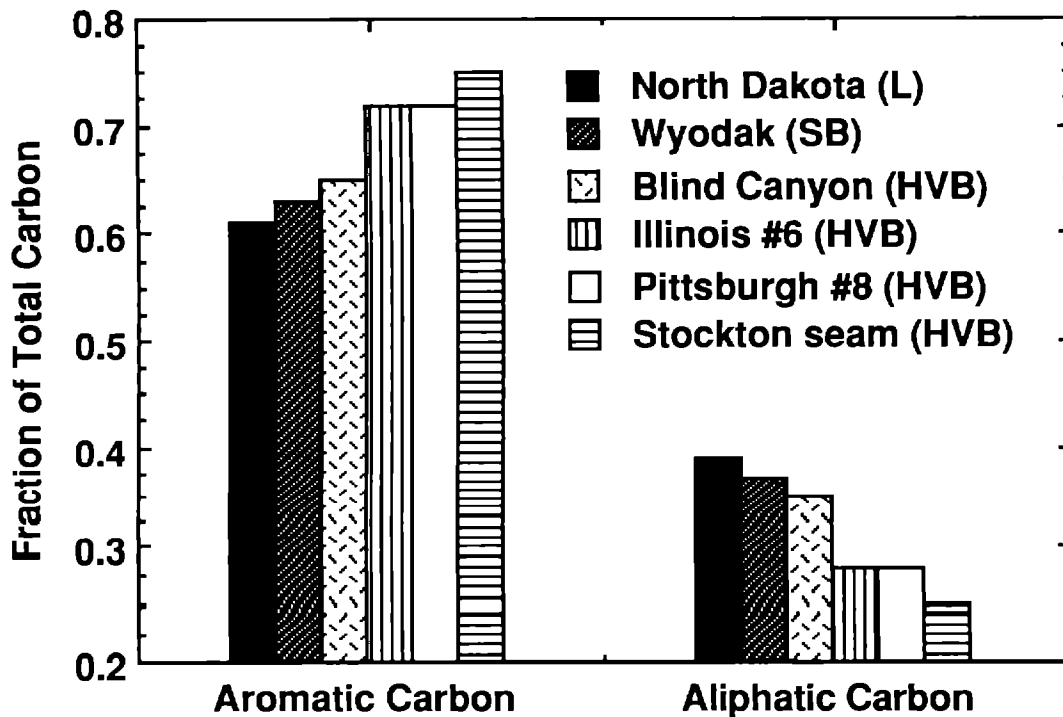


Figure 3.12 Comparison of the chemical composition of Argonne coal bank samples [Solum et al., 1989] contrasting the Blind Canyon coal with coals similar to several used in these experiments.

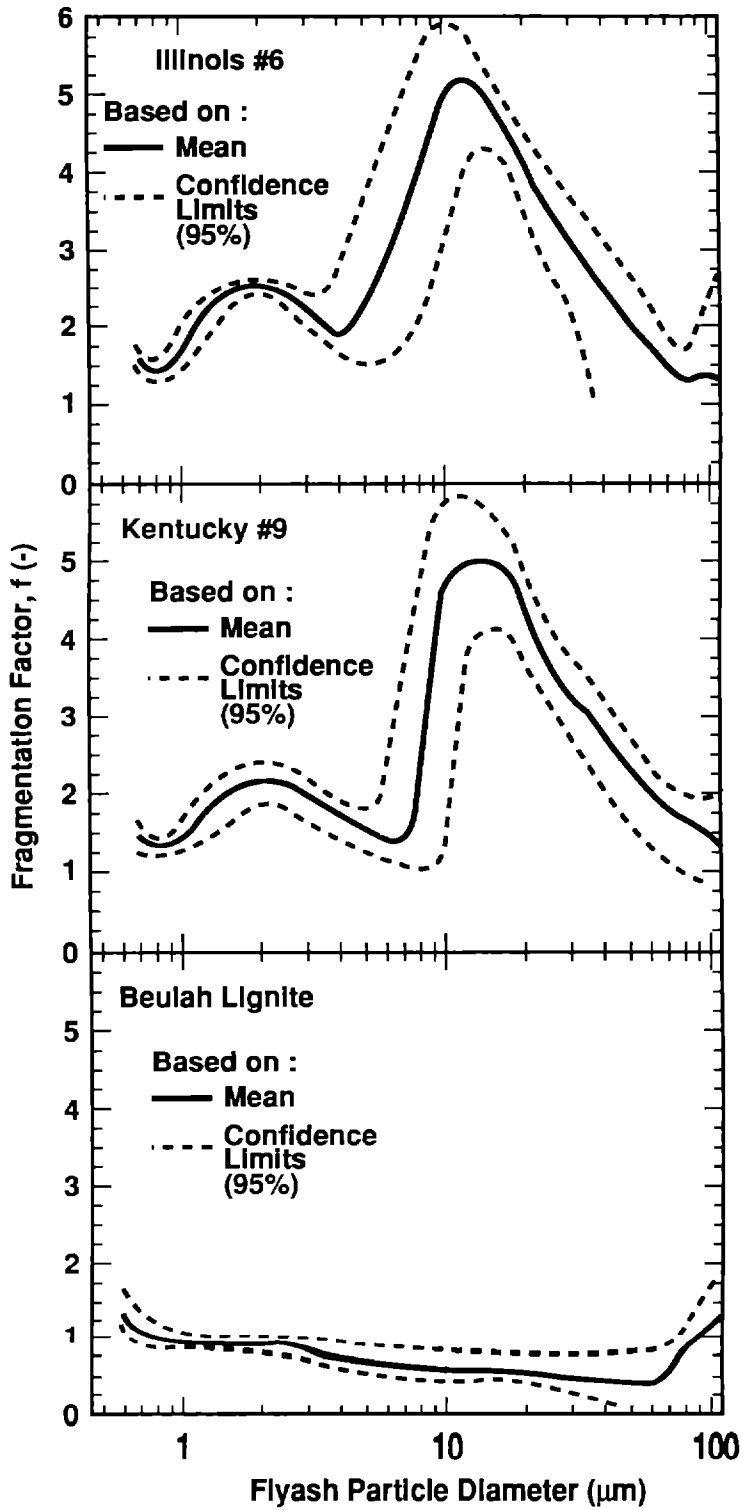


Figure 3.13 Variation of the fragmentation factor as a function of fly ash particle size for the Illinois #6 (1) hv C bituminous coal, the Kentucky #9 hv C bituminous coal, and the Beulah lignite.

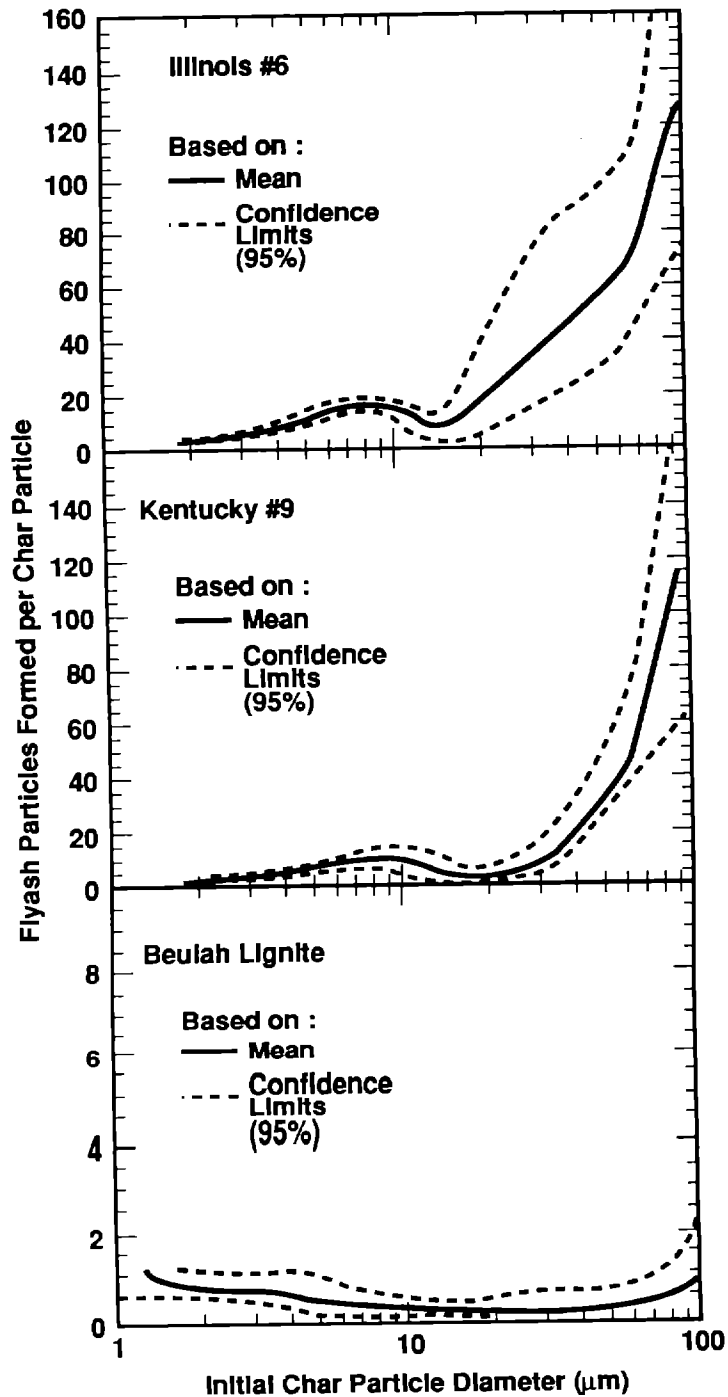


Figure 3.14 Variation of the number of fly ash particles produced per char particle as a function of initial char particle size for the Illinois #6 (1) hv C bituminous coal, the Kentucky #9 hv C bituminous coal, and the Beulah lignite.

Future Work

All of the data presented thus far have been analyzed assuming a value of the size ratio, s , of unity. This assumption is not critical to the evaluation of the extent of fragmentation. Analyses of the same data when the size ratio is assumed to scale with the initial char particle size (a more realistic assumption) will be completed and reported in the future. Preliminary results indicate that this will not alter the qualitative observations, i.e., that the extent of fragmentation increases with increasing initial char particle size, decreases with increasing ash loading, and increases with increasing rank (up to bituminous). It does, however, significantly alter the number of fly ash particles predicted to form from a given size initial char particle, in particular for large particles.

SUBTASK 3.3 THEORETICAL AND EXPERIMENTAL STUDIES OF ASH DEPOSITION

Improvements to the ADLVIC ash deposition code are being incorporated. These include establishing more fundamental relationships between the propensity of a particle to stick to a surface and its chemical/physical transformations during combustion, incorporating the kinetics of heterogenous reactions with ash deposits, and validating the model predictions by comparison with several additional sets of data. These changes will be discussed more fully next quarter.

Ash deposition experiments in the MFC are also progressing. Significant equipment repair and maintenance of the MFC were completed this quarter.

TECHNOLOGY EXCHANGE FOR TASK 3

Sandia, Livermore is involved in two close collaborations with industrial partners. The purpose of these interactions is to gain access to large pilot scale and commercial-scale equipment and data from this equipment with which to validate fundamental understanding of fly ash formation and ash deposition processes being developed under this program. In these collaborations, the industrial partners supply coal samples, chemical analysis and physical characterization services, access to large pilot-scale and commercial scale facilities and data from these facilities, and industrial perspective of the most significant aspects of ash deposition. In exchange, Sandia shares research results arising from this program. Evaluation and interpretation of results is conducted jointly. Several personnel exchanges have also occurred during critical portions of experimentation or model development.

COLLABORATION WITH CONSOL

During this quarter, approximately 80 analyses of samples of coal, char, fly ash, water wall deposits, and deposits on tubes in cross flow collected in the MFC were returned from Consol. These analyses include: (1) moisture content; (2) proximate analysis; (3) ultimate analysis; (4) ash chemistry; (5) ash fusion temperatures under reducing and oxidizing environments; (6) sulfur forms; (7) particle size distributions determined by sieves; and (8) particle size distributions determined by Malvern optical analyses.

COLLABORATION WITH CENTRAL ILLINOIS PUBLIC SERVICES

Collaborations with Central Illinois Public Services (CIPS) center around combustion tests in utility-scale boilers.

CIPS is helping evaluate the ash deposition code by providing data and services from utility-scale facilities regarding ash deposit properties as a function of location in the boiler, coal type, and boiler operating conditions. Data are collected during regularly scheduled test burns of several coals. One test burn, together with data collection and comparison of predictions and measurements has already been completed and documented. A second full scale test burn was completed late this quarter, together with chemical analyses of ash deposits. These results will be discussed in the future.

Also, abstracts for two papers discussing these test burns were accepted this quarter for presentation at technical meetings. Richard DeSollar, fuels coordinator for CIPS, coauthors both papers and will present one of them.

PLANS FOR NEXT QUARTER

In the next quarter, the first version of ADLVIC will be completed. The code will be prepared for release to PETC and other interested parties. A complete discussion of ADLVIC will be presented as part of the next quarterly report. This discussion and documentation will include validation of the model predictions at many different combustion scales. Also, progress in developing ADLVIC II, a more detailed ash deposition model, will be reported.

ACKNOWLEDGMENTS

Several visitors at the Sandia Combustion Research Facility (CRF) and the MFC laboratory have contributed to this work. The assistance of Eric Harwood and James Brandt in performing experiments and maintenance of the MFC during this quarter are gratefully acknowledged. Eric Harwood is a student at the University of California at Davis. James Brandt is a recent graduate of Livermore High School who will be studying in the Mechanical Engineering Department at Los Positas College this fall. The assistance of Alan Salmi and Ephraim Arquitolola, both from Sandia, in maintaining the MFC is also gratefully acknowledged.



REFERENCES FOR TASK 3

- Baxter, L.L., "Char Fragmentation and Fly Ash Formation During Pulverized-Coal Combustion," to appear in *Comb. and Flame*, 1991
- Baxter, L.L., "Task 3: Fate of Mineral Matter During Pulverized Coal Combustion," in "Coal Combustion Science: Quarterly Progress Report" Hardesty, D.R., ed., Sandia Report SAND90-8247, February, 1990.
- Canavos, G.C. *Applied Probability and Statistical Methods*, Little, Brown, 1984.
- Dunn-Rankin, D. and Kerstein, A.R.: *Comb. and Flame*, 74, 207, (1988).
- Holve, D.J. "A Single Particle Counting Diagnostic System for measuring fine particulates at high number densities in research and industrial applications — Final report summarizing instrument development, validation, and operating instructions," SAND83-8246, Sandia Report.
- Kerstein, A.R. and Edwards, B.F.: *Chem. Eng. Sci.*, 42, 1629 (1987).
- Nsakala, N.Y., Patel, R.L., Raymond, D.R., Hargrove, M. J., Hurley, J., and Benson, S., "Effects of Coal Natures and Cleaning Processes on the Physicochemical and Reactivity Characteristics of Beneficiated Coal-Based Products," The Sixteenth International Conference on Coal and slurry Technologies, Clearwater, Florida, April 22-25, 1991.
- Quann, R.J. and Sarofim, A.F.: *Fuel*, 65, 40 (1986).
- Solum, M. S., Pugmire, R. J., and Grant, D.M., *Energy & Fuels*, 3, 187 (1989).

PUBLICATIONS, PAPERS AND PRESENTATIONS FOR TASK 3

The following publications, papers and presentations were completed under Task 3 during this quarter:

- Baxter, L.L. "The Fate of Mineral Matter During Coal Combustion," presented at the PSI review meeting, Pittsburgh, PA, February 4-5, 1991.
- Yang, N.Y.C., and L.L. Baxter, "Instrument and Sample Preparation Considerations for Computer-Controlled Scanning Electron Microscopy (CCSEM) Analyses," presented at the Engineering Foundation Conference on Ash Deposition, Palm Coast, FL, March 10-15, 1991.
- Baxter, L.L., M.F. Abbott, and R.E. Douglas, "Dependence of Elemental Ash Deposit Composition on Coal Ash Chemistry and Combustor Environment," presented at the Engineering Foundation Conference on Ash Deposition, Palm Coast, FL, March 10-15, 1991.

APPENDIX FOR TASK 3

The tables in this appendix summarize the chemical and physical properties of the coals being used to study mineral matter transformations, fly ash formation, and ash deposition. The tables are arranged in order of decreasing coal rank, with blends being grouped separately at the end of the appendix.

The Parr values are used to rank the coals, with results as indicated in Table 3.A.1.

Table 3.A.1

Parr values for fixed carbon, volatile matter, and heating value and associated coal rank for the suite of coals being studied in this project.

Coal	Parr Values			Rank
	Fixed Carbon [-]	Volatile Matter [-]	Heating Value Btu/lb	
Upper Freeport	71.45	28.55	15342	mv Bituminous
Pittsburgh-Seam	59.01	40.99	15154	hv A Bituminous
Pittsburgh #8 (2)	61.51	38.49	14843	hv A Bituminous
Eastern Kentucky	59.76	40.24	14724	hv A Bituminous
Pittsburgh #8 (1)	56.44	43.56	14695	hv A Bituminous
Utah Blind Canyon	51.92	48.08	14276	hv A Bituminous
Kentucky #11	57.38	42.62	13269	hv B Bituminous
Illinois #6 (2)	56.34	43.66	13083	hv B Bituminous
Kentucky #9	57.15	42.85	12791	hv C Bituminous
Hanna Basin	57.59	42.41	12053	hv C Bituminous
Illinois #6 (1)	55.68	44.32	11997	hv C Bituminous
Roland-Seam	52.85	47.15	11494	Subbituminous A
Decker	53.92	46.08	10726	Subbituminous A
Wyodak	51.79	48.21	10059	Subbituminous B
Eagle Butte	51.68	48.32	9286	Subbituminous C
Beulah Lignite	51.28	48.72	8202	Lignite A
Texas Lignite	39.98	60.02	7513	Lignite A
Blends				
Eastern Blend	67.77	32.23	15312	hv A Bituminous
Pitt. #8/Decker	61.3	38.7	13599	hv B Bituminous
Roland/Illinois #6	54.3	45.7	12467	hv B Bituminous

Table 3.A.2

Chemical and Physical Analyses of the Upper Freeport Coal

Analyses			Analyses				
Proximate	Dry	As Rec'd	Size Distribution		Sieves	mass % In size bin	cum. mass %
Fixed Carbon	54.25	53.85	dp>600µm		+28	0	0
Volatile Matter	24.09	23.91	600µm>dp>300µm		28x48	0.55	0.55
Moisture	0.74		300µm>dp>149µm		48x100	6.4	6.95
Ultimate	Dry	As Rec'd	149µm>dp>74µm		100x200	20.55	27.5
C	66.15	65.66	74µm>dp>44µm		200x325	20.2	47.7
H	4.16	4.13	44µm>dp		-325	52.3	100
O	4.48	4.45	Size Distribution (Malvern)*			Size Distribution (Malvern)*	
N	1.51	1.50	Diameter (µm)	% in size bin	cum. vol. per.	Diameter (µm)	% in size bin
S	2.00	1.98	188	0	100	118.4	
Ash	21.66	21.50	162	0	100	102.1	
Ash Chemistry	% dry coal	% ash	140	0	100	88.1	
SiO2	11.06	51.08	121	0	100	76	
Al2O3	5.27	24.34	104	0	100	65.6	
TiO2	0.25	1.15	89.9	0.18	99.8	56.6	
Fe2O3	2.90	13.39	77.5	0.30	99.5	48.8	
CaO	0.53	2.44	66.9	0.30	99.2	42.1	
MgO	0.29	1.32	57.7	0.73	98.5	36.3	
K2O	0.66	3.04	49.8	3.70	94.8	31.3	
Na2O	0.06	0.29	42.9	6.33	88.5	27	
SO3	0.53	2.45	37.1	8.38	80.1	23.3	
P2O5	0.03	0.13	32	8.55	71.6	20.1	
Und. Ash	0.20	0.93	27.6	7.33	64.2	17.4	
Free Silica/Total Silicon	0.29		23.8	6.10	58.1	15	
Pyritic Iron/Total Iron	0.66		20.5	5.40	52.7	12.9	
Chlorine	Dry	As Rec'd	17.7	6.08	46.7	11.1	
Cl (bomb)	0.18	0.18	15.3	6.73	39.9	9.6	
Cl (In ash)			13.2	6.20	33.7	8.3	
Forms of Sulfur	Dry	As Rec'd	11.4	5.10	28.6	7.2	
Sulfatic	0.0775	0.08	9.8	3.68	25.0	6.2	
Pyritic	1.52	1.51	8.5	3.18	21.8	5.3	
Organic	0.48	0.47	7.3	3.38	18.4	4.6	
Heating Value (Btu/lb)	Dry	As Rec'd	6.3	3.78	14.6	4	
As Fired	11800	11713	5.4	3.50	11.1	3.4	
Dulong	11836	11748	4.7	2.65	8.48	3	
Acid Soluble Alkall (ppm)	Dry	As Rec'd	4.1	1.85	6.63	2.6	
Na	343	341	3.5	1.23	5.40	2.2	
Mg	1208	1199	3	1.03	4.38	1.9	
Ca	3767	3739	2.6	1.00	3.38	1.6	
K	2292	2275	2.2	0.98	2.40	1.4	
Fusion Temp. (Reducing)	°F	°C	1.9	2.35	0.05	1.2	
Initial Deformation	2173	1190	Size Distribution			For -325 Mesh Data	
Spherical	2302	1261	D(v,0.5) (µm)			16.55	
Hemispherical	2364	1295	D(v,0.9) (µm)			38.23	
Fluid	2420	1327	D(v,0.1) (µm)			4.45	
Fusion Temp. (Oxidizing)	°F	°C	D(4,3) (µm)			19.75	
Initial Deformation	2435	1335	D(3,2) (µm)			9.5	
Spherical	2507	1375	Span			2.05	
Hemispherical	2540	1393	Spec. Surf. Area (sq.m./cc.)			0.68	
Fluid	2595	1424					

*These Malvern data are for the -325 mesh size fractions.

Table 3.A.3

Chemical and Physical Analyses of the Pittsburgh-Seam Coal

Analyses			Analyses				
Proximate	Dry	As Rec'd	Size Distribution		Sieves	mass % in size bin	cum. mass %
Fixed Carbon	53.10	52.45	dp>600µm	+28		0	0.00
Volatle Matter	38.51	38.04	600µm>dp>300µm	28x48		1.1	1.10
Moisture	1.22		300µm>dp>149µm	48x100		3.55	4.65
Ultimate	Dry	As Rec'd	149µm>dp>74µm	100x200		24.15	28.80
C	77.90	76.95	74µm>dp>44µm	200x325		22.15	50.95
H	5.16	5.10	44µm>dp	-325		49.05	100.00
O	3.83	3.78	Size Distribution (Malvern)*		Size Distribution (Malvern)*		
N	1.38	1.36	Diameter	% in	cum. vol.	Diameter	% in
S	3.23	3.19	(µm)	size bin	per.	(µm)	size bin
Ash	8.40	8.29	188	0	100	118.4	
Ash Chemistry	% dry coal	% ash	162	0	100	102.1	
SiO2	3.29	39.18	140	0	100	88.1	
Al2O3	1.66	19.82	121	0	100	76	
TiO2	0.07	0.86	104	0	100	65.6	
Fe2O3	2.16	25.78	89.9	0.05	100	56.6	
CaO	0.39	4.68	77.5	0.5	99.5	48.8	
MgO	0.07	0.86	66.9	1.45	98.0	42.1	
K2O	0.10	1.25	57.7	2.95	95.1	36.3	
Na2O	0.08	0.98	49.8	5.25	89.8	31.3	
SO3	0.38	4.55	42.9	8.15	81.7	27	
P2O5	0.03	0.34	37.1	11.15	70.5	23.3	
Und. Ash	0.14	1.69	32	10.45	60.0	20.1	
Free Silica/Total Silicon	0.24		27.6	7.05	53.0	17.4	
Pyritic Iron/Total Iron	0.92		23.8	5.75	47.2	15	
Chlorine	Dry	As Rec'd	20.5	5.95	41.3	12.9	
Cl (bomb)	0.12	0.12	17.7	6.15	35.1	11.1	
Cl (in ash)			15.3	5.85	29.3	9.6	
Forms of Sulfur	Dry	As Rec'd	13.2	4.65	24.6	8.3	
Sulfatic	0.04	0.03	11.4	3.7	20.9	7.2	
Pyritic	1.61	1.59	9.8	2.95	18.0	6.2	
Organic	1.59	1.57	8.5	2.65	15.3	5.3	
Heating Value (Btu/lb)	Dry	As Rec'd	7.3	2.45	12.9	4.6	
As Fired	13859	13690	6.3	2.3	10.6	4	
Dulong			5.4	2.2	8.4	3.4	
Acid Soluble Alkali (ppm)	Dry	As Rec'd	4.7	1.95	6.45	3	
Na			4.1	1.4	5.05	2.6	
Mg			3.5	1.2	3.85	2.2	
Ca			3	0.85	3.00	1.9	
K			2.6	0.7	2.30	1.6	
Fusion Temp. (Reducing)	°F	°C	2.2	0.6	1.70	1.4	
Initial Deformation	2003	1095	1.9	1.45	0.25	1.2	
Spherical	2049	1121	Size Distribution		For -325 Mesh Data		
Hemispherical	2119	1159	D(v,0.5) (µm)		22.10		
Fluid	2269	1243	D(v,0.9) (µm)		43.20		
Fusion Temp. (Oxidizing)	°F	°C	D(v,0.1) (µm)		5.30		
Initial Deformation	2378	1303	D(4,3) (µm)		23.9		
Spherical	2425	1329	D(3,2) (µm)		11.85		
Hemispherical	2472	1355	Span		1.70		
Fluid	2524	1384	Spec. Surf. Area (sq.m./cc.)		0.53		

*These Malvern data are for the -325 mesh size fractions.

Table 3.A.4

Chemical and Physical Analyses of the Pittsburgh #8 (2)

Analyses			Analyses			Analyses		
Proximate	Dry	As Rec'd	Size Distribution		Sieves	mass % in size bin		cum. mass %
Fixed Carbon	56.87	55.92	dp>800µm		+28	0.00		0.00
Volatile Matter	36.58	35.98	800µm>dp>300µm		28x48	0.27		0.27
Moisture	1.66		300µm>dp>149µm		48x100	1.40		1.67
Ultimate	Dry	As Rec'd	149µm>dp>74µm		100x200	27.83		29.50
C	78.62	77.32	74µm>dp>44µm		200x325	30.83		60.33
H	5.14	5.06	44µm>dp		-325	39.67		100.00
O	6.52	6.41	Size Distribution (Malvern)*			Size Distribution (Malvern)*		
N	1.50	1.48	Diameter	% In	cum. vol.	Diameter	% In	cum. vol.
S	1.57	1.54	(µm)	size bin	per.	(µm)	size bin	per.
Ash	6.55	6.44	188	0	100	118.40	0.75	99.9
Ash Chemistry	% dry coal	% ash	162	0	100	102.1	0.15	99.8
SiO2	3.02	46.08	140	0	100	88.1	0.175	99.6
Al2O3	1.54	23.50	121	0	100	76	0.125	99.5
TiO2	0.07	1.02	104	0	100	65.6	1.325	98.2
Fe2O3	1.17	17.93	89.9	0.25	99.8	56.6	5.3	92.9
CaO	0.24	3.73	77.5	0.4	99.4	48.8	9.875	83.0
MgO	0.05	0.84	66.9	0.35	99.0	42.1	11.45	71.5
K2O	0.11	1.72	57.7	1.05	98.0	36.3	10.025	5
Na2O	0.03	0.45	49.8	5.35	92.6	31.3	8.025	53.5
SO3	0.22	3.34	42.9	9.45	83.2	27	8	45.5
P2O5	0.04	0.64	37.1	12.6	70.6	23.3	8.875	36.6
Und. Ash	0.05	0.74	32	11.95	58.6	20.1	7.225	29.4
Free Silica/Total Silicon	0.23		27.6	8.55	50.1	17.4	4.425	25.0
Pyritic Iron/Total Iron	0.74		23.8	6.6	43.5	15	3.7	21.3
Chlorine	Dry	As Rec'd	20.5	6	37.5	12.9	4.4	16.9
Cl (bomb)	0.10	0.09	17.7	6.35	31.1	11.1	3.9	13.0
Cl (in ash)			15.3	6.4	24.7	9.6	2.875	10.1
Forms of Sulfur	Dry	As Rec'd	13.2	5.25	19.5	8.3	1.625	8.45
Sulfatic	0.05	0.05	11.4	4.05	15.4	7.2	1.45	7.00
Pyritic	0.69	0.68	9.8	2.85	12.6	6.2	1.5	5.50
Organic	0.82	0.81	8.5	2.25	10.3	5.3	1.325	4.17
Heating Value (Btu/lb)	Dry	As Rec'd	7.3	2	8.30	4.6	1.2	2.97
As Fired	13994	13762	6.3	1.8	6.50	4	0.925	2.05
Dulong			5.4	1.65	4.85	3.4	0.875	1.17
Acid Soluble Alkali (ppm)	Dry	As Rec'd	4.7	1.35	3.50	3	0.7	0.47
Na			4.1	0.9	2.60	2.6	0.3	0.17
Mg			3.5	0.8	1.80	2.2	0.125	0.05
Ca			3	0.5	1.30	1.9	0	0.05
K			2.6	0.35	0.95	1.6	0.05	0.00
Fusion Temp. (Reducing)	°F	°C	2.2	0.25	0.70	1.4	0	0.00
Initial Deformation	2109	1154	1.9	0.55	0.15	1.2	0	0.00
Spherical	2268	1242	Size Distribution			For -325 Mesh Data		
Hemispherical	2383	1306	D(v,0.5) (µm)			24.78		
Fluid	2481	1360	D(v,0.9) (µm)			44.78		
Fusion Temp. (Oxidizing)	°F	°C	D(v,0.1) (µm)			18.55		
Initial Deformation	2472	1356	D(4,3) (µm)			25.5167		
Spherical	2519	1382	D(3,2) (µm)			14.80		
Hemispherical	2550	1399	Span			1.48		
Fluid	2604	1429	Spec. Surf. Area (sq.m./cc.)			0.39		

*These Malvern data are for the -325 mesh size fractions.

Table 3.A.5

Chemical and Physical Analyses of the Eastern Kentucky Coal

Analyses			Analyses					
Proximate	Dry	As Rec'd	Size Distribution	Sieves	mass % In size bin	cum. mass %		
Fixed Carbon	53.03	52.41	dp>600µm	+28	0.00	0.00		
Volatlie Matter	36.82	36.39	600µm>dp>300µm	28x48	0.07	0.07		
Moisture	1.17		300µm>dp>149µm	48x100	1.50	1.57		
Ultimate	Dry	As Rec'd	149µm>dp>74µm	100x200	32.10	33.67		
C	75.02	74.15	74µm>dp>44µm	200x325	30.80	64.47		
H	4.99	4.93	44µm>dp	-325	35.53	100.00		
O	7.32	7.23	Size Distribution (Malvern)*		Size Distribution (Malvern)*			
N	1.46	1.44	Diameter (µm)	% In size bin	cum. vol. per.	Diameter (µm)	% In size bin	cum. vol. per.
S	0.98	0.97	188	0	100	118.4	0.05	99.95
Ash	10.15	10.03	162	0.1	99.9	102.1	0.13	99.825
Ash Chemistry	% dry coal	% ash	140	0.1	99.8	88.1	0.15	99.675
SiO2	5.89	58.01	121	0.1	99.7	76	0.23	99.45
Al2O3	3.08	30.40	104	0.1	99.6	65.6	1.98	97.475
TiO2	0.21	2.04	89.9	0.35	99.3	56.6	5.58	91.9
Fe2O3	0.49	4.86	77.5	1.25	98.0	48.8	9.70	82.2
CaO	0.11	1.12	66.9	2.6	95.4	42.1	10.70	71.5
MgO	0.04	0.39	57.7	4.3	91.1	36.3	8.63	62.875
K2O	0.10	0.96	49.8	6.45	84.7	31.3	6.40	56.475
Na2O	0.01	0.11	42.9	8.6	76.1	27	6.98	49.5
SO3	0.13	1.28	37.1	10.65	65.4	23.3	8.98	40.525
P2O5	0.01	0.13	32	10.1	55.3	20.1	7.55	32.975
Und. Ash	0.07	0.72	27.6	7.7	47.6	17.4	4.28	28.7
Free Silica/Total Silicon	0.21		23.8	6.05	41.6	15	3.30	25.4
Pyritic Iron/Total Iron	0.83		20.5	5.35	36.2	12.9	4.13	21.275
Chlorine	Dry	As Rec'd	17.7	5.3	30.9	11.1	4.35	16.925
Cl (bomb)	0.09	0.09	15.3	5.25	25.7	9.6	3.90	13.025
Cl (in ash)			13.2	4.6	21.1	8.3	2.40	10.625
Forms of Sulfur	Dry	As Rec'd	11.4	3.85	17.2	7.2	1.63	9
Sulfatic	0.003	0.003	9.8	2.9	14.3	6.2	1.68	7.325
Pyritic	0.33	0.32	8.5	2.4	11.9	5.3	1.78	5.55
Organic	0.65	0.64	7.3	2.15	9.8	4.6	1.60	3.95
Heating Value (Btu/lb)	Dry	As Rec'd	6.3	2.1	7.7	4	1.40	2.55
As Fired	13254	13099	5.4	2	5.7	3.4	1.15	1.4
Dulong			4.7	1.7	4.0	3	0.93	0.475
Acid Soluble Alkali (ppm)	Dry	As Rec'd	4.1	1.2	2.8	2.6	0.45	0.025
Na			3.5	1	1.8	2.2	0.15	-0.125
Mg			3	0.65	1.1	1.9	0	-0.125
Ca			2.6	0.4	0.7	1.6	0	-0.125
K			2.2	0.3	0.4	1.4	0	-0.125
Fusion Temp. (Reducing)	°F	°C	1.9	0.5	-0.1	1.2	0	-0.125
Initial Deformation	2948	1620	Size Distribution		For -325 Mesh Data			
Spherical	2980	1638	D(v,0.5) (µm)		24.03			
Hemispherical	2992	1644	D(v,0.9) (µm)		47.63			
Fluid	3000	1649	D(v,0.1) (µm)		6.70			
Fusion Temp. (Oxidizing)	°F	°C	D(4,3) (µm)		25.88			
Initial Deformation	2961	1627	D(3,2) (µm)		13.72			
Spherical	2998	1648	Span		1.70			
Hemispherical	3000	1649	Spec. Surf. Area (sq.m./cc.)		0.42			
Fluid	3000	1649						

*These Malvern data are for the -325 mesh size fractions.

Table 3.A.6

Chemical and Physical Analyses of the Pittsburgh #8 (1) Coal

Analyses			Analyses				
Proximate	Dry	As Rec'd	Size Distribution		Sieves	mass % in size bin	cum. mass %
Fixed Carbon	49.16	48.66	dp>600µm		+28	0	0.00
Volatile Matter	40.16	39.75	600µm>dp>300µm		28x48	0.2	0.20
Moisture	1.02		300µm>dp>149µm		48x100	0.8	1.00
Ultimate	Dry	As Rec'd	149µm>dp>74µm		100x200	22.1	23.10
C	71.51	70.78	74µm>dp>44µm		200x325	34.8	57.90
H	5.03	4.98	44µm>dp		-325	42.1	100.00
O	6.76	6.69	Size Distribution (Malvern)*		Size Distribution (Malvern)*		
N	1.24	1.23	Diameter	% In	cum. vol.	Diameter	% In
S	4.78	4.73	(µm)	size bin	per.	(µm)	size bin
Ash	10.68	10.57	188			118.4	
Ash Chemistry	% dry coal	% ash	162			102.1	
SiO2	4.42	41.40	140			88.1	
Al2O3	2.19	20.51	121			76	
TiO2	0.10	0.89	104			65.6	
Fe2O3	3.10	29.03	89.9			56.6	
CaO	0.22	2.07	77.5			48.8	
MgO	0.08	0.78	66.9			42.1	
K2O	0.18	1.73	57.7			36.3	
Na2O	0.04	0.40	49.8			31.3	
SO3	0.25	2.33	42.9			27	
P2O5	0.02	0.15	37.1			23.3	
Und. Ash	0.08	0.71	32			20.1	
Free Silica/Total Silicon	0.26		27.6			17.4	
Pyritic Iron/Total Iron	0.73		23.8			15	
Chlorine	Dry	As Rec'd	20.5			12.9	
Cl (bomb)			17.7			11.1	
Cl (in ash)			15.3			9.6	
Forms of Sulfur	Dry	As Rec'd	13.2			8.3	
Sulfatic	0.15	0.15	11.4			7.2	
Pyritic	1.81	1.79	9.8			6.2	
Organic	2.82	2.79	8.5			5.3	
Heating Value (Btu/lb)	Dry	As Rec'd	7.3			4.6	
As Fired	13004	12871	6.3			4	
Dulong			5.4			3.4	
Acid Soluble Alkali (ppm)	Dry	As Rec'd	4.7			3	
Na			4.1			2.6	
Mg			3.5			2.2	
Ca			3			1.9	
K			2.6			1.6	
Fusion Temp. (Reducing)	°F	°C	2.2			1.4	
Initial Deformation	1917	1047	1.9			1.2	
Spherical	1980	1082	Size Distribution		For -325 Mesh Data		
Hemispherical	2154	1179	D(v,0.5) (µm)				
Fluid	2232	1222	D(v,0.9) (µm)				
Fusion Temp. (Oxidizing)	°F	°C	D(v,0.1) (µm)				
Initial Deformation	2438	1337	D(4,3) (µm)				
Spherical	2502	1372	D(3,2) (µm)				
Hemispherical	2518	1381	Span				
Fluid	2532	1389	Spec. Surf. Area (sq.m./cc.)				

*These Malvern data are for the -325 mesh size fractions.

Table 3.A.7

Chemical and Physical Analyses of the Utah Blind Canyon Coal

Analyses			Analyses				
Proximate	Dry	As Rec'd	Size Distribution		Sieves	mass % in size bin	cum. mass %
Fixed Carbon	46.03	44.51	dp>600µm		+28	0	0.00
Volatile Matter	43.58	42.14	600µm>dp>300µm		28x48	0.2	0.20
Moisture	3.30		300µm>dp>149µm		48x100	5.3	5.50
Ultimate	Dry	As Rec'd	149µm>dp>74µm		100x200	25.25	30.75
C	72.98	70.58	74µm>dp>44µm		200x325	22.4	53.15
H	5.54	5.35	44µm>dp		-325	46.85	100.00
O	9.27	8.96	Size Distribution (Malvern)*			Size Distribution (Malvern)*	
N	1.32	1.28	Diameter (µm)	% in size bin	cum. vol. per.	Diameter (µm)	% in size bin
S	0.46	0.44					
Ash	10.40	10.06	188	0	100	118.4	
Ash Chemistry	% dry coal	% ash	162	0	100	102.1	
SiO2	5.86	56.35	140	0	100	88.1	
Al2O3	1.87	17.97	121	0	100	76	
TiO2	0.10	0.94	104	0	100	65.6	
Fe2O3	0.43	4.13	89.9	0.15	99.9	56.6	
CaO	0.65	6.23	77.5	0.45	99.4	48.8	
MgO	0.19	1.84	66.9	0.9	98.5	42.1	
K2O	0.12	1.14	57.7	1.9	96.6	36.3	
Na2O	0.53	5.06	49.8	4.85	91.8	31.3	
SO3	0.57	5.46	42.9	7.9	83.8	27	
P2O5	0.03	0.32	37.1	10.65	73.2	23.3	
Und. Ash	0.06	0.58	32	10.45	62.7	20.1	
Free Silica/Total Silicon	0.52		27.6	8.1	54.6	17.4	
Pyritic Iron/Total Iron	0.29		23.8	6.15	48.5	15	
Chlorine	Dry	As Rec'd	20.5	5.15	43.3	12.9	
Cl (bomb)	0.04	0.04	17.7	5.5	37.8	11.1	
Cl (in ash)			15.3	6.05	31.8	9.6	
Forms of Sulfur	Dry	As Rec'd	13.2	5.5	26.3	8.3	
Sulfatic	0.00	0.00	11.4	4.5	21.8	7.2	
Pyritic	0.10	0.10	9.8	3.15	18.6	6.2	
Organic	0.36	0.35	8.5	2.6	16.0	5.3	
Heating Value (Btu/lb)	Dry	As Rec'd	7.3	2.6	13.4	4.6	
As Fired	13146	12713	6.3	2.7	10.7	4	
Dulong			5.4	2.55	8.20	3.4	
Acid Soluble Alkali (ppm)	Dry	As Rec'd	4.7	2.1	6.10	3	
Na			4.1	1.25	4.85	2.6	
Mg			3.5	1.05	3.80	2.2	
Ca			3	0.75	3.05	1.9	
K			2.6	0.7	2.35	1.6	
Fusion Temp. (Reducing)	°F	°C	2.2	0.65	1.70	1.4	
Initial Deformation	2181	1194	1.9	1.6	0.10	1.2	
Spherical	2247	1231	Size Distribution		For -325 Mesh Data		
Hemispherical	2358	1292	D(v,0.5) (µm)		21.30		
Fluid	2621	1438	D(v,0.9) (µm)		41.30		
Fusion Temp. (Oxidizing)	°F	°C	D(v,0.1) (µm)		5.25		
Initial Deformation	2214	1212	D(4,3) (µm)		22.75		
Spherical	2255	1235	D(3,2) (µm)		11.45		
Hemispherical	2389	1309	Span		1.70		
Fluid	2670	1465	Spec. Surf. Area (sq.m./cc.)		0.55		

*These Malvern data are for the -325 mesh size fractions.

Table 3.A.8

Chemical and Physical Analyses of the Kentucky #11 Coal

Analyses			Analyses			Analyses	
Proximate	Dry	As Rec'd	Size Distribution	Sieves	mass % in size bin	cum. mass %	
Fixed Carbon	42.82	41.12	dp>800µm	+28	0	0.00	
Volatiles Matter	34.97	33.58	600µm>dp>300µm	28x48	0.2	0.20	
Molsture	3.97		300µm>dp>149µm	48x100	2.7	2.90	
Ultimate	Dry	As Rec'd	149µm>dp>74µm	100x200	15.4	18.30	
C	59.15	56.81	74µm>dp>44µm	200x325	22.7	41.00	
H	4.44	4.26	44µm>dp	-325	59	100.00	
O	8.25	7.93	Size Distribution (Malvern)*			Size Distribution (Malvern)*	
N	1.16	1.11	Diameter (µm)	% In size bin	cum. vol. per.	Diameter (µm)	% In size bin
S	4.78	4.59	188	0	100	118.4	
Ash	22.21	21.33	162	0	100	102.1	
Ash Chemistry	% dry coal	% ash	140	0	100	88.1	
SiO2	10.14	45.65	121	0	100	76	
Al2O3	4.14	18.62	104	0	100	65.6	
TiO2	0.19	0.86	89.9	0.15	99.9	56.6	
Fe2O3	4.67	21.05	77.5	0.45	99.4	48.8	
CaO	0.96	4.30	66.9	0.8	98.8	42.1	
MgO	0.21	0.96	57.7	1.6	97.2	36.3	
K2O	0.49	2.19	49.8	3.85	93.3	31.3	
Na2O	0.07	0.33	42.9	6.65	86.7	27	
SO3	1.02	4.58	37.1	9.55	77.1	23.3	
P2O5	0.04	0.19	32	9.9	67.2	20.1	
Und. Ash	0.11	0.48	27.6	8.15	59.1	17.4	
Free Silica/Total Silicon	0.39		23.8	6.85	52.2	15	
Pyritic Iron/Total Iron	0.80		20.5	6.2	46.0	12.9	
Chlorine	Dry	As Rec'd	17.7	6.2	39.8	11.1	
Cl (bomb)	0.03	0.03	15.3	6.35	33.5	9.6	
Cl (In ash)	0.02	0.02	13.2	5.7	27.8	8.3	
Forms of Sulfur	Dry	As Rec'd	11.4	4.75	23.0	7.2	
Sulfatic	0.20	0.20	9.8	3.5	19.5	6.2	
Pyritic	2.99	2.87	8.5	2.9	16.6	5.3	
Organic	1.59	1.53	7.3	2.8	13.8	4.6	
Heating Value (Btu/lb)	Dry	As Rec'd	6.3	2.75	11.1	4	
As Fired	10524	10107	5.4	2.6	8.5	3.4	
Dulong			4.7	2.2	6.3	3	
Acid Soluble Alkali (ppm)	Dry	As Rec'd	4.1	1.55	4.7	2.6	
Na	400	384	3.5	1.15	3.6	2.2	
Mg	1037	995	3	0.85	2.7	1.9	
Ca	4981	4783	2.6	0.7	2.0	1.6	
K	3578	3436	2.2	0.55	1.5	1.4	
Fusion Temp. (Reducing)	°F	°C	1.9	1.25	0.2	1.2	
Initial Deformation	2238	1226	Size Distribution			For -325 Mesh Data	
Spherical	2270	1243	D(v,0.5) (µm)			19.55	
Hemispherical	2310	1266	D(v,0.9) (µm)			39.75	
Fluid	2352	1289	D(v,0.1) (µm)			5.20	
Fusion Temp. (Oxidizing)	°F	°C	D(4,3) (µm)			21.75	
Initial Deformation	2314	1268	D(3,2) (µm)			11.25	
Spherical	2354	1290	Span			1.80	
Hemispherical	2404	1318	Spec. Surf. Area (sq.m./cc.)			0.55	
Fluid	2446	1341					

*These Malvern data are for the -325 mesh size fractions.

Table 3.A.9

Chemical and Physical Analyses of the Illinois #6 (2) Coal

Analyses			Analyses			Analyses		
Proximate	Dry	As Rec'd	Size Distribution		Sieves	mass % In size bin	cum. mass %	
Fixed Carbon	48.28	47.05	dp>600µm		+28	0	0.00	
Volatile Matter	39.40	38.40	600µm>dp>300µm		28x48	0	0.00	
Moisture	2.54		300µm>dp>149µm		48x100	1.75	1.75	
Ultimate	Dry	As Rec'd	149µm>dp>74µm		100x200	30.85	32.60	
C	69.18	67.43	74µm>dp>44µm		200x325	28.3	60.90	
H	4.82	4.69	44µm>dp		-325	39.1	100.00	
O	8.86	8.63	Size Distribution (Malvern)*			Size Distribution (Malvern)*		
N	1.21	1.17	Diameter (µm)	% In size bin	cum. vol. per.	Diameter (µm)	% In size bin	cum. vol. per.
S	3.51	3.42	188	0	100	118.4		
Ash	12.33	12.02	162	0	100	102.1		
Ash Chemistry	% dry coal	% ash	140	0	100	88.1		
SiO ₂	6.10	49.50	121	0	100	76		
Al ₂ O ₃	2.31	18.74	104	0	100	65.6		
TiO ₂	0.11	0.90	89.9	0.1	99.9	56.6		
Fe ₂ O ₃	2.13	17.29	77.5	0.45	99.5	48.8		
CaO	0.11	0.90	66.9	1.85	97.6	42.1		
MgO	2.13	17.29	57.7	4	93.6	36.3		
K ₂ O	0.37	2.99	49.8	6.55	87.1	31.3		
Na ₂ O	0.56	4.55	42.9	8.65	78.4	27		
SO ₃	0.13	1.07	37.1	10.4	68.0	23.3		
P ₂ O ₅	0.26	2.12	32	10.1	57.9	20.1		
Und. Ash	0.16	1.27	27.6	8.15	49.8	17.4		
Free Silica/Total Silicon	0.43		23.8	6.35	43.4	15		
Pyritic Iron/Total Iron	0.37		20.5	5.25	38.2	12.9		
Chlorine	Dry	As Rec'd	17.7	5.4	32.8	11.1		
Cl (bomb)	0.10	0.10	15.3	5.65	27.1	9.6		
Cl (In ash)			13.2	4.85	22.3	8.3		
Forms of Sulfur	Dry	As Rec'd	11.4	3.8	18.5	7.2		
Sulfatic	0.26	0.25	9.8	2.65	15.8	6.2		
Pyritic	1.33	1.30	8.5	2.25	13.6	5.3		
Organic	1.99	1.94	7.3	2.3	11.3	4.6		
Heating Value (Btu/lb)	Dry	As Rec'd	6.3	2.4	8.9	4		
As Fired	12233	11923	5.4	2.3	6.6	3.4		
Dulong			4.7	1.85	4.7	3		
Acid Soluble Alkali (ppm)	Dry	As Rec'd	4.1	1.15	3.6	2.6		
Na			3.5	0.95	2.6	2.2		
Mg			3	0.7	1.9	1.9		
Ca			2.6	0.5	1.4	1.6		
K			2.2	0.4	1.0	1.4		
Fusion Temp. (Reducing)	°F	°C	1.9	0.9	0.1	1.2		
Initial Deformation Spherical	2014	1101	Size Distribution			For -325 Mesh Data		
Hemispherical	2071	1133	D(v,0.5) (µm)			23.95		
Fluid	2202	1205	D(v,0.9) (µm)			45.70		
	2382	1305	D(v,0.1) (µm)			5.85		
Fusion Temp. (Oxidizing)	°F	°C	D(4,3) (µm)			25.25		
Initial Deformation Spherical	2285	1251	D(3,2) (µm)			13.10		
Hemispherical	2334	1279	Span			1.70		
Fluid	2449	1343	Spec. Surf. Area (sq.m./cc.)			0.47		
	2530	1388						

*These Malvern data are for the -325 mesh size fractions.

Table 3.A.10

Chemical and Physical Analyses of the Kentucky #9 Coal

Analyses			Analyses			Analyses	
Proximate	Dry	As Rec'd	Size Distribution	Sieves	mass % In size bin	cum. mass %	
Fixed Carbon	47.47	43.53	dp>600µm	+28	0	0	
Volatiles Matter	37.88	34.74	600µm>dp>300µm	28x48	0.1	0.1	
Moisture	8.30		300µm>dp>149µm	48x100	1.75	1.85	
Ultimate	Dry	As Rec'd	149µm>dp>74µm	100x200	14.15	16	
C	66.00	60.52	74µm>dp>44µm	200x325	28.25	44.25	
H	4.69	4.30	44µm>dp	-325	55.75	100	
O	9.07	8.32	Size Distribution (Malvern)*			Size Distribution (Malvern)*	
N	1.70	1.56	Diameter	% In	cum. vol.	Diameter	% In
S	3.88	3.56	(µm)	size bin	per.	(µm)	size bin
Ash	14.64	13.43	188	0	100	118.4	
Ash Chemistry	% dry coal	% ash	162	0	100	102.1	
SiO2	6.59	44.99	140	0.05	100	88.1	
Al2O3	2.97	20.25	121	0.05	99.9	76	
TiO2	0.15	1.03	104	0	99.9	65.6	
Fe2O3	3.37	23.03	89.9	0.15	99.8	56.6	
CaO	0.44	3.00	77.5	0.75	99.0	48.8	
MgO	0.16	1.08	66.9	1.85	97.2	42.1	
K2O	0.37	2.52	57.7	3.45	93.7	36.3	
Na2O	0.14	0.98	49.8	5.65	88.1	31.3	
SO3	0.60	4.10	42.9	7.95	80.1	27	
P2O5	0.02	0.12	37.1	10.4	69.7	23.3	
Und. Ash	0.03	0.18	32	10.65	59.1	20.1	
Free Silica/Total Silicon	0.32		27.6	9.05	50.0	17.4	
Pyritic Iron/Total Iron	0.61		23.8	7.4	42.6	15	
Chlorine	Dry	As Rec'd	20.5	5.95	36.6	12.9	
Cl (bomb)	0.07	0.06	17.7	5.55	31.1	11.1	
Cl (In ash)	0.03	0.02	15.3	5.45	25.6	9.6	
Forms of Sulfur	Dry	As Rec'd	13.2	5	20.6	8.3	
Sulfatic	0.18	0.16	11.4	4.2	16.4	7.2	
Pyritic	1.66	1.52	9.8	3.05	13.4	6.2	
Organic	2.04	1.87	8.5	2.35	11.0	5.3	
Heating Value (Btu/lb)	Dry	As Rec'd	7.3	2	9.0	4.6	
As Fired	11847	10864	6.3	1.9	7.1	4	
Dulong	12053	11053	5.4	1.8	5.3	3.4	
Acid Soluble Alkali (ppm)	Dry	As Rec'd	4.7	1.65	3.7	3	
Na	694	636	4.1	1.1	2.6	2.6	
Mg	830	761	3.5	0.95	1.6	2.2	
Ca	2835	2600	3	0.6	1.0	1.9	
K	2225	2040	2.6	0.4	0.6	1.6	
Fusion Temp. (Reducing)	°F	°C	2.2	0.3	0.3	1.4	
Initial Deformation	1981	1083	1.9	0.5	-0.2	1.2	
Spherical	2050	1121	Size Distribution			For -325 Mesh Data	
Hemispherical	2200	1204	D(v,0.5) (µm)			23.80	
Fluid	2324	1274	D(v,0.9) (µm)			44.85	
Fusion Temp. (Oxidizing)	°F	°C	D(v,0.1) (µm)			6.75	
Initial Deformation	2318	1270	D(4,3) (µm)			25.55	
Spherical	2415	1324	D(3,2) (µm)			14.00	
Hemispherical	2465	1352	Span			1.60	
Fluid	2518	1381	Spec. Surf. Area (sq.m./cc.)			0.43	

*These Malvern data are for the -325 mesh size fractions.

Table 3.A.11

Chemical and Physical Analyses of the Hanna Basin Coal

Analyses			Analyses			Analyses		
Proximate	Dry	As Rec'd	Size Distribution		Sieves	mass % in size bin		cum. mass %
Fixed Carbon	50.60	45.03	dp>600µm		+28			
Volatile Matter	38.40	34.16	600µm>dp>300µm		28x48			
Moisture	11.00		300µm>dp>149µm		48x100			
Ultimate	Dry	As Rec'd	149µm>dp>74µm		100x200			
C	65.00	57.85	74µm>dp>44µm		200x325			
H	5.00	4.45	44µm>dp		-325			
O	16.85	15.00	Size Distribution (Malvern)*			Size Distribution (Malvern)*		
N	1.40	1.25	Diameter	% in	cum. vol.	Diameter	% in	cum. vol.
S	0.70	0.62	(µm)	size bin	per.	(µm)	size bin	per.
Ash	11.05	9.83	188			118.4		
Ash Chemistry	% dry coal	% ash	162			102.1		
SiO ₂	3.65	33.00	140			88.1		
Al ₂ O ₃	1.60	14.50	121			76		
TiO ₂	0.11	1.00	104			65.6		
Fe ₂ O ₃	0.88	8.00	89.9			56.6		
CaO	2.98	27.00	77.5			48.8		
MgO	0.44	4.00	66.9			42.1		
K ₂ O	0.07	0.60	57.7			36.3		
Na ₂ O	0.17	1.50	49.8			31.3		
SO ₃	0.88	8.00	42.9			27		
P ₂ O ₅	0.07	0.60	37.1			23.3		
Und. Ash	0.09	0.80	32			20.1		
Free Silica/Total Silicon	0.34		27.6			17.4		
Pyritic Iron/Total Iron	0.24		23.8			15		
Chlorine	Dry	As Rec'd	20.5			12.9		
Cl (bomb)			17.7			11.1		
Cl (in ash)			15.3			9.6		
Forms of Sulfur	Dry	As Rec'd	13.2			8.3		
Sulfatic	0.01	0.01	11.4			7.2		
Pyritic	0.17	0.15	9.8			6.2		
Organic	0.51	0.45	8.5			5.3		
Heating Value (Btu/lb)	Dry	As Rec'd	7.3			4.6		
As Fired	12093	10763	6.3			4		
Dulong			5.4			3.4		
Acid Soluble Alkali (ppm)	Dry	As Rec'd	4.7			3		
Na			4.1			2.6		
Mg			3.5			2.2		
Ca			3			1.9		
K			2.6			1.6		
Fusion Temp. (Reducing)	°F	°C	2.2			1.4		
Initial Deformation	2300	1260	1.9			1.2		
Spherical	2350	1288	Size Distribution		For -325 Mesh Data			
Hemispherical	2360	1293	D(v,0.5) (µm)					
Fluid	2400	1316	D(v,0.9) (µm)					
Fusion Temp. (Oxidizing)	°F	°C	D(v,0.1) (µm)					
Initial Deformation	2375	1302	D(4,3) (µm)					
Spherical	2425	1329	D(3,2) (µm)					
Hemispherical	2450	1343	Span					
Fluid	2475	1357	Spec. Surf. Area (sq.m./cc.)					

*These Malvern data are for the -325 mesh size fractions.

Table 3.A.12

Chemical and Physical Analyses of the Illinois #6 (1) Coal

Analyses			Analyses			Analyses		
Proximate	Dry	As Rec'd	Size Distribution		Sieves	mass % in size bin		cum. mass %
Fixed Carbon	48.91	43.12	dp>600µm		+28	0.00		0.00
Volatiles Matter	40.95	36.10	600µm>dp>300µm		28x48	0.07		0.07
Moisture	11.83		300µm>dp>149µm		48x100	1.80		1.87
Ultimate	Dry	As Rec'd	149µm>dp>74µm		100x200	15.17		17.03
C	68.76	60.63	74µm>dp>44µm		200x325	29.20		46.23
H	5.09	4.49	44µm>dp		-325	55.43		101.67
O	10.19	8.99	Size Distribution (Malvern)*			Size Distribution (Malvern)*		
N	1.47	1.30	Diameter	% In	cum. vol.	Diameter	% In	cum. vol.
S	4.33	3.82	(µm)	size bin	per.	(µm)	size bin	per.
Ash	10.13	8.93	188	0	100	118.4	0.05	99.95
Ash Chemistry	% dry coal	% ash	162	0	100	102.1	0.15	99.8
SiO ₂	4.70	46.41	140	0	100	88.1	0.15	99.65
Al ₂ O ₃	1.71	16.87	121	0	100	76	0.1	99.55
TiO ₂	0.09	0.89	104	0	100	65.6	1.65	97.9
Fe ₂ O ₃	2.06	20.30	89.9	0.05	100	56.6	5.4	92.5
CaO	0.53	5.20	77.5	0.55	99.4	48.8	9.55	82.95
MgO	0.08	0.75	66.9	1.65	97.8	42.1	10.95	72
K ₂ O	0.20	2.01	57.7	3.4	94.4	36.3	9.55	62.45
Na ₂ O	0.13	1.31	49.8	5.8	88.6	31.3	7.75	54.7
SO ₃	0.50	4.89	42.9	8.6	80.0	27	8.2	46.5
P ₂ O ₅	0.02	0.15	37.1	11.45	68.5	23.3	9.55	36.95
Und. Ash	0.07	0.71	32	11.6	56.9	20.1	7.55	29.4
Free Silica/Total Silicon	0.45		27.6	9.4	47.5	17.4	4.15	25.25
Pyritic Iron/Total Iron	0.78		23.8	7.1	40.4	15	3.65	21.6
Chlorine	Dry	As Rec'd	20.5	5.6	34.8	12.9	4.9	16.7
Cl (bomb)	0.11	0.10	17.7	5.8	29.0	11.1	4.2	12.5
Cl (In ash)	0.02	0.01	15.3	6.1	22.9	9.6	3	9.5
Forms of Sulfur	Dry	As Rec'd	13.2	5.25	17.7	8.3	1.6	7.9
Sulfatic	0.27	0.23	11.4	3.95	13.7	7.2	1.2	6.7
Pyritic	1.28	1.13	9.8	2.5	11.2	6.2	1.55	5.15
Organic	2.79	2.46	8.5	1.9	9.3	5.3	1.35	3.8
Heating Value (Btu/lb)	Dry	As Rec'd	7.3	1.8	7.5	4.6	1.15	2.65
As Fired	12226	10779	6.3	1.9	5.6	4	0.8	1.85
Dulong	12615	11122	5.4	1.6	4.0	3.4	0.75	1.1
Acid Soluble Alkali (ppm)	Dry	As Rec'd	4.7	1.3	2.7	3	0.7	0.4
Na	2256	1989	4.1	0.9	1.8	2.6	0.1	0.3
Mg	1766	1557	3.5	0.65	1.15	2.2	0.1	0.2
Ca	5977	5270	3	0.4	0.75	1.9	0	0.2
K	2380	2099	2.6	0.2	0.55	1.6	0	0.2
Fusion Temp. (Reducing)	°F	°C	2.2	0.2	0.35	1.4	0	0.2
Initial Deformation	1938	1059	1.9	0.3	0.05	1.2	0	0.2
Spherical	1994	1090	Size Distribution			For -325 Mesh Data		
Hemispherical	2112	1155	D(v,0.5) (µm)			24.85		
Fluid	2279	1248	D(v,0.9) (µm)			45.63		
Fusion Temp. (Oxidizing)	°F	°C	D(v,0.1) (µm)			8.18		
Initial Deformation	2262	1239	D(4,3) (µm)			26.15		
Spherical	2287	1253	D(3,2) (µm)			15.6		
Hemispherical	2373	1300	Span			1.53		
Fluid	2510	1376	Spec. Surf. Area (sq.m./cc.)			0.38		

*These Malvern data are for the -325 mesh size fractions.

Table 3.A.13

Chemical and Physical Analyses of the Roland-Seam Coal

Analyses			Analyses			Analyses	
Proximate	Dry	As Rec'd	Size Distribution		Sieves	mass % in size bin	cum. mass %
Fixed Carbon	49.20	44.33	dp>600µm		+28	0	0.00
Volatile Matter	44.52	40.11	600µm>dp>300µm		28x48	0.1	0.10
Moisture	9.89		300µm>dp>149µm		48x100	1.6	1.70
Ultimate	Dry	As Rec'd	149µm>dp>74µm		100x200	24.75	26.45
C	70.36	63.40	74µm>dp>44µm		200x325	29.8	56.25
H	4.62	4.16	44µm>dp		-325	43.75	100.00
O	17.19	15.49	Size Distribution (Malvern)*			Size Distribution (Malvern)*	
N	0.89	0.80	Diameter (µm)	% in size bin	cum. vol. per.	Diameter (µm)	% in size bin
S	0.44	0.40					
Ash	6.29	5.67	188	0	100	118.4	
Ash Chemistry	% dry coal	% ash	162	0	100	102.1	
SiO ₂	1.91	30.31	140	0	100	88.1	
Al ₂ O ₃	0.91	14.54	121	0	100	76	
TiO ₂	0.07	1.07	104	0	100	65.6	
Fe ₂ O ₃	0.47	7.50	89.9	0.05	100	56.6	
CaO	1.21	19.31	77.5	0.25	99.7	48.8	
MgO	0.31	4.88	66.9	1.2	98.5	42.1	
K ₂ O	0.03	0.41	57.7	2.7	95.8	36.3	
Na ₂ O	0.13	2.08	49.8	4.85	91.0	31.3	
SO ₃	1.14	18.13	42.9	7.5	83.5	27	
P ₂ O ₅	0.06	1.00	37.1	10.15	73.3	23.3	
Und. Ash	0.08	1.29	32	9.75	63.6	20.1	
Free Silica/Total Silicon	0.28		27.6	7.05	56.5	17.4	
Pyritic Iron/Total Iron	0.11		23.8	5.6	50.9	15	
Chlorine	Dry	As Rec'd	20.5	5.4	45.5	12.9	
Cl (bomb)	0.04	0.04	17.7	5.8	39.7	11.1	
Cl (in ash)			15.3	5.85	33.9	9.6	
Forms of Sulfur	Dry	As Rec'd	13.2	4.9	29.0	8.3	
Sulfatic	0.00	0.00	11.4	3.9	25.1	7.2	
Pyritic	0.07	0.06	9.8	3.1	22.0	6.2	
Organic	0.27	0.24	8.5	3	19.0	5.3	
Heating Value (Btu/lb)	Dry	As Rec'd	7.3	3.1	15.9	4.6	
As Fired	11969	10785	6.3	3.15	12.7	4	
Dulong			5.4	2.9	9.80	3.4	
Acid Soluble Alkali (ppm)	Dry	As Rec'd	4.7	2.4	7.40	3	
Na			4.1	1.85	5.55	2.6	
Mg			3.5	1.3	4.25	2.2	
Ca			3	1	3.25	1.9	
K			2.6	0.9	2.35	1.6	
Fusion Temp. (Reducing)	°F	°C	2.2	0.65	1.70	1.4	
Initial Deformation	2059	1126	1.9	1.6	0.10	1.2	
Spherical	2108	1153	Size Distribution			For -325 Mesh Data	
Hemispherical	2126	1163	D(v,0.5) (µm)			20.05	
Fluid	2176	1191	D(v,0.9) (µm)			42.00	
Fusion Temp. (Oxidizing)	°F	°C	D(v,0.1) (µm)			4.75	
Initial Deformation	2132	1167	D(4,3) (µm)			21.8	
Spherical	2176	1191	D(3,2) (µm)			10.55	
Hemispherical	2203	1206	Span			1.85	
Fluid	2262	1239	Spec. Surf. Area (sq.m./cc.)			0.59	

*These Malvern data are for the -325 mesh size fractions.

Table 3.A.14

Chemical and Physical Analyses of Decker Coal

Analyses			Analyses			Analyses		
Proximate	Dry	As Rec'd	Size Distribution		Sieves	mass % In size bin		cum. mass %
Fixed Carbon	50.87	41.72	dp>600µm		+28	0		0.00
Volatile Matter	44.03	36.11	600µm>dp>300µm		28x48	0.15		0.15
Moisture	17.99		300µm>dp>149µm		48x100	4.3		4.45
Ultimate	Dry	As Rec'd	149µm>dp>74µm		100x200	23.2		27.65
C	72.25	59.26	74µm>dp>44µm		200x325	25.05		52.70
H	5.03	4.13	44µm>dp		-325	47.3		100.00
O	16.07	13.18	Size Distribution (Malvern)*			Size Distribution (Malvern)*		
N	1.00	0.82	Diameter (µm)	% In size bin	cum. vol. per.	Diameter (µm)	% In size bin	cum. vol. per.
S	0.53	0.43	188	0	100	118.4		
Ash	5.11	4.19	162	0	100	102.1		
Ash Chemistry	% dry coal	% ash	140	0	100	88.1		
SiO2	1.29	25.31	121	0	100	76		
Al2O3	0.84	16.45	104	0	100	65.6		
TiO2	0.06	1.12	89.9	0.1	99.9	56.6		
Fe2O3	0.31	6.12	77.5	0.6	99.3	48.8		
CaO	0.72	14.03	66.9	1.65	97.7	42.1		
MgO	0.15	3.03	57.7	3.2	94.5	36.3		
K2O	0.03	0.49	49.8	5.5	89.0	31.3		
Na2O	0.43	8.45	42.9	8.65	80.3	27		
SO3	1.14	22.27	37.1	11.95	68.4	23.3		
P2O5	0.04	0.84	32	11.5	56.9	20.1		
Und. Ash	0.08	1.64	27.6	8.05	48.8	17.4		
Free Silica/Total Silicon	0.03		23.8	5.8	43.0	15		
Pyritic Iron/Total Iron	0.72		20.5	5.1	37.9	12.9		
Chlorine	Dry	As Rec'd	17.7	6	31.9	11.1		
Cl (bomb)	0.03	0.03	15.3	6.5	25.4	9.6		
Cl (In ash)			13.2	5.3	20.1	8.3		
Forms of Sulfur	Dry	As Rec'd	11.4	3.95	16.2	7.2		
Sulfatic	0.03	0.02	9.8	2.65	13.5	6.2		
Pyritic	0.19	0.15	8.5	2.3	11.2	5.3		
Organic	0.32	0.26	7.3	2.4	8.8	4.6		
Heating Value (Btu/lb)	Dry	As Rec'd	6.3	2.3	6.5	4		
As Fired	12483	10238	5.4	2	4.5	3.4		
Dulong			4.7	1.5	3.0	3		
Acid Soluble Alkali (ppm)	Dry	As Rec'd	4.1	0.95	2.05	2.6		
Na			3.5	0.75	1.3	2.2		
Mg			3	0.45	0.85	1.9		
Ca			2.6	0.2	0.65	1.6		
K			2.2	0.2	0.45	1.4		
Fusion Temp. (Reducing)	°F	°C	1.9	0.3	0.15	1.2		
Initial Deformation	2080	1138	Size Distribution			For -325 Mesh Data		
Spherical	2152	1178	D(v,0.5) (µm)			24.50		
Hemispherical	2170	1188	D(v,0.9) (µm)			44.05		
Fluid	2202	1206	D(v,0.1) (µm)			6.85		
Fusion Temp. (Oxidizing)	°F	°C	D(4,3) (µm)			25.3		
Initial Deformation	2326	1274	D(3,2) (µm)			14.60		
Spherical	2459	1348	Span			1.50		
Hemispherical	2476	1358	Spec. Surf. Area (sq.m./cc.)			0.41		
Fluid	2506	1374						

*These Malvern data are for the -325 mesh size fractions.

Table 3.A.15

Chemical and Physical Analyses of the Wyodak Coal

Analyses			Analyses			Analyses		
Proximate	Dry	As Rec'd	Size Distribution		Sieves	mass % in size bin		cum. mass %
Fixed Carbon	48.24	38.36	dp>600µm		+28	0.00		0.00
Volatile Matter	45.55	36.22	600µm>dp>300µm		28x48	0.00		0.00
Moisture	20.48		300µm>dp>149µm		48x100	3.87		3.87
Ultimate	Dry	As Rec'd	149µm>dp>74µm		100x200	19.13		23.00
C	70.01	55.67	74µm>dp>44µm		200x325	20.70		43.70
H	4.99	3.97	44µm>dp		-325	56.30		100.00
O	17.24	13.71	Size Distribution (Malvern)*			Size Distribution (Malvern)*		
N	0.93	0.74	Diameter (µm)	% In size bin	cum. vol. per.	Diameter (µm)	% In size bin	cum. vol. per.
S	0.56	0.44	188	0	100	118.4	0.08	99.9
Ash	6.22	4.94	162	0	100	102.1	0.13	99.8
Ash Chemistry	% dry coal	% ash	140	0	100	88.1	0.15	99.7
SiO2	1.62	26.06	121	0	100	76	0.10	99.6
Al2O3	0.86	13.82	104	0	100	65.6	0.38	99.2
TiO2	0.08	1.26	89.9	0.05	100	56.6	3.45	95.7
Fe2O3	0.32	5.11	77.5	0.50	99.5	48.8	7.43	88.3
CaO	1.45	23.37	66.9	1.40	98.1	42.1	9.40	78.9
MgO	0.25	4.06	57.7	2.80	95.3	36.3	9.35	69.6
K2O	0.01	0.19	49.8	4.85	90.4	31.3	8.50	61.1
Na2O	0.05	0.86	42.9	7.45	83.0	27	8.20	52.9
SO3	1.40	22.59	37.1	10.20	72.8	23.3	8.10	44.8
P2O5	0.06	0.93	32	10.35	62.4	20.1	6.75	38.0
Und. Ash	0.11	1.78	27.6	8.35	54.1	17.4	5.15	32.9
Free Silica/Total Silicon	0.21		23.8	6.60	47.5	15	4.90	28.0
Pyritic Iron/Total Iron	0.50		20.5	5.45	42.0	12.9	5.35	22.6
Chlorine	Dry	As Rec'd	17.7	5.50	36.5	11.1	4.58	18.0
Cl (bomb)	0.06	0.05	15.3	5.80	30.7	9.6	3.70	14.3
Cl (in ash)			13.2	5.50	25.2	8.3	2.68	11.7
Forms of Sulfur	Dry	As Rec'd	11.4	4.75	20.5	7.2	2.18	9.48
Sulfatic	0.04	0.03	9.8	3.60	16.8	6.2	2.13	7.35
Pyritic	0.13	0.11	8.5	2.90	13.9	5.3	1.90	5.45
Organic	0.38	0.30	7.3	2.55	11.4	4.6	1.53	3.92
Heating Value (Btu/lb)	Dry	As Rec'd	6.3	2.45	8.95	4	1.28	2.65
As Fired	11970	9519	5.4	2.30	6.65	3.4	1.13	1.52
Dulong			4.7	1.95	4.70	3	0.88	0.65
Acid Soluble Alkali (ppm)	Dry	As Rec'd	4.1	1.25	3.45	2.6	0.45	0.20
Na			3.5	1.10	2.35	2.2	0.10	0.10
Mg			3	0.70	1.65	1.9	0	0.10
Ca			2.6	0.45	1.20	1.6	0	0.10
K			2.2	0.40	0.80	1.4	0	0.10
Fusion Temp. (Reducing)	°F	°C	1.9	0.75	0.05	1.2	0	0.10
Initial Deformation Spherical	2153	1178	Size Distribution			For -325 Mesh Data		
Hemispherical	2207	1209	D(v,0.5) (µm)			22.05		
Fluid	2230	1221	D(v,0.9) (µm)			43.00		
	2278	1248	D(v,0.1) (µm)			6.23		
Fusion Temp. (Oxidizing)	°F	°C	D(4,3) (µm)			23.75		
Initial Deformation Spherical	2150	1177	D(3,2) (µm)			13.47		
Hemispherical	2198	1203	Span			1.68		
Fluid	2224	1218	Spec. Surf. Area (sq.m./cc.)			0.45		
	2281	1250						

*These Malvern data are for the -325 mesh size fractions.

Table 3.A.16

Chemical and Physical Analyses of Eagle Butte

Analyses			Analyses				
Proximate	Dry	As Rec'd	Size Distribution		Sieves	mass % in size bin	cum. mass %
Fixed Carbon	48.05	36.64	dp>600µm		+28	0	0
Volatile Matter	45.55	34.73	600µm>dp>300µm		26x48	0.2	0.2
Moisture	23.74		300µm>dp>149µm		48x100	2.55	2.75
Ultimate	Dry	As Rec'd	149µm>dp>74µm		100x200	17.55	20.3
C	66.81	50.94	74µm>dp>44µm		200x325	22.95	43.25
H	4.93	3.76	44µm>dp		-325	56.75	100
O	20.18	15.39	Size Distribution (Malvern)*			Size Distribution (Malvern)*	
N	1.20	0.92	Diameter (µm)	% in size bin	cum. vol. per.	Diameter (µm)	% in size bin
S	0.47	0.36					
Ash	6.40	4.88	188	0	100	118.4	
Ash Chemistry	% dry coal	% ash	162	0	100	102.1	
SiO2	1.79	27.89	140	0	100	88.1	
Al2O3	0.91	14.24	121	0	100	76	
TiO2	0.05	0.84	104	0	100	65.6	
Fe2O3	0.39	6.04	89.9	0.1	99.9	56.6	
CaO	1.62	25.34	77.5	0.25	99.7	48.8	
MgO	0.38	6.00	66.9	0.975	98.7	42.1	
K2O	0.02	0.27	57.7	2.2	96.5	36.3	
Na2O	0.12	1.83	49.8	4.5	92.0	31.3	
SO3	1.05	16.34	42.9	7.175	84.8	27	
P2O5	0.04	0.66	37.1	9.975	74.8	23.3	
Und. Ash	0.04		32	10.375	64.5	20.1	
Free Silica/Total Silicon	0.24		27.6	8.75	55.7	17.4	
Pyritic Iron/Total Iron	0.20		23.8	7.325	48.4	15	
Chlorine	Dry	As Rec'd	20.5	6.375	42.0	12.9	
Cl (bomb)	0.03	0.02	17.7	6.3	35.7	11.1	
Cl (In ash)			15.3	6.325	29.4	9.6	
Forms of Sulfur	Dry	As Rec'd	13.2	5.575	23.8	8.3	
Sulfatic	0.01	0.00	11.4	4.6	19.2	7.2	
Pyritic	0.06	0.05	9.8	3.425	15.8	6.2	
Organic	0.41	0.31	8.5	2.8	13.0	5.3	
Heating Value (Btu/lb)	Dry	As Rec'd	7.3	2.55	10.4	4.6	
As Fired	11534	8796	6.3	2.425	8.0	4	
Dulong	11289	8608	5.4	2.175	5.8	3.4	
Acid Soluble Alkall (ppm)	Dry	As Rec'd	4.7	1.775	4.1	3	
Na	822	627	4.1	1.075	3.0	2.6	
Mg	1891	1442	3.5	0.925	2.1	2.2	
Ca	7250	5529	3	0.575	1.5	1.9	
K	75	57	2.6	0.4	1.1	1.6	
Fusion Temp. (Reducing)	°F	°C	2.2	0.3	0.8	1.4	
Initial Deformation Spherical	2224	1218	1.9	0.25	0.5	1.2	
Spherical	2253	1234	Size Distribution			For -325 Mesh Data	
Hemispherical	2260	1238	D(v,0.5) (µm)			21.275	
Fluid	2270	1243	D(v,0.9) (µm)			40.98	
Fusion Temp. (Oxidizing)	°F	°C	D(v,0.1) (µm)			6.20	
Initial Deformation Spherical	2181	1194	D(4,3) (µm)			22.675	
Spherical	2212	1211	D(3,2) (µm)			12.9	
Hemispherical	2226	1219	Span			1.63	
Fluid	2243	1228	Spec. Surf. Area (sq.m./cc.)			0.47	

*These Malvern data are for the -325 mesh size fractions.

Table 3.A.17

Chemical and Physical Analyses of Beulah Lignite

Analyses			Analyses			Analyses		
Proximate	Dry	As Rec'd	Size Distribution		Sieves	mass % In size bin		cum. mass %
Fixed Carbon	43.36	31.70	dp>600µm		+28	0.075		0.08
Volatile Matter	42.78	31.28	600µm>dp>300µm		28x48	2.45		2.53
Molsture	26.89		300µm>dp>149µm		48x100	11.44		13.97
Ultimate	Dry	As Rec'd	149µm>dp>74µm		100x200	22.08		36.05
C	60.72	44.39	74µm>dp>44µm		200x325	17.54		53.59
H	4.09	2.99	44µm>dp		-325	46.92		100.51
O	18.35	13.42	Size Distribution (Malvern)*			Size Distribution (Malvern)*		
N	1.05	0.77	Diameter	% In	cum. vol.	Diameter	% In	cum. vol.
S	1.84	1.35	(µm)	size bin	per.	(µm)	size bin	per.
Ash	13.86	10.13	188	0	100	118.4	0.08	99.925
Ash Chemistry	% dry coal	% ash	162	0	100	102.1	0.13	99.8
SiO2	2.92	21.07	140	0	100	88.1	0.13	99.675
Al2O3	1.92	13.88	121	0	100	76	0.1	99.575
TiO2	0.06	0.41	104	0	100	65.6	0	99.575
Fe2O3	1.68	12.15	89.9	0.27	99.7	56.6	1.525	98.05
CaO	2.26	16.28	77.5	0.43	99.3	48.8	4.55	93.5
MgO	0.60	4.33	66.9	0.43	98.9	42.1	6.43	87.075
K2O	0.03	0.21	57.7	0.75	98.1	36.3	7.13	79.95
Na2O	0.89	6.42	49.8	3.87	94.3	31.3	7.2	72.75
SO3	3.32	23.92	42.9	6.43	87.8	27	7.28	65.475
P2O5	0.00	0.00	37.1	8.07	79.8	23.3	7.3	58.175
Und. Ash	-0.01	-0.1	32	7.73	72.0	20.1	6.43	51.75
Free Silica/Total Silicon	0.14		27.6	6.90	65.1	17.4	5.55	46.2
Pyritic Iron/Total Iron	0.33		23.8	6.43	58.7	15	5.73	40.475
Chlorine	Dry	As Rec'd	20.5	6.10	52.6	12.9	6.15	34.325
Cl (bomb)	0.04	0.03	17.7	6.07	46.5	11.1	5.3	29.025
Cl (in ash)			15.3	6.10	40.4	9.6	4.6	24.425
Forms of Sulfur	Dry	As Rec'd	13.2	5.60	34.8	8.3	3.93	20.5
Sulfatic	0.14	0.10	11.4	5.03	29.8	7.2	3.73	16.775
Pyritic	0.44	0.32	9.8	4.23	25.5	6.2	3.65	13.125
Organic	1.27	0.93	8.5	3.73	21.8	5.3	3.08	10.05
Heating Value (Btu/lb)	Dry	As Rec'd	7.3	3.50	18.3	4.6	2.38	7.675
As Fired	10000	7311	6.3	3.50	14.8	4	2.15	5.525
Dulong	9909	7244	5.4	3.33	11.5	3.4	2.25	3.275
Acid Soluble Alkali (ppm)	Dry	As Rec'd	4.7	3	8.5	3	2.075	1.2
Na	7357	4210	4.1	2.5	6.0	2.6	0.725	0.475
Mg	3321	2428	3.5	1.70	4.3	2.2	0.4	0.075
Ca	14036	10262	3	1.27	3.0	1.9	0	0.075
K	152	111	2.6	1.17	1.8	1.6	0.03	0.05
Fusion Temp. (Reducing)	°F	°C	2.2	0.87	1.0	1.4	0	0.05
Initial Deformation	2017	1103	1.9	2.0333	-1.1	1.2	0	0.05
Spherical	2139	1170	Size Distribution			For -325 Mesh Data		
Hemispherical	2165	1185	D(v,0.5) (µm)			16.47		
Fluid	2179	1193	D(v,0.9) (µm)			38.01		
Fusion Temp. (Oxidizing)	°F	°C	D(v,0.1) (µm)			4.40		
Initial Deformation	2286	1252	D(4,3) (µm)			19.53		
Spherical	2354	1290	D(3,2) (µm)			9.93		
Hemispherical	2367	1297	Span			2.04		
Fluid	2383	1306	Spec. Surf. Area (sq.m./cc.)			0.62		

*These Malvern data are for the -325 mesh size fractions.

Table 3.A.18

Chemical and Physical Analyses of the Texas Lignite

Analyses			Analyses			Analyses		
Proximate	Dry	As Rec'd	Size Distribution		Sieves	mass % in size bin		cum. mass %
Fixed Carbon	17.42	14.10	dp>600µm		+28	0.00		0.00
Volatile Matter	30.62	24.77	600µm>dp>300µm		28x48	2.07		2.07
Moisture	19.09		300µm>dp>149µm		48x100	10.13		12.20
Ultimate	Dry	As Rec'd	149µm>dp>74µm		100x200	18.70		30.90
C	29.36	23.75	74µm>dp>44µm		200x325	17.57		48.47
H	3.25	2.63	44µm>dp		-325	51.53		100.00
O	14.15	11.45	Size Distribution (Malvern)*			Size Distribution (Malvern)*		
N	0.51	0.41	Diameter (µm)	% in size bin	cum. vol. per.	Diameter (µm)	% in size bin	cum. vol. per.
S	1.75	1.41	188	0	100	118.4	0.10	99.9
Ash	51.96	42.04	162	0	100	102.1	0.35	99.6
Ash Chemistry	% dry coal	% ash	140	0	100	88.1	0.40	99.2
SiO2	34.07	65.58	121	0	100	76	0.35	98.8
Al2O3	10.22	19.67	104	0	100	65.6	0.25	98.6
TiO2	0.45	0.87	89.9	0.13	99.9	56.6	1.80	96.8
Fe2O3	0.88	1.70	77.5	0.20	99.7	48.8	4.90	91.9
CaO	1.58	3.04	66.9	0.20	99.5	42.1	6.85	85.0
MgO	0.25	0.48	57.7	0.30	99.2	36.3	7.55	77.5
K2O	0.97	1.87	49.8	1.40	97.8	31.3	7.50	70.0
Na2O	1.33	2.55	42.9	3.63	94.2	27	7.30	62.7
SO3	1.46	2.81	37.1	6.45	87.7	23.3	6.75	55.9
P2O5	0.00	0.00	32	7.70	80.0	20.1	6.05	49.9
Und. Ash	1.10	2.13	27.6	7.43	72.6	17.4	5.60	44.3
Free Silica/Total Silicon	0.55		23.8	7.00	65.6	15	5.60	38.7
Pyritic Iron/Total Iron	0.43		20.5	6.55	59.0	12.9	5.55	33.1
Chlorine	Dry	As Rec'd	17.7	6.60	52.4	11.1	4.80	28.3
Cl (bomb)	0.08	0.06	15.3	6.70	45.7	9.6	4.30	24.0
Cl (In ash)	0.01	0.01	13.2	6.33	39.4	8.3	3.90	20.1
Forms of Sulfur	Dry	As Rec'd	11.4	5.75	33.6	7.2	3.55	16.6
Sulfatic	0.09	0.07	9.8	4.73	28.9	6.2	3.30	13.3
Pyritic	0.31	0.25	8.5	4.10	24.8	5.3	2.85	10.4
Organic	1.35	1.09	7.3	3.83	21.0	4.6	2.40	8.00
Heating Value (Btu/lb)	Dry	As Rec'd	6.3	3.83	17.2	4	2.20	5.80
As Fired	5085	4114	5.4	3.60	13.6	3.4	2.10	3.70
Dulong			4.7	3.13	10.4	3	1.75	1.95
Acid Soluble Alkali (ppm)	Dry	As Rec'd	4.1	2.45	8.00	2.6	0.80	1.15
Na	8788	6097	3.5	1.70	6.30	2.2	0.60	0.55
Mg	1156	935	3	1.33	4.97	1.9	0.30	0.25
Ca	7628	6172	2.6	1.20	3.77	1.6	0.00	0.25
K	5862	4743	2.2	1.13	2.65	1.4	0.10	0.15
Fusion Temp. (Reducing)	°F	°C	1.9	2.68	-0.03	1.2	0.10	0.05
Initial Deformation	2349	1287	Size Distribution			For -325 Mesh Data		
Spherical	2454	1345	D(v,0.5) (µm)			15.53		
Hemispherical	2569	1409	D(v,0.9) (µm)			35.77		
Fluid	2736	1502	D(v,0.1) (µm)			4.15		
Fusion Temp. (Oxidizing)	°F	°C	D(4,3) (µm)			18.35		
Initial Deformation	2340	1282	D(3,2) (µm)			8.88		
Spherical	2432	1333	Span			2.03		
Hemispherical	2565	1407	Spec. Surf. Area (sq.m./cc.)			0.70		
Fluid	2743	1506						

*These Malvern data are for the -325 mesh size fractions.

Table 3.A.19

Chemical and Physical Analyses of the Eastern Blend

Analyses			Analyses			Analyses		
Proximate	Dry	As Rec'd	Size Distribution	Sieves	mass % in size bin	cum. mass %		
Fixed Carbon	61.06	60.62	dp>600µm	+28	0	0.00		
Volatlie Matter	30.27	30.05	600µm>dp>300µm	28x48	0	0.00		
Molsture	0.72		300µm>dp>149µm	48x100	1.3	1.30		
Ultimate	Dry	As Rec'd	149µm>dp>74µm	100x200	26.3	27.60		
C	77.95	77.39	74µm>dp>44µm	200x325	26.3	53.90		
H	4.79	4.76	44µm>dp	-325	46.1	100.00		
O	5.51	5.47	Size Distribution (Malvern)*			Size Distribution (Malvern)*		
N	1.43	1.42	Diameter	% In	cum. vol.	Diameter	% in	cum. vol.
S	1.65	1.64	(µm)	size bin	per.	(µm)	size bin	per.
Ash	8.67	8.61	188			118.4		
Ash Chemistry	% dry coal	% ash	162			102.1		
SiO2	4.25	49.03	140			88.1		
Al2O3	2.13	24.53	121			76		
TiO2	0.09	1.00	104			65.6		
Fe2O3	1.48	17.03	89.9			56.6		
CaO	0.20	2.31	77.5			48.8		
MgO	0.07	0.86	66.9			42.1		
K2O	0.17	1.99	57.7			36.3		
Na2O	0.03	0.36	49.8			31.3		
SO3	0.17	1.92	42.9			27		
P2O5	0.03	0.37	37.1			23.3		
Und. Ash	0.05	0.60	32			20.1		
Free Silica/Total Silicon	0.25		27.6			17.4		
Pyritic Iron/Total Iron	0.75		23.8			15		
Chlorine	Dry	As Rec'd	20.5			12.9		
Cl (bomb)			17.7			11.1		
Cl (in ash)			15.3			9.6		
Forms of Sulfur	Dry	As Rec'd	13.2			8.3		
Sulfatic	0.01	0.01	11.4			7.2		
Pyritic	0.89	0.88	9.8			6.2		
Organic	0.75	0.74	8.5			5.3		
Heating Value (Btu/lb)	Dry	As Rec'd	7.3			4.6		
As Fired	13933	13833	6.3			4		
Dulong			5.4			3.4		
Acid Soluble Alkali (ppm)	Dry	As Rec'd	4.7			3		
Na			4.1			2.6		
Mg			3.5			2.2		
Ca			3			1.9		
K			2.6			1.6		
Fusion Temp. (Reducing)	°F	°C	2.2			1.4		
Initial Deformation	2133	1167	1.9			1.2		
Spherical	2429	1332	Size Distribution			For -325 Mesh Data		
Hemispherical	2449	1343	D(v,0.5) (µm)					
Fluid	2500	1371	D(v,0.9) (µm)					
Fusion Temp. (Oxidizing)	°F	°C	D(v,0.1) (µm)					
Initial Deformation	2497	1369	D(4,3) (µm)					
Spherical	2574	1412	D(3,2) (µm)					
Hemispherical	2602	1428	Span					
Fluid	2632	1444	Spec. Surf. Area (sq.m./cc.)					

*These Malvern data are for the -325 mesh size fractions.

Table 3.A.20

Chemical and Physical Analyses of the Pittsburgh #8 (2)/Decker Blend

Analyses			Analyses					
Proximate	Dry	As Rec'd	Size Distribution	Sieves	mass % in size bin	cum. mass %		
Fixed Carbon	56.45	52.60	dp>600µm	+28	0.00	0.00		
Volatiles Matter	36.59	34.10	600µm>dp>300µm	28x48	0.03	0.03		
Moisture	6.81		300µm>dp>149µm	48x100	2.47	2.50		
Ultimate	Dry	As Rec'd	149µm>dp>74µm	100x200	25.67	28.17		
C	76.26	71.06	74µm>dp>44µm	200x325	26.67	54.83		
H	4.94	4.60	44µm>dp	-325	45.20	100.03		
O	9.21	8.58	Size Distribution (Malvern)*		Size Distribution (Malvern)*			
N	1.31	1.22	Diameter (µm)	% In size bin	cum. vol. per.	Diameter (µm)	% In size bin	cum. vol. per.
S	1.28	1.19	188	0	100	118.4		
Ash	6.96	6.49	162	0	100	102.1		
Ash Chemistry	% dry coal	% ash	140	0	100	88.1		
SiO2	2.96	42.54	121	0	100	76		
Al2O3	1.55	22.32	104	0	100	65.6		
TiO2	0.07	1.01	89.9	0.05	100	56.6		
Fe2O3	0.99	14.28	77.5	0.4	99.6	48.8		
CaO	0.39	5.64	66.9	1.55	98.0	42.1		
MgO	0.09	1.35	57.7	3.35	94.7	36.3		
K2O	0.11	1.51	49.8	5.8	88.9	31.3		
Na2O	0.17	2.43	42.9	8.25	80.6	27		
SO3	0.50	7.25	37.1	10.75	69.9	23.3		
P2O5	0.04	0.57	32	10.8	59.1	20.1		
Und. Ash	0.08	1.10	27.6	8.95	50.1	17.4		
Free Silica/Total Silicon	0.20		23.8	7.05	43.1	15		
Pyritic Iron/Total Iron	0.74		20.5	5.7	37.4	12.9		
Chlorine	Dry	As Rec'd	17.7	5.7	31.7	11.1		
Cl (bomb)	0.07	0.06	15.3	5.95	25.7	9.6		
Cl (in ash)			13.2	5.2	20.5	8.3		
Forms of Sulfur	Dry	As Rec'd	11.4	4.15	16.4	7.2		
Sulfatic	0.04	0.04	9.8	2.9	13.5	6.2		
Pyritic	0.59	0.55	8.5	2.25	11.2	5.3		
Organic	0.65	0.60	7.3	2.05	9.2	4.6		
Heating Value (Btu/lb)	Dry	As Rec'd	6.3	1.95	7.2	4		
As Fired	13540	12617	5.4	1.8	5.4	3.4		
Dulong			4.7	1.5	3.9	3		
Acid Soluble Alkali (ppm)	Dry	As Rec'd	4.1	0.95	3.0	2.6		
Na			3.5	0.85	2.1	2.2		
Mg			3	0.5	1.6	1.9		
Ca			2.6	0.35	1.3	1.6		
K			2.2	0.3	1.0	1.4		
Fusion Temp. (Reducing)	°F	°C	1.9	0.55	0.4	1.2		
Initial Deformation	2144	1173	Size Distribution		For -325 Mesh Data			
Spherical	2283	1251	D(v,0.5) (µm)		23.85			
Hemispherical	2319	1271	D(v,0.9) (µm)		44.20			
Fluid	2397	1314	D(v,0.1) (µm)		6.85			
Fusion Temp. (Oxidizing)	°F	°C	D(4,3) (µm)		24.55			
Initial Deformation	2381	1305	D(3,2) (µm)		13.85			
Spherical	2418	1326	Span		1.60			
Hemispherical	2460	1349	Spec. Surf. Area (sq.m./cc.)		0.43			
Fluid	2502	1372						

*These Malvern data are for the -325 mesh size fractions.

Table 3.A.21

Chemical and Physical Analyses of the 70 % Roland/ 30 % Illinois #6 (2) Blend

Analyses			Analyses					
Proximate	Dry	As Rec'd	Size Distribution	Sieves	mass % in size bin	cum. mass %		
Fixed Carbon	48.83	45.62	dp>600µm	+28	0	0.00		
Volatile Matter	42.20	39.43	600µm>dp>300µm	28x48	0.1	0.10		
Moisture	6.57		300µm>dp>149µm	48x100	1.6	1.70		
Ultimate	Dry	As Rec'd	149µm>dp>74µm	100x200	28.85	30.55		
C	69.97	65.37	74µm>dp>44µm	200x325	28.95	59.50		
H	4.77	4.46	44µm>dp	-325	40.5	100.00		
O	13.81	12.90	Size Distribution (Malvern)*		Size Distribution (Malvern)*			
N	1.03	0.96	Diameter (µm)	% in size bin	cum. vol. per.	Diameter (µm)	% in size bin	cum. vol. per.
S	1.42	1.32	188	0	100	118.4		
Ash	8.97	8.38	162	0	100	102.1		
Ash Chemistry	% dry coal	% ash	140	0	100	88.1		
SiO2	3.34	37.29	121	0	100	76		
Al2O3	1.41	15.70	104	0	100	65.6		
TiO2	0.09	0.95	89.9	0.05	100	56.6		
Fe2O3	0.94	10.50	77.5	0.6	99.4	48.8		
CaO	1.02	11.42	66.9	1.95	97.4	42.1		
MgO	0.27	2.96	57.7	4	93.4	36.3		
K2O	0.10	1.15	49.8	6.55	86.9	31.3		
Na2O	0.14	1.57	42.9	8.9	78.0	27		
SO3	1.54	17.14	37.1	10.95	67.0	23.3		
P2O5	0.05	0.56	32	9.95	57.1	20.1		
Und. Ash	0.16	1.77	27.6	7.1	50.0	17.4		
Free Silica/Total Silicon	0.37		23.8	5.85	44.1	15		
Pyritic Iron/Total Iron	0.36		20.5	5.85	38.3	12.9		
Chlorine	Dry	As Rec'd	17.7	5.85	32.4	11.1		
Cl (bomb)	0.05	0.04	15.3	5.45	27.0	9.6		
Cl (in ash)			13.2	4.3	22.6	8.3		
Forms of Sulfur	Dry	As Rec'd	11.4	3.45	19.2	7.2		
Sulfatic	0.05	0.05	9.8	2.7	16.5	6.2		
Pyritic	0.56	0.52	8.5	2.5	14.0	5.3		
Organic	0.85	0.79	7.3	2.4	11.6	4.6		
Heating Value (Btu/lb)	Dry	As Rec'd	6.3	2.2	9.40	4		
As Fired	12110	11314	5.4	2.05	7.35	3.4		
Dulong			4.7	1.8	5.55	3		
Acid Soluble Alkali (ppm)	Dry	As Rec'd	4.1	1.25	4.30	2.6		
Na			3.5	1.15	3.15	2.2		
Mg			3	0.8	2.35	1.9		
Ca			2.6	0.6	1.75	1.6		
K			2.2	0.5	1.25	1.4		
Fusion Temp. (Reducing)	°F	°C	1.9	1.05	0.20	1.2		
Initial Deformation	2048	1120	Size Distribution		For -325 Mesh Data			
Spherical	2126	1163	D(v,0.5) (µm)		23.90			
Hemispherical	2207	1208	D(v,0.9) (µm)		45.90			
Fluid	2306	1263	D(v,0.1) (µm)		5.75			
Fusion Temp. (Oxidizing)	°F	°C	D(4,3) (µm)		25.6			
Initial Deformation	2176	1191	D(3,2) (µm)		12.75			
Spherical	2202	1205	Span		1.70			
Hemispherical	2282	1250	Spec. Surf. Area (sq.m./cc.)		0.49			
Fluid	2373	1301						

*These Malvern data are for the -325 mesh size fractions.

Initial Distribution
Unlimited Release

Dr. Ralph Carabetta
Associate Director, Project Management
U.S. DOE/PETC, Bldg. 922-Rm. 206
P.O. Box 10940
Pittsburgh, PA 15236-0940

Ms. Kay Downey
MS 58-M217
U.S. DOE/PETC
P.O. Box 10940
Pittsburgh, PA 15236-0940

Mr. James M. Ekmann
Director, Coal Combustion Division
U.S. DOE/PETC
P.O. Box 10940, MS 84-307
Pittsburgh, PA 15241

Mr. Charles Garrett
Office of Technical Coordination
U.S. DOE/GTN
FE 14, Room B-107
Washington, DC 20545

Mr. Philip M. Goldberg
Coal Utilization Division
U.S. DOE/PETC, 922-H
P.O. Box 10940
Pittsburgh, PA 15236-0940

Dr. Martin Hertzberg
Pittsburgh Research Center
U.S. Bureau of Mines
P.O. Box 18070
Pittsburgh, PA 15236

Mr. James Hickerson
Coal Utilization Division
U.S. DOE/PETC, 922-H
P.O. Box 10940
Pittsburgh, PA 15236-0940

Ms. Marilyn Keane
PM-01, MS922-206
U.S. DOE/PETC
P.O. Box 10940
Pittsburgh, PA 15236-0940

Dr. Dan Maloney
U.S. DOE/METC
P.O. Box 880
Morgantown, WV 26507

Dr. Mahendra P. Mathur
Chief, Fundamentals of Combustion Branch
U.S. DOE/PETC
Post Office Box 10940
Pittsburgh, PA 15236

Dr. Tom O'Brien
U.S. DOE/METC - B-010
P.O. Box 880
Morgantown, WV 26507

Mr. Larry Ruth
Director, Coal Utilization Division
U.S. DOE/PETC, 922-H
P.O. Box 10940
Pittsburgh, PA 15236-0940

Mr. Scott M. Smouse
Coal Combustion Division
U.S. DOE/PETC
P.O. Box 10940
Pittsburgh, PA 15236

U.S. DOE
Office of Patent Counsel
Chicago Operations Office
9800 South Cass Avenue
Argonne, IL 60439

Mr. John C. Winslow
Project Manager, Coal Utilization
U.S. DOE/PETC
P.O. Box 10940
Pittsburgh, PA 15236

Mr. Ian W. Smith
Leader--Combustion Group
CSIRO
51 Delhi Road, P.O. Box 136
North Ryde, NSW, 2113
AUSTRALIA

Professor John Beer
Department of Chemical Engineering
Massachusetts Institute of Technology
66-552
Cambridge, MA 02139

Dr. Steve Benson
Energy and Mineral Research Center
University of North Dakota
Box 8213, University Station
Grand Forks, ND 58202

Dr. Alan W. Cramb
Associate Director, CISR
Carnegie Mellon University
Dept. of Metallurgical Engr. & Materials Science
Pittsburgh, PA 15213-3890

Dr. Boyd Edwards
Associate Professor
West Virginia University
Department of Physics
Morgantown, WV 26505

Professor Robert Essenhigh
Mechanical Engineering Department
Ohio State University
206 West 18th Avenue
Columbus, OH 43210

Professor Richard Flagan
Environmental Engineering Department
California Institute of Technology
138-78
Pasadena, CA 91125

Dr. Richard J. Fruehan
Director, CISR
Carnegie Mellon University
Dept. of Metallurgical Engr. & Materials Science
Pittsburgh, PA 15213-3890

Professor David Grant
Department of Chemistry
University of Utah
Salt Lake City, UT 84112

Professor John Harb
Department of Chemical Engineering
Brigham Young University
350 Clyde Building
Provo, UT 84602

Professor Bill Hecker
Brigham Young University
350 CB
Provo, UT 84602

Professor J. B. Howard
Chemical Engineering Department
Massachusetts Institute of Technology
66-454
Cambridge MA 02139

Dr. Michael L. Jones
Energy and Mineral Research Center
University of North Dakota
Box 8213, University Station
Grand Forks, ND 58202

Professor Herman Krier
140 Mechanical Engineering Bldg.
University of Illinois at Urbana
1206 W. Green Street
Urbana, IL 61801

Professor John Larsen
Department of Chemistry
Lehigh University
Bethlehem, PA 18015

Professor John P. Longwell
Chemical Engineering Department
Massachusetts Institute of Technology
Room 66554
Cambridge, MA 02139

Dr. Henk Meuzelaar
Center for Microanalysis & Reaction Chemistry
University of Utah
214 EMRL
Salt Lake City, UT 84112

Professor Reginald E. Mitchell
High Temperature Gasdynamics Lab.
Stanford University
Mechanical Engineering Department
Palo Alto, CA 94305

Professor Steve Niksa
Mechanical Engineering Department
Stanford University
Palo Alto, CA 94305

Professor Howard B. Palmer
Senior Associate Dean
Pennsylvania State University
113 Kern Building
University Park, PA 16802

Professor David W. Pershing
Dean, College of Engineering
University of Utah
2202 Merrill Engineering Bldg.
Salt Lake City, UT 84112

Professor Ron Pugmire
Vice President for Research
University of Utah
210 Park Building
Salt Lake City, UT 84112

Professor Daniel E. Rosner
Director, High Temperature Chem. Engr. Lab.
Yale University
P.O. Box 2159
New Haven CT 06520-8167

Professor Adel Sarofim
Department of Chemical Engineering
Massachusetts Institute of Technology
66-466
Cambridge, MA 02139

Dr. Alan Scaroni
Pennsylvania State University
404 Academic Activities Building
University Park, PA 16802

Professor Philip Smith
Department of Chemical Engineering
University of Utah
2250 Merrill Engineering Bldg.
Salt Lake City, UT 84112

Professor L. Douglas Smoot
Dean, College of Engineering & Technology
Brigham Young University
270 CB
Provo, UT 84602

Professor Eric Suuberg
Division of Engineering
Brown University
Box D
Providence, RI 02913

Mr. Charles L. Wagoner
Senior Research Engineer
University of Tennessee Space Inst.
Fuels and Environmental Department
Tullahoma, TN 37388-8897

Professor Terry Wall
Department of Chemical & Materials Engr.
The University of Newcastle
Rankin Drive
Newcastle, NSW 2308
AUSTRALIA

Professor Mark S. Wrighton
Chemistry Department
Massachusetts Institute of Technology
Cambridge, MA 02139

Murray Abbott
Supervisor, Combustion Group
Consolidation Coal Company
4000 Brownsviolle Road
Library, PA 15129

Dr. Seymour B. Alpert
P.O. Box 10412
Electric Power Research Institute
3412 Hillview Avenue
Palo Alto, CA 94308

Dr. Arthur Boni
President
PSI Technology Company
20 New England Business Center
Andover, MA 01810

Mr. Richard W. Borio
Combustion Engineering Inc.
1000 Prospect Hill Road, P.O. Box 500
Windsor, CT 06095

Dr. Robert W. Bouman
Manager, Process Research
Bethlehem Steel Corporation
Homer Research Laboratories
Bethlehem, PA 18016

Joseph N. Brobjorg
Senior Research Engineer
Northern States Power Company
414 Nicolet Mall
Minneapolis, MN 55401

Mr. Richard Bryers
Applied Thermo & Processes Dept.
Foster Wheeler Development Corp.
12 Peach Tree Hill Road
Livingston, NJ 07039

Donald L. Bull
Engineering Services
Northern Indiana Public Service Co.
5265 Hohman Avenue
Hammond, IN 46320-1755

Dr. Hartwell F. Calcote
Aerochem Research Laboratories
Director of Research
P.O. Box 12
Princeton, NJ 08540

Mr. Richard W. DeSollar
Fuels Coordinator, Power Production
Central Illinois Public Service Company
607 East Adams Street
Springfield, IL 62701

Dr. Richard Diehl
AVCO Everett Research Lab
2385 Revere Beach Parkway
Everett, MA 02149

Dr. W. A. Fiveland
Heat Transfer & Fluid Mechanics Sec.
Babcock & Wilcox
1562 Beeson Street
Alliance, OH 44601

Dr. Patrick F. Flynn
Vice President, Research & Technology
Cummins Engine Company
Mail Code 50181, Box 3005
Columbus, IN 47202-3005

Dr. Anthony Fonseca
Research and Development
Consolidation Coal Company
4000 Brownsville Road
Library, PA 15129

Dr. James Freihaut
United Technologies Research Center
Combustion Sciences
Silver Lane, MS 30
East Hartford, CT 06108

Mr. William R. Gould
Southern California Edison
P.O. Box 800
Rosemead, CA 91770

Dr. N. Stanley Harding
Reaction Engineering International
317 Marion Drive
McMurray PA 15317

Mr. Michael J. Hargrove
Power Systems
Combustion Engineering, Inc.
1000 Prospect Hill Rd., P.O. Box 500
Windsor, CT 06095-0500

Rod Hatt
Director, Technical Marketing
Island Creek Corporation
P.O. Box 11430
Lexington, KY 40575-1430

Dr. Michael Heap
Reaction Engineering International
48 W. 300 Street, Suite 605N
Salt Lake City, UT 84101

Mr. Michael C. Ingham
Manager, Transportation Fuels Performance
Chevron Research & Technology
Room 10-3618, P.O. Box 1627
Richmond, CA 93802-0627

Dr. A. S. Jamaluddin
Combustion/Reaction Engineering
Shell Development Company
P.O. Box 1380
Houston, TX 77251-1380

Dr. Flynt Kennedy
Vice President, Research & Development
Consolidation Coal Co.
4000 Brownsville Road
Library, PA 15129

Dr. Hisashi Kobayashi
Linde Division
Union Carbide Corporation
Tarrytown Technical Center
Tarrytown, NY 10591

Dr. Donald R. Mac Rae
Research Department
Bethlehem Steel Corporation
Technology Center
Bethlehem, PA 18016

Mr. John L. Marion
Manager, Fuel Systems Development
Kreisinger Development Laboratory
1000 Prospect Hill Road, P.O. Box 500
Windsor, CT 06095-0500

Dr. John S. Maulbetsch
Exploratory Research
EPRI
3412 Hillview Ave., P.O. Box 10412
Palo Alto, CA 94303

Dr. Arun K. Mehta
P.O. Box 10412
Electric Power Research Institute
3412 Hillview Avenue
Palo Alto, CA 94308

Mr. E. R. Michaud
Director, Mechanical Engr. Lab
Babcock & Wilcox
1562 Beeson Street
Alliance, OH 44601

Dr. Nsakala ya Nsakala
Combustion Engineering Inc.
1000 Prospect Hill Road, P.O. Box 500
Windsor, CT 06095

Dr. Jack Oakey
Technology Department
National Steel Corporation
20 Stanwix Street
Pittsburgh, PA 15222

Mr. William J. Oberjohn
Technical Advisor, Alliance Research Center
Babcock & Wilcox
1562 Beeson Street
Alliance, OH 44601

Dr. Myungsook S. Oh
Texaco, Inc.
P.O. Box 509
Beacon, NY 12508

Mr. John M. Rackley
Director, Energy Systems Lab
Babcock & Wilcox
1562 Beeson Street
Alliance, OH 44601

Dr. Dee P. Rees
Combustion Research
Consolidation Coal Co.
4000 Brownsville Road
Library, PA 15129

Mr. Eric H. Reichl
P.O. Box 472
Princeton, NJ 08542

Mr. Michael J. Rini, PE
Fuel Systems Development
Kreisinger Development Laboratory
1000 Prospect Hill Road, P.O. Box 500
Windsor, CT 06095-0500

Dr. Peter Roberts
Manager, Combustion Engineering
Solar Turbines, Inc.
Box 85376
San Diego, CA 92138-5376

Dr. Robert Schwartz
Senior Vice President
John Zink Company
P.O. Box 702220
Tulsa, OK 74170-2220

Dr. W. Randall Seeker
Environmental Management Services
Energy and Environmental Research Corp.
18 Mason
Irvine, CA 92718

Dr. Daniel Seery
United Technologies Research Center
Combustion Sciences
Silver Lane, MS 30
East Hartford, CT 06108

Dr. Peter Solomon
P.O. Box 18343
Advance Fuel Research
87 Church Street
East Hartford, CT 06108

Dr. A. Turan
Principal Research Scientist
AVCO Everett Research Lab
2385 Revere Beach Parkway
Everett, MA 02149

Dr. Joel Vatsky
Director, Combustion and Environ. Sys.
Foster Wheeler Energy Corp.
Clinton, NJ 08809-4000

Mr. Craig G. Vogel, P.E.
Manager, Technical Sales
Cyprus Coal Company
9100 East Mineral Circle
Englewood, CO 80112

Dr. Harold W. Wahle
Manager, Heat Transfer & Fluid Mech.
Babcock & Wilcox
1562 Beeson St.
Alliance, OH 44601

Mr. Colin Wilkes
Supervisor, Coal Tech. & Research
Allison Gas Turbines
Speed Code T14, P.O. Box 420
Indianapolis, IN 46206

Mr. Kurt Yeager
Vice President, Generation & Storage Div.
Electric Power Research Institute
P.O. Box 10412
Palo Alto, CA 94303

Roy R. Ziemer, PE
Fuel Services Analysis Supervisor
Wisconsin Public Service Corp.
600 N. Adams, P.O. Box 19002
Green Bay, WI 54307-9002

1800 R. J. Eagan
ATTN: 1810 D. W. Schaefer
1820 J. Q. Searcy

6000 D. L. Hartley
6200 B. W. Marshall
ATTN: 6201 D. Engi
6211 G. A. Carlson
6211 A. P. Sylvester
6212 H. R. Stephens

8000 J. C. Crawford
ATTN: 8100 E. E. Ives
8200 R. J. Detry
8400 R. C. Wayne
8500 P. E. Brewer

8300 P. L. Mattern
8300A J. S. Binkley
ATTN: T. T. Bramlette
T. M. Dyer
S. C. Johnston

8310 D. L. Lindner
ATTN: 8311 J. E. Costa
8312 K. W. Mahin
8313 J. M. Hruby
8316 R. E. Stoltz

8313 D. K. Ottesen
8314 N. Y. C. Yang
8340 W. Bauer

8350 W. J. McLean
ATTN: 8351 D. W. Sweeney
8353 D. W. Chandler
8354 R. P. Lucht
8362 R. W. Carling

8361 M. D. Allendorf
E. R. Arquitola
S. M. Ferko
A. R. Kerstein
A. J. Salmi

8361 L. L. Baxter

8361 T. H. Fletcher

8361 D. R. Hardesty (10)

8361 R. H. Hurt

8535 Publications Division

8535 Publications Division for OSTI (10)

8524-2 Central Technical Files (2)

3141 Technical Library Processes (3)